Radio Frequency and Terahertz Signals Generated by Passively Mode-Locked Semiconductor Lasers

Sylwester Latkowski

B.Eng., M.Sc., MIEEE

A dissertation submitted in part fulfilment of the

requirement for the award of

Doctor of Philosophy (Ph.D.)

to the

Dublin City University

Faculty of Engineering and Computing

School of Electronic Engineering

Research Supervisor:

Dr. Pascal Landais

September of 2010

Declaration

I hereby certify that this material, which I now submit for assessment on the programme of study leading to the award of Doctor of Philosophy is entirely my own work, that I have exercised reasonable care to ensure that the work is original, and does not to the best of my knowledge breach any law of copyright, and has not been taken from the work of others save and to the extent that such work has been cited and acknowledged within the text of my work.

Signed:	
Student ID:	56102771
Date:	December 14, 2010

To Mam

Mojej Mamie

Acknowledgements

This dissertation is the result of research work that I have conducted in DCU over past four years. While doing so, I have received support from many people to whom I would like to express my gratitude.

Dr. Pascal Landais for allowing me to join his group, and making all this work possible. For his support, guidance, patience and attitude all of which make him not only great research supervisor but also a good friend.

Dr. Ramón Maldonado-Basilio for everything, as research cannot be fruitful without friendship (and a coffee).

To all radio and optical communications laboratory members I had the honor to work with (in random order, ladies first): Dr. Aisling Clarke, Elif Degirmenci, Dr. Ola Kaszubowska - Anandarajah, Jennifer Stopford, Dr. Severine Phillippe, Dr. Frederic Surre, Dr. Prince Anandarajah, Dr. Robert Maher, Dr. Douglas Reid, Dr. Krzysztof Bondarczuk, Dr. Frank Smyth, Dr. Paul Maguire, Dr. Karl Dexter, Prof. Liam Barry, Dr. Philip Perry, Josué Parra-Cetina, Kevin Carney, Haymen Shams Eldin, Kai Shi, Daniele Tafani, Colm Browning, Antonio Castillo, Marc Rensing, Dr. Brendan Kennedy, and Dr. Eoin Connolly. For all the priceless conversations, advice, comments, and the friendly atmosphere not only in the workplace but also beyond of it. All of you will remain my friends for a lifetime.

I am in debt to all Irish friends who were always willing to help me to overcome my English language deficiencies, especially: Kevin, Rob, Karl, Paul, and Darragh Buffini.

To the technical staff I could always rely on: Robert Clare, Conor Maguire, Liam Meany, Billy Roarty, and Paul Wogan.

Important experiments were carried out in external laboratories, with the kind support from: Dr. Stephen A. Lynch, Prof.Dr. Wolfgang Elser, and Dr. Jean-François Lampin.

To my family: Irena, Maria, Natasza, Antoni, Jerzy, Marek, Ireneusz for their everlasting support and belief in me. I am who I am because of all of you.

To my beloved girlfriend Karolina for all the support and love I get from her - it wouldn't happen without you.

Abstract

There are several different approaches to generating periodic signals using semiconductor lasers, for example: Q-switching, gain switching or mode-locking schemes. In general the active or passive mode-locking techniques require the use of a modulator or a saturable absorber in order to achieve the phase synchronisation. The laser diodes studied in this thesis, are demonstrated to operate in the mode-locked regime, while not requiring any direct or external modulation, nor the saturable absorbtion element in order to achieve the phase synchronisation. It has been demonstrated previously, that in a multimode semiconductor laser, the third order nonlinearities of a gain medium resulting in the four-wave-mixing effects, are responsible for the phase synchronisation and lead to phase locking. The repetition rate of the generated signal is fixed by the free-spectral range of the longitudinal spectrum. Therefore, with a passively mode-locked laser (PMLL) it is possible to cover a wide range of frequencies from the Radio-Frequency (RF) to the TeraHertz (THz) domain. Radio frequency signals generated by semiconductor lasers have many applications in optical communications, such as radio-over-fibre, or all-optical clock extraction. Terahertz signals are the focus of many research bodies nowadays, due to their interaction with matter. They have potential applications in areas like: industry, pharmacy, security (military), telecommunication and medicine. With continuous improvement of materials processing and technology, new ways of generation and detection of such types of signals have appeared. The key advantage of the optical RF or THz generation is that this type of device is direct current biased and operates at room temperature. In this thesis, a comprehensive study of various PMLLs, from distributed Bragg reflector bulk laser to quantum dashed Fabry-Perot lasers is given, demonstrating the origin of the phase synchronisation in these structures and some applications for these lasers such as all-optical clock recovery or THz signal generation.

Contents

List of Figures

List of Tables

List of Acronyms

AMP	Amplifier
BPF	Band-Pass Filter
CDM	Carrier Density Modulation
CH	Carrier Heating
CW	Continuous Wave
DBR	Distributed Bragg Reflector
DC	Direct Current
DFB	Distributed FeedBack
EDFA	Erbium Doped Fibre Amplifier
EM	ElectroMagnetic
ESA	Electrical Spectrum Analyzer
FP	Fabry-Pérot
FROG	Frequency Resolved Optical Gating
FSR	Free Spectral Range
FT-IR	Fourier Transform-Infrared
FWHM	Full Width at Half Maximum
FWM	Four Wave Mixing
GEN	Signal Generator
GS-MBE	Gas Source Molecular Beam Epitaxy
GVD	Group Velocity Dispersion
HEB	Hot Electron Bolometer
IF	Intermediate Frequency
ISO	Optical Isolator
LI	Power versus Current
LD	Laser Diode
LO	Local Oscillator
MBE	Molecular Beam Epitaxy
MMIC	Monolithic Microwave Integrated Circuit
MIX	Mixer
mmW	Millimeter Wave
MOVPE	Metalorganic Vapour Phase Epitaxy
MQW	Multi Quantum Well
MZM	Mach-Zhender Modulator
NRZ	None Return to Zero

OBPF	Optical Band-Pass Filter
OMUX	Optical Multiplexer
OSA	Optical Spectrum Analyzer
OSO	Optical Sampling Oscilloscope
OTDM	Optical Time Division Multiplexing
PC	Polarization Controller
PD	Photo Diode
PM	Phase Modulator
PML	Passive Mode-Locking
POL	Polarizer
PPG	Pulse Pattern Generator
PRBS	Pseudo Random Bit Sequence
QD	Quantum Dot
QDash	Quantum Dash
RF	Radio Frequency
RZ	Return to Zero
SCH	Separate Confinement Heterostructure
SHB	Spectral Hole Burning
SHG	Second Harmonic Generation
SIS	Superconductor-Insulator-Superconductor
SMF	Polarization Maintaining Fibre
SMSR	Side Mode Suppression Ration
S/N	Singal to Noise
SOA	Semiconductor Optical Amplifier
SQW	Single Quantum Well
TE	Transverse Electric
TM	Transverse Magnetic
TMLL	Tunable Mode-Locked Laser
TPA	Two Photon Absorption
TPX	Polymethylpentene
UTC-PD	Uni-Traveling Carrier Photo Diode
VCO	Voltage Controlled Oscillator
VCSEL	Vertical Cavity Surface Emitting Laser
VECSEL	Vertical Extended Cavity Surface Emitting Laser
VI	Voltage versus Current
VOA	Variable Optical Attenuator

Chapter 1

Introduction

1.1 General Introduction and Rationale

The semiconductor laser's range of applications is expanding. Their compactness, relatively low power consumption, and feasibility, combined with great operation parameters, allow for use in many areas. Semiconductor lasers play key roles in today's optical communication systems. Fast photonic devices seem to be the only reasonable solution able to cope with the increasing demand for the networks speed and capacity. At first glance, a single longitudinal mode operation of the laser device is most desirable from optical communications point of view. Great improvement in recent years in semiconductor laser science and technology allowes to achieve excellent parameters of such devices in terms of spectral purity, stability and emitted power. However, it has also allowed for better understanding of the mechanisms affecting the optical fields inside the active semiconductor material, and opened new possible areas of applications for devices operating in a multicolour regime. Advances in epitaxy resulted in techniques like gas source molecular beam epitaxy (GS-MBE), which allows controlling growth on the atomic scale, and makes it possible to create active materials based on quantum dots, while quantum well based devices manufactured in metalorganic vapour phase epitaxy (MOVPE) processes are most commonly used nowadays. Better control over the epitaxial growth and regrowth processes resulted in development of new sophisticated techniques and improvement of those already known, allowing engineering of the spectral output of the laser diode in terms of emission wavelengths, number of longitudinal modes and separation frequency between those. Such laser diodes can operate in a stable multimode regime. Parameters of the optical modes present in the output spectrum of such multimode semiconductor laser are nearly as good as the ones which originate from a single-mode semiconductor device in terms of wavelength stability and optical linewidth. However, they can also benefit from the nonlinear nature of the semiconductor material that they simultaneously originate from, which can result in correlation of the phase noise associated with each mode and lead to high coherence between them. While the semiconductor laser operates in the multimode regime, and there exists a mechanism providing the phase information exchange among the modes inside the laser cavity, pulse stream formation may occur as a result of mode-locking. Very short pulse durations with repetition rates reaching terahertz frequencies are possible. Generation of signals related to the free spectral range is possible via photomixing providing that a sufficiently fast photodetector is used. Signals generated in this fashion feature a stable central frequency which spans from RF to terahertz band, as the separation between optical modes is limited by the gain bandwidth of the active structure and can reach up to several terahertz. Additionally the linewidth of such a signal can benefit from the phase correlation of the modes originating from a single semiconductor cavity. Furthermore, as a result of strong nonlinear interactions between electro-magnetic fields associated with laser modes, the semiconductor active material undergoes modulation with the frequency corresponding to the beat tone produced by the longitudinal modes difference frequency. An extensive experimental study of three different types of semiconductor laser structures operating in a multi longitudinal mode regime is described in this thesis.

1.2 Thesis Overview

This dissertation consists of eight chapters of which the first comprises this introduction and the remaining are organized in the following order:

Chapter 2 contains a basic background associated with operation of semiconductor laser. Information provided spans from an ordinary p-n junction based laser to sophisticated quantum structures utilized as an active medium. A number of techniques used for profiling of the spectral output of semiconductor material based laser is presented, all of which were developed in order to achieve single longitudinal mode operation. However, when such a technique is applied in a proper manner this can lead to multi longitudinal mode operation. Among others, the method based on introduction of a one-dimensional photonic bandgap along the laser cavity in order to control its spectral output is presented, as many experimental examples of multimode operation of such a semiconductor laser are presented and discussed across this thesis.

Physical interactions of the electro-magnetic fields associated with the number of optical longitudinal modes inside the semiconductor laser cavity are analyzed in Chapter 3. Different mode-locking scenarios are presented, and the chapter concludes with a discussion of the mode-locking via four wave mixing interactions in a single section semiconductor laser.

Chapter 4 deals with generation of radio frequency signals by semiconductor lasers operating in a multimode regime. The presence of passive mode-locking mechanisms in tested structures is experimentally investigated.

The formation of short optical events with high repetition rates as a consequence of passive mode-locking by laser diodes of different structure is studied in Chapter 5.

In Chapter 6 the ability of the multimode semiconductor lasers introduced in former chapters to alter the free running frequency to the externally injected signal is demonstrated. This leads to potential applications as a clock recovery elements in all-optical communications systems.

The ability to generate terahertz signals by multimode semiconductor lasers is discussed and experimentally investigated in Chapter 7. Terahertz generation by direct and indirect means are demonstrated.

The thesis is concluded in Chapter 8, with a brief discussion of possible further research directions linked with the scope of presented work.

Chapter 2

Semiconductor lasers

The aim of this chapter is to provide a brief background on the physics of the devices that are the subject of discussion and investigation in subsequent chapters.

2.1 Laser - Introduction

The word laser emerged as an acronym for light amplification by stimulated emission of radiation. The first laser action at optical wavelengths was proposed in 1957 by Schawlow and Tones [1], and demonstrated in 1960 by T.H. Maiman [2]. It followed presentation of the maser (microwave amplification by stimulated emission of radiation) in 1954 by C.H. Townes, N.G. Basov and A.M. Prokhorov. The principle underlying both is a process of stimulated emission introduced by A. Einstein in 1917 [3]. The research and development of lasers has been vast since then, and new applications for such are being found on nearly daily basis in present times [4]. Today various types of semiconductor lasers are used as a source of coherent light for various applications, including optical fibre communication systems and optical disk memory systems. Advanced functions and high performance have been realized through distributed feedback and quantum well lasers following the development of Fabry-Pérot type lasers. Accordingly new applications previously unfeasible (or difficult with other conventional lasers) have been found, and replacement of gas and solid-state lasers is in progress [5]. The laser is an optical oscillator, which comprises an optical amplifier with a positive feedback. The oscillation process may be initiated by the noise containing frequency components lying in the gain bandwidth of the amplifier, and continues to grow until saturation of the amplifier gain is reached and the system settles in a steady state with an output signal at single or multiple resonant frequencies. Two conditions have to be satisfied for such a process to occur: the amplifier gain must equal the losses in the feedback system and phase shift in a single round trip must fulfill the condition of positive feedback (in particular to be an integer multiple of 2π). Once saturation of the amplifier occurs, gain is reduced from its initial value and in stable condition the gain compensates for the losses in the system, and a steady state oscillation occurs.

2.2 Semiconductor laser

The laser is an externally pumped, self sustained oscillator, and consists of a gain medium placed into an optical resonator, which provides necessary feedback [6]. A semiconductor laser comprises of gain medium which is an electrically pumped, forward biased $p - n$ junction (diode), where charge carriers injected into a thin active region may contribute to the optical gain. The optical feedback can be provided by the edges of the semiconductor material, cleaved along the crystal planes. Refractive index difference created at the contact of the cleaved facet and the air act as a reflector. If the gain coefficient is sufficiently large, and a phase condition for positive feedback is satisfied, such semiconductor crystal forms an optical oscillator, or in other words a laser. External pumping is governed by injected current density J. The threshold condition is achieved when the injected current density equals a value J_{th}, at which optical gain is sufficient to overcome the losses [6, 7]. This type of device is called a semiconductor injection laser or a laser diode (LD).

In semiconductor laser, electrons contributing to the processes of spontaneous emission, absorption, and stimulated emission as depicted in Fig. 2.2, should be treated collectively, as they interact with each other through various intraband processes. The electrons and holes diffuse spatially, which leads to a spatially inhomogeneous gain profile, and spatial variation of the optical mode through stimulated emission. The optical modes in semiconductor laser

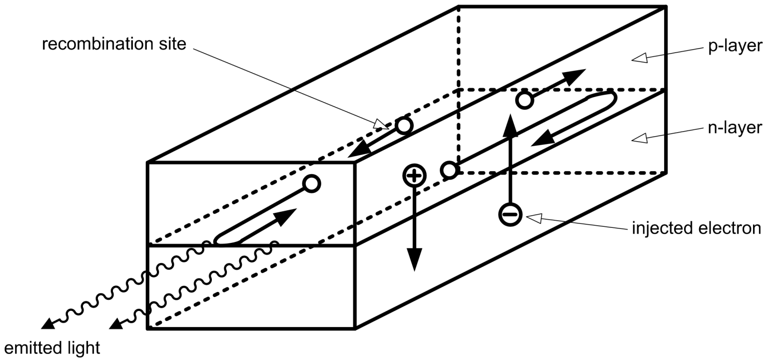

Figure 2.1: Schematic picture of semiconductor laser.

resulting from dielectric wave-guiding, are transverse electric (TE) or transverse magnetic (TM). The cold-cavity modes are affected by external pumping (the injected current density J), which changes both the gain and the refractive index, and has an impact on the operating characteristics of the laser diode [6].

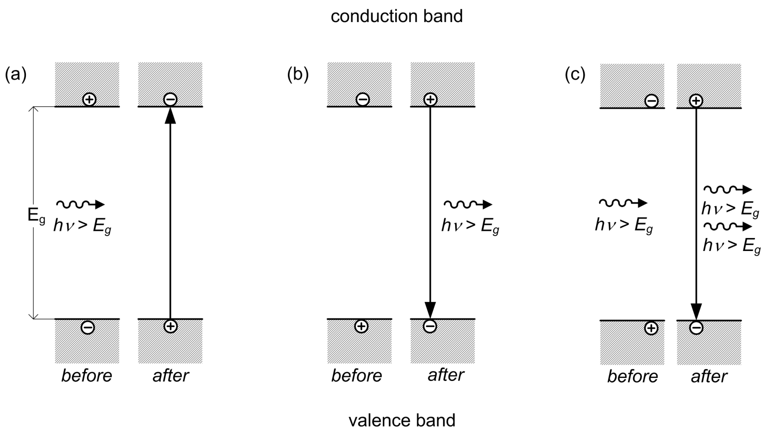

Figure 2.2: Photon-electron transitions in semiconductor material: a) absorption, b) spontaneous emission, c) stimulated emission.

2.2.1 Light amplification

The gain coefficient $\gamma_0(\nu)$ of a semiconductor laser amplifier has a peak value γ_p can be approximated proportional to the injected current density J [7].

$$\gamma_p \approx \alpha(\frac{J}{J_T}) \tag{2.1}$$

$$J_T = \frac{el}{\eta_i \tau_r} \Delta n_T \tag{2.2}$$

where τ_r is the radiative electron-hole recombination lifetime, $\eta_i = \tau/\tau_r$ is the internal quantum efficiency with τ being carrier lifetime, l is the thickness of active region, α is the thermal equilibrium absorption coefficient, and Δn_T and J_T are the injected carrier concentration and current density required to achieve the semiconductor transparency.

2.2.2 Optical feedback

The optical feedback is usually provided by cleaved crystal planes normal to the junction plane. In such case, the active region of the $p-n$ junction serves as an optical resonator of length L, with planar mirrors. The reflectance at the semiconductor-air contact can be written as [7]:

$$R = \left(\frac{n-1}{n+1}\right)^2 \tag{2.3}$$

with n being the refractive index of the semiconductor material.

2.2.3 Resonator losses

Dominant loss of the resonator results from partial reflection at the facets. For the resonator of length L, and reflectance of the mirrors R_1 and R_2, their total loss α_m can be written [7]:

$$\alpha_m = \alpha_{m1} + \alpha_{m2} = \frac{1}{2L} ln \frac{1}{R_1 R_2} \tag{2.4}$$

with α_{m1} and α_{m2} losses on both mirrors respectively.This loss includes the useful, transmitted part of light. The total loss coefficient α_r can be written in the form [7]:

$$\alpha_r = \alpha_s + \alpha_m \tag{2.5}$$

where α_s represent other sources of loss, like free carrier absorption in semiconductor and scattering from optical inhomogeneities. The part of the optical field outside the active layer - in perpendicular direction to its plane - also contributes to the overall loss. Losses caused by this effect can be taken into account by definition of the confinement factor Γ in order to represent the part of the optical field lying in the active region and assuming that the remaining part isunaffected by gain. Then Γ is the ratio by which the gain coefficient g should be reduced or the loss coefficient increased. To follow the latter, the loss coefficient takes a form [7]:

$$\alpha_r = \frac{1}{\Gamma}(\alpha_s + \alpha_m) \tag{2.6}$$

2.2.4 Gain condition

In order to satisfy the laser oscillation condition, the gain must equal the losses, $\gamma_p = \alpha_r$. The threshold gain is then equal to the loss α_r [7]:

$$\Gamma g = \alpha_r \tag{2.7}$$

and then the threshold current density J_t can be found from [7]:

$$J_t = \frac{\alpha_r + \alpha}{\alpha} J_T \tag{2.8}$$

2.2.5 The p-n junction lasers

In a semiconductor lasers a p-n junction serves as the active medium. In order to achieve a laser action, requirements for population inversion and optical feedback have to be fulfilled. To obtain stimulated emission, there must be a region of the device where there are many exited electrons and vacant states (i.e. holes) present together. This can be achieved by forward biasing a junction formed from heavily doped materials denoted as $p+$ and $n+$. In such type of semiconductors Fermi levels may lie within the valence and conduction bands in case of type $p+$ and $n+$ respectively. The equilibrium and forward biased energy bands are presented in Fig. 2.3. When forward bias voltage is nearly equal to the energy gap voltage E_g/e, electrons and holes injected across the junction are in sufficient amounts to create a population inversion in a narrow zone called active region. In case of direct band-gap materials such as $GaAs$, electrons and holes have a high probability of recombining

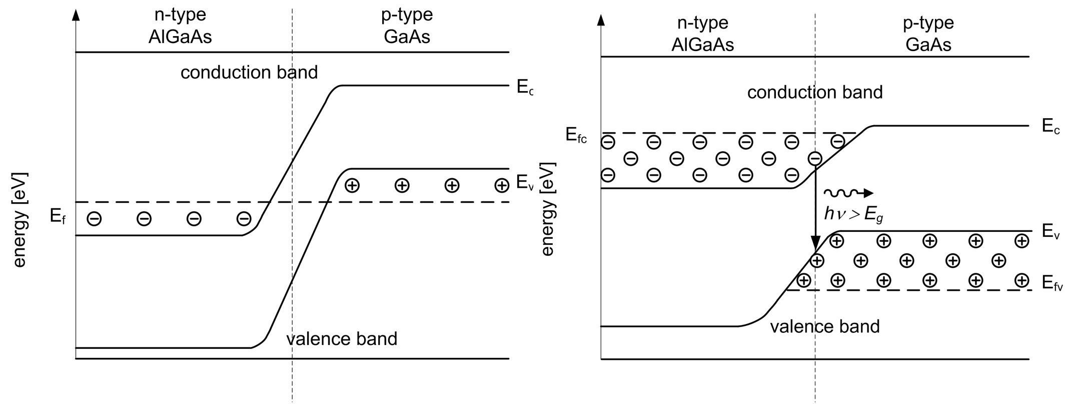

(a) Eequilibrium state.
(b) Forward biased.

Figure 2.3: Energy band distributions of a p-n junction.

radiatively. The recombination radiation may interact with electrons in the valence band and be absorbed, or interact with electrons in conduction band and stimulate production of photons of the same energy:

$$\nu = \frac{E_g}{h} \tag{2.9}$$

For a high enough injection current, stimulated emission can exceed absorption process and optical gain can be achieved in the active region.

The optical feedback is provided by reflections form the interface between material and air due to high value of the refractive index of the semiconductor material as given by Equation 2.3. Reflectance provided is sufficient even though it is only about 0.32 for $GaAs$.

The end facets of the diode are created by cleaving the device along natural crystal planes normal to the plane of the junction and in such a form create a resonant cavity. Additional optical coating may be applied on the facets. The radiation generated in the active region spreads out into the surrounding material ($GaAs$); however there is some confinement of the radiation within the region called mode volume. The refractive index in the active region is affected by additional carriers and effectively increased to a higher value than surroundings what results in formation of dielectric waveguide. The onset of laser action at the threshold current density can be detected by an abrupt increase of the radiance of emitting region which is accompanied by a narrowing of the spectral width of emission [5] following the relation between optical linewidth $\Delta\nu$ and optical power P:

$$\Delta\nu \propto \frac{1}{P} \tag{2.10}$$

2.2.6 Heterojunction lasers

Use of heterojunction instead of homojunction in the semiconductor laser allows for significant reduction of the threshold current density, and a stable CW operation at room temperature conditions. These are achieved because of better optical and carrier confinements. The origin of these properties in the heterojunction based on a $GaAs$ layer sandwiched between wider band-gap, $Al_xGa_{x-1}As$, is presented in Fig. 2.4.

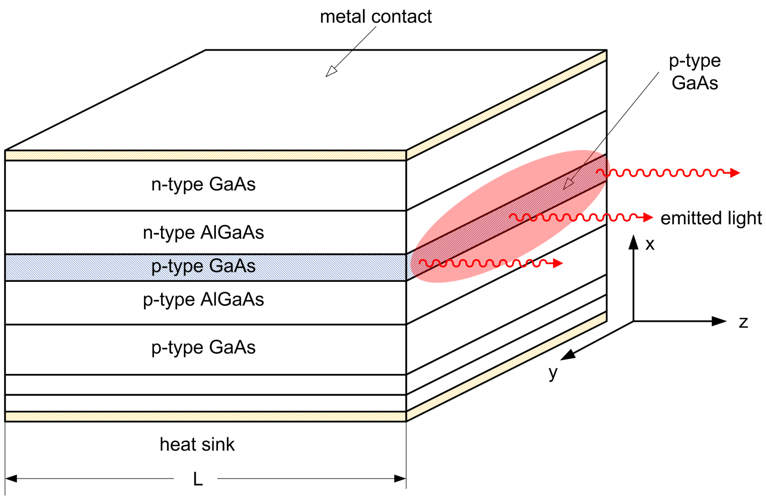

Figure 2.4: Heterostructure based FabryP'erot laser. Scale not maintained.

Both carrier and photon confinements can be achieved simultaneously by use of the double heterojunction, which is shown in Fig. 2.5 and Fig. 2.6. Band-gap energy differences from potential barriers in conduction and valence bands prevent diffusion of the electrons and the holes injected into $GaAs$ layer, which becomes an active region. There is also a step change in the refractive index, which leads to improved wave-guiding compared to the devices based on homojunction.

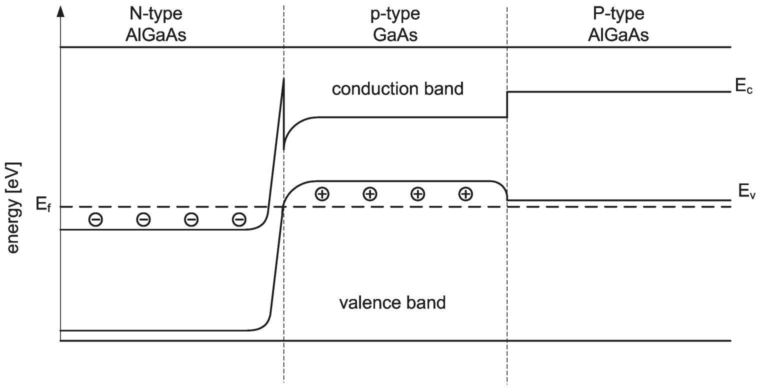

Figure 2.5: Energy bands diagram of a double-heterostructure in equilibrium state.

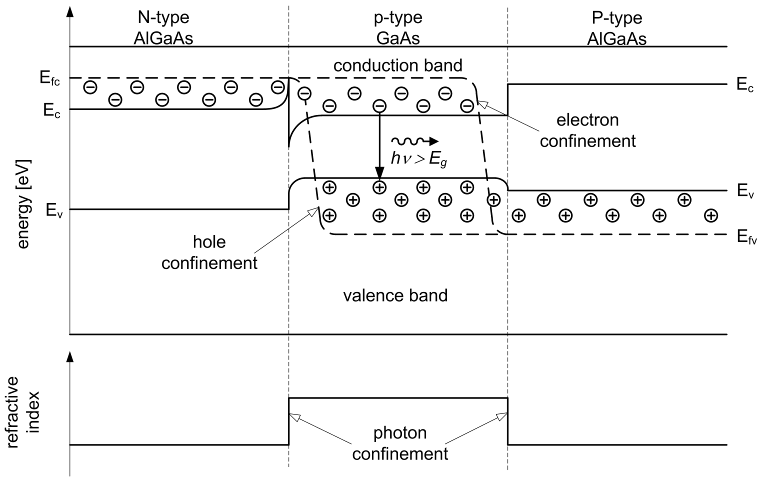

Figure 2.6: Energy bands diagram of a double-heterostructure with forward voltage applied and refractive index variation level across such a structure.

2.2.7 Quantum well lasers

A double heterojunction, that consists of a layer of a semiconductor material, whose thickness is around or less than its de Broglie wavelength (around $50\ nm$ for $GaAs$) [5], and a band-gap smaller than that of the surrounding material, forms a quantum well as depicted in Fig. 2.7.

The increased density of states in the narrow semiconductor layer, at the bottom of the conduction band and at the top of the valence band, makes achievement of population inversion easier, while small volume of active region leads to further reduction of the threshold current in the quantum well lasers. Quantum well lasers are also characterized by a low

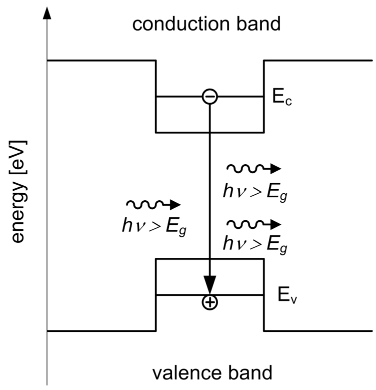

Figure 2.7: Band diagram of stimulated emission from single quantum well, after [5].

temperature sensitivity. In a single quantum well (SQW) structure as depicted in Fig. 2.7 the narrowness of its active region results in poor optical confinement, and results in a lower gain. One approach to minimize the low confinement is to use the multi quantum well (MQW) structure, Fig. 2.8.

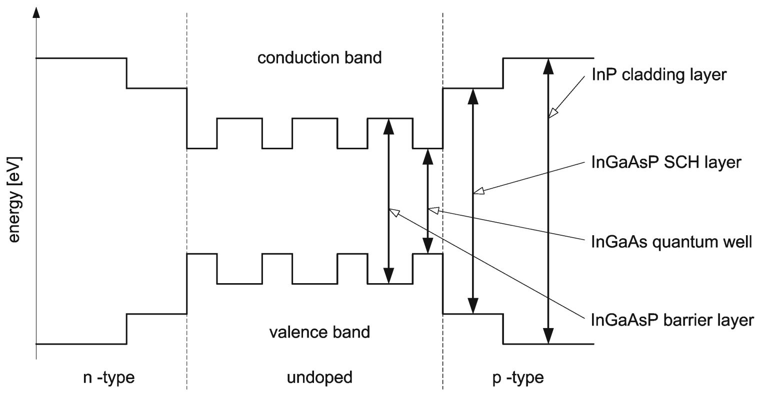

Figure 2.8: The energy band diagram of MQW structure. The light confinement occurs between cladding layers, after [5].

In such a device, several quantum wells of $GaAs$ may be coupled by $AlGaAs$ barrier layers. This is results in the increase of a thickness of the active region, which allows carriers which were not captured and recombined in a first well, to be captured in a subsequent one. MQW based lasers have higher value of threshold current than SQW devices, however they are able to emit more power, and offer better optical confinement.

Both optical and carrier confinements can be further improved by incorporation of cladding layers and separate confinement heterostructure (SCH) layers. The refractive index of the SCH layers is greater than that of cladding layers, assuring total internal reflection at the boundary. The energy gap of SCH and barrier layers is between those of cladding layers and quantum wells to confine the charge carriers between cladding layers. Cladding layers are n- and p-type doped while MQW layers are undoped. Under forward bias condition electrons and holes are injected from cladding layers, diffuse across SCH layers and recombine in MQW structure.

2.3 Spatial distribution

The transverse modes in semiconductor laser can be determined by analysis of the rectangular optical waveguide with dimensions l and w corresponding to the dimensions of the active region. In most cases, semiconductor lasers (usually double-heterostructure), l/λ_0 is small enough to admit only a single mode in the epitaxial growth direction. However the w dimension is usually larger than λ_0, which allows for the waveguide to support several modes in direction parallel to the plane of the junction. Modes that are parallel to the junction plane are called lateral modes. Reduction of the number of lateral modes can be achieved by reduction of the dimension w of the active layer, which also results in reduction of the threshold current.

2.3.1 Stripe geometry semiconductor lasers

Improvement in the meaning of the reduction of the threshold current can be made by the reduction of the junction plane into a narrow stripe [5]. Stripe geometry lasers offer a smaller area that radiation is emitted from, which results in a more stable output when compared to the other types of lasers, and also makes it easier to be coupled to the optical fibres. The emission filament is not uniform along the active region, which results in its lateral displacement. This effect is caused by interactions of the optical and carrier densities and arises from refractive index profile. Wave-guiding can be achieved only by carrier distribution in the active region. Thus the use of the narrow stripe regions reduces possibility of the displacement of the radiation filament, hence improves lateral output stability.

2.3.1.1 Gain guided structures

Structures in which the width of the gain section is determined by the restriction of the extent of the current flow are referred to as gain guided, the example of such a structure is shown in Fig. 2.9.

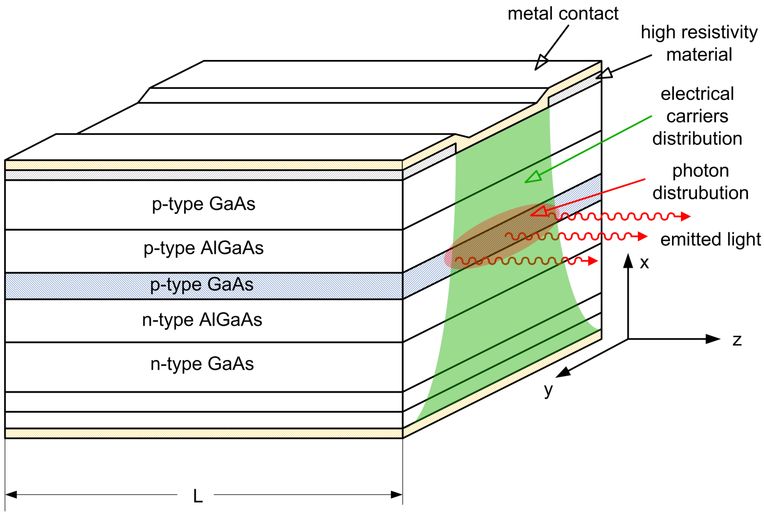

Figure 2.9: Gain guided stripe geometry lase structure. High resistivity layer restricts current injection to narrow extent in lateral (y) direction.

2.3.1.2 Index guided structures

Stripe structure lasers can also be created by formation of the optical waveguide with use of index guided structures. These can be realized as a buried heterostructure, where the active region is surrounded by regions with a lower value of refractive index, Fig. 2.10. An alternative option is to introduce a change in the thickness of the layer next to the waveguide, which results in effective refractive index changes in the active layer, Fig. 2.11. Index guided structures are more difficult to fabricate than gain guided structures, but they offer better optical confinement, which leads to more stable operation.

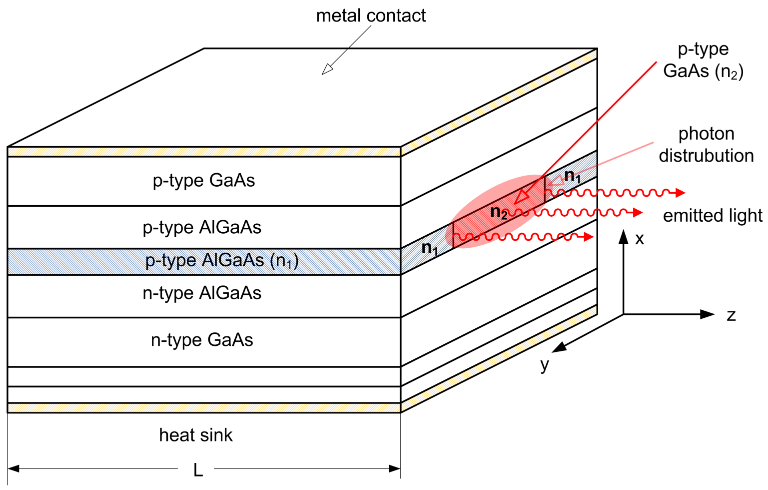

Figure 2.10: Buried heterostructure laser diode. Active layer is surrounded by semiconductor material with lower refractive index, which results in light confinement.

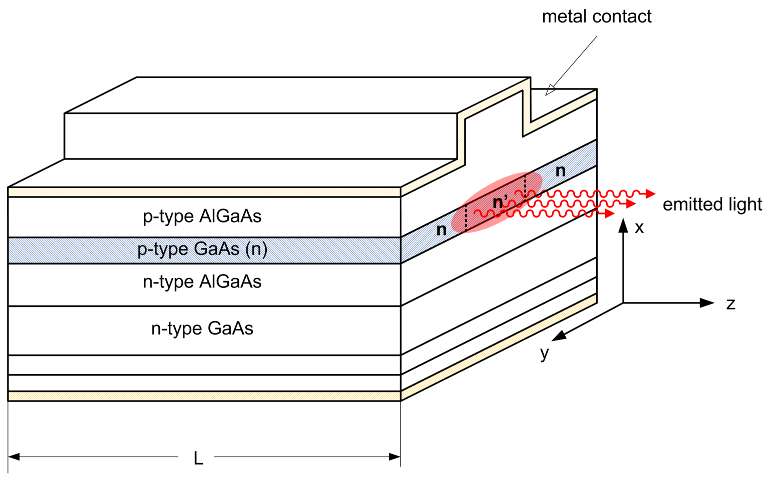

Figure 2.11: Edge emitting laser diode featuring ridge waveguide. Lateral change of thickness in a top layer of semiconductor material results in a step change of the effective refractive index in the active layer underneath such as $n' > n$.

2.4 Spectral distribution

It is desirable from the view of many applications that the laser should operate in a single longitudinal mode regime. The gain curve of the semiconductor structure covers a number of longitudinal modes supported by the laser cavity length, so the output of a simple semiconductor laser based on a Fabry-Pérot resonator, being biased above the threshold, consists of many longitudinal modes separated by free spectral range (FSR), characteristic for a resonator of given length, as schematically depicted in Fig. 2.12. Spectral distribution of the

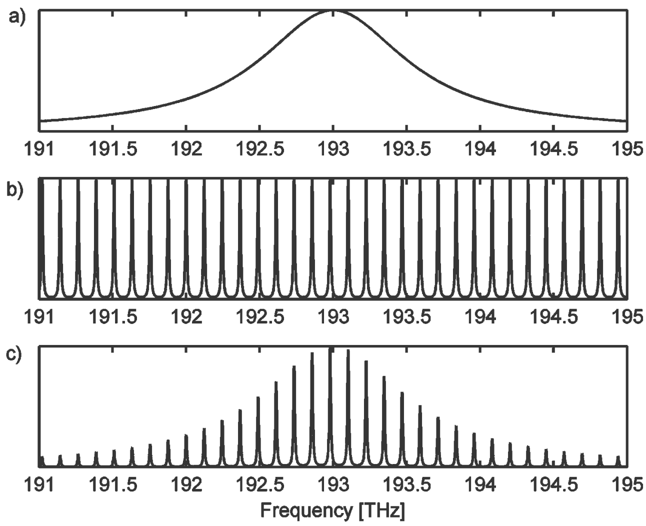

Figure 2.12: a) Lorentzian gain curve with 600 GHz bandwidth, b) Fabry-Pérot modes for 350 μm long resonator; c) Cold cavity modes, FSR at 123 GHz corresponding to given cavity length and 3.5 refractive index.

generated light in semiconductor lasers is determined by both the gain profile of the active medium including its homogeneous or inhomogeneous broadening, and resonator modes. Only a finite number of oscillation frequencies is possible. Cold cavity modes - no chromatic dispersion or mode pulling effects taken into account - are presented, and as a result, only a finite number of discrete frequencies is possible, with a free spectral range (FSR) between them of $\nu_f = c/2L$. However, the power distribution among these possible modes depends on the nature of broadening mechanism [7]. The linewidth of each laser mode is limited by Schawlow-Townes linewidth [1], which decreases inversely with the optical power. Most of the lasers have larger values of the linewidth than the Schawlow-Townes limit, due to extraneous effects such as acoustic and thermal fluctuations of the crystalline structure.

There have been many efforts in order to develop techniques of a spectral tailoring of the output of the semiconductor laser, with the aim of achieving a single mode operation.

Some of those techniques can be also be used, in order to produce a multimode output, with controlled FSR and number of lasing modes. There are potential applications for such a multimode laser diode, such as clock recovery or short pulse generation as it will be proposed in further chapters. Reduction of the length of the laser cavity, in order to increase the FSR to the value at which only one resonant frequency will be in the scope of the gain of used semiconductor material could be a solution, however this also leads to reduction of the power emitted by the device. Therefore a number of techniques based on the coupled cavity or Bragg's effect schemes, have been developed and are in practical use nowadays.

2.4.1 Bragg reflector

A Bragg reflector can be formed by periodical corrugations which form a grating. Such grating results in periodical perturbations of the refractive index in the active region and provides feedback by means of Bragg scattering and leads to coupling between fields propagating in both directions [6] along the laser cavity. Bragg condition expressed by Equation 2.11 governs the mode selection mechanism, coherent coupling between counter-propagating waves occurs for wavelengths λ_m inside the laser, satisfying the Bragg condition:

$$\Lambda = \frac{m\lambda_m}{2} \tag{2.11}$$

where Λ represents the Bragg diffraction length, and m being an order of this diffraction ($m = 1$ for a grating of first order). First lasing device based on structure comprising a Bragg reflector was reported by Kogelnik and Shank [8].

Number of structures have been developed making use of this effect, some of which are described in following sections.

2.4.2 Distributed Bragg reflector laser

A Distributed Bragg reflector (DBR) laser operates on the Bragg's scattering principle, where distributed feedback is placed outside of the active section. The DBR laser employs the grating, which is etched at one or both unpumped cavity ends, which then act as wavelength dependent mirrors.

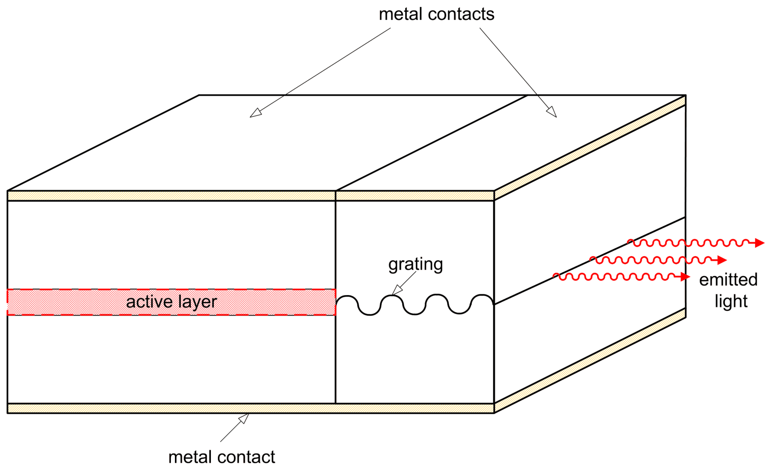

Figure 2.13: Schematic picture of distributed Bragg reflector laser. The grating etched at both ends of the cavity, provides wavelength dependent feedback.

This type of a laser diode can be designed to operate in multi longitudinal mode output, and the example of such a laser will be experimentally investigated in further chapters of this dissertation.

2.4.3 Vertical cavity surface emitting laser

A special kind of DBR laser is a vertical cavity surface emitting laser (VCSEL). In the VCSEL the resonant cavity is perpendicular to the active region plane, as opposed to the previously described edge emitting structures, where the resonant cavity was in plane of the active region. The mirrors in the form of the Bragg reflectors at the top and bottom of the wafer form a resonant cavity Fig. 2.14. Reflectivity of the mirrors is much higher than those in the edge emitting devices in order to compensate for lower gain due to much shorter length of active medium [5].

The active region of the VCSEL device is usually smaller than 1 μm, and comprises SQW or MQW structure. Considerable efforts have been put into research of mode-locked lasers based on VCSEL structure, an example of this type of the mode-locked laser is disclosed in chapter 3.

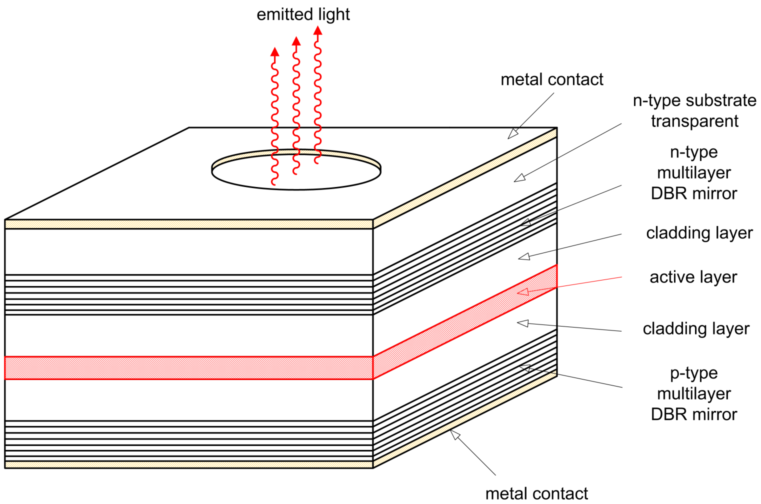

Figure 2.14: Structure of VCSEL laser diode.

2.4.4 Distributed feedback laser

In distributed feedback (DFB) lasers, the feedback necessary for lasing is not localized at the facets of the device but is distributed through the device's cavity [6]. This is achieved by etching periodical perturbations in the thickness of one of the layers composing the heterostructure, as schematically depicted in Fig. 2.15. For a single longitudinal mode operation a $\lambda/4$ step has to be introduced in the middle of the grating.

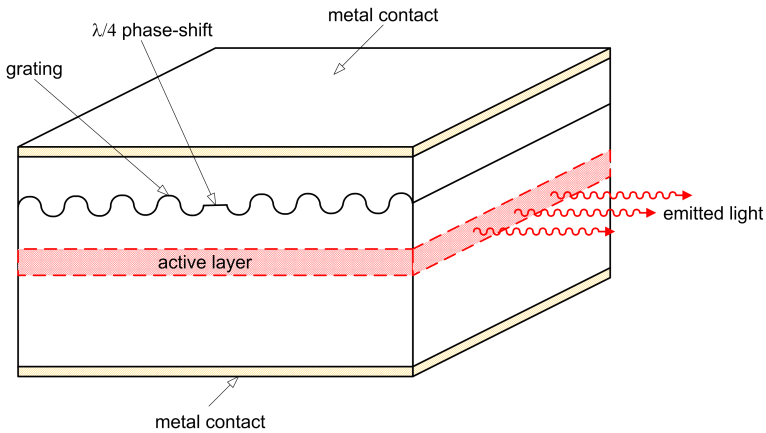

Figure 2.15: Schematic picture of distributed feedback laser. The grating etched in the top cladding layer results in perturbations of the effective refractive index in the active layer.

2.4.5 Slotted Fabry-Pérot

A semiconductor laser based on the ridge waveguide structure which features shallow etched grooves (slots) at the top of the ridge waveguide, forms a so called slotted Fabry-Pérot laser diode. The ridge is 2 μm high and 2.5 μm wide, while the slots are around 1 μm in depth and length and span across the ridge as presented in Fig. 2.16.

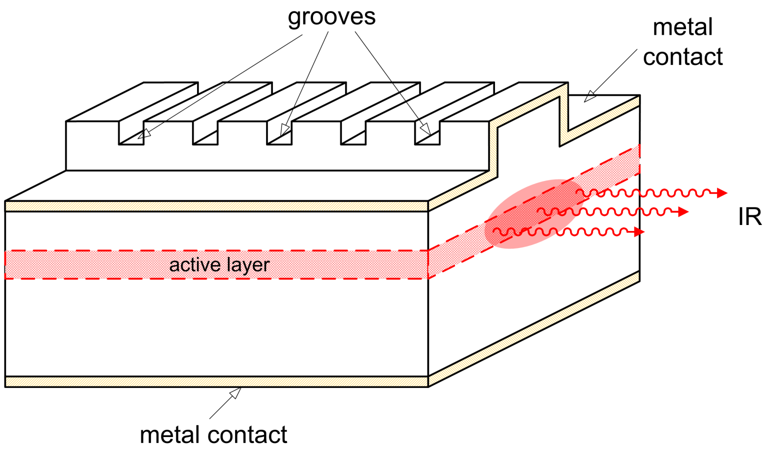

Figure 2.16: Slotted Fabry-Pérot laser schematic structure of the device, scale not maintained.

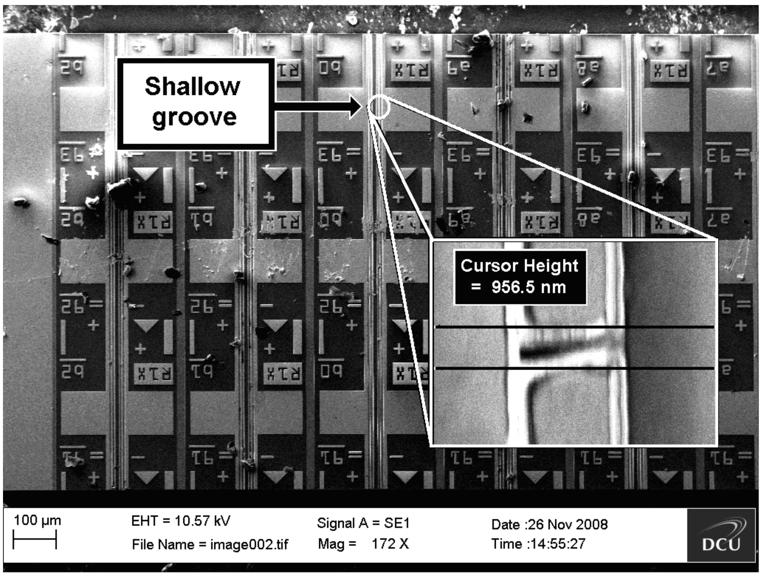

Figure 2.17: Scattering Electron Microscope image of a wafer bar consisting of FP lasers with slots introduced at the top of the ridge waveguide.

These grooves result in perturbations of the effective refractive index in the active region underneath. Top plane of the slot can take different shapes in order to introduce different gradients of the refractive index for example rectangular will result in step, while trapezoidal provide gradual change. An example of 1 mm slotted FP laser is presented in Fig. 2.17, where scattered electron microscope is used to investigate surface of the wafer bar consisting of multiple of slotted FP lasers, magnification of a single slot is also depicted with longitudinal dimension provided. These features on the waveguide, followed by refractive index variations along the laser cavity, act as a one-dimensional photonic band-gap. This effectively allows for optical filtering of the laser output initially predefined by resonator length and the gain profile of used active material [9]. These have a two-fold application: allows for selection of a single longitudinal mode and improve its spectral purity (reduce the linewidth) or select a number of modes allowed by laser cavity and gain profile at given bias and temperature conditions.

2.5 Summary

This chapter provided the basics of the operation of semiconductor lasers. Various active material structures and wavelength selection approaches were presented that are presently being used in many applications or actively investigated in research laboratories.

Three types of multimode lasers based on DBR, FP, and slotted FP approaches with active cores made of bulk, quantum well, and quantum dash semiconductor materials, will be investigated through this dissertation, and potential applications for such laser diodes will be demonstrated.

Bibliography

[1] A. L. Schawlow and C. H. Townes, “Infrared and optical masers,” *Physical Review*, vol. 112, p. 1940, Dec. 1958.

[2] T. H. Maiman, “Stimulated optical radiation in ruby,” *nature*, vol. 187, no. 4736, pp. 493–494, 1960.

[3] A. Einstein, “On the quantum theory of radiation,” *Phys. Z*, vol. 18, p. 121, 1917.

[4] J. Wilson and J. Hawkes, *Lasers: Principles and Applications*. Prentice Hall International Series in Optoelectronics, Prentice Hall, 1987.

[5] J. Wilson and J. F. B. Hawkes, *Optoelectronics (2nd ed.): an introduction*. Prentice-Hall, Inc., 1989.

[6] G. P. Agrawal and N. K. Dutta, *Long wavelength semiconductor lasers*. United States: Van Nostrand Reinhold Co. Inc.,New York, NY, 1986.

[7] S. BE’A and M. C. Teich, *Fundamentals of photonics*. Wiley, New York, 1991.

[8] H. Kogelnik and C. V. Shank, “Stimulated emission in a periodic structure,” *Applied Physics Letters*, vol. 18, pp. 152–154, Feb. 1971.

[9] J. C. O’Gorman, P. McEvoy, D. McDonald, F. P. Logue, and P. M. Landais, “Optical waveguide and a method for providing an optical waveguide,” Patent W 6978057, 12 2005.

Chapter 3

Passively mode-locked semiconductor lasers

3.1 Mode-locking introduction

Mode-locking is a process of generation of inter-modal phase correlations in the laser cavity [1–3]. Thus, the mode-locking is also often referred to as phaselocking. If there are several longitudinal optical modes present in the laser cavity at the same time and a fixed phase relationship between those optical modes exists, short pulse formation occurs. This phase relationship can be introduced by a variety of techniques, which are mainly divided in two groups: active and passive. Pulse repetition rates achieved from such lasers correspond to the round-trip time of the resonator in case of fundamental mode-locking, and its multiples in case of harmonic mode-locking. Repetition rates can be as high as several hundreds of GHz [4], while pulse durations can be a few femtoseconds [5].

Synthesis of a pulse train can be considered as a superposition of electric fields associated with axial modes of a resonant cavity of the mode-locked laser, as shown in Fig. 3.1. The following formula is used to simulate coherent interaction of n electromagnetic fields resulting with total field E_{tot}:

$$\vec{E}_{tot} = \sum_{k=1}^{n} \vec{E}_k \tag{3.1}$$

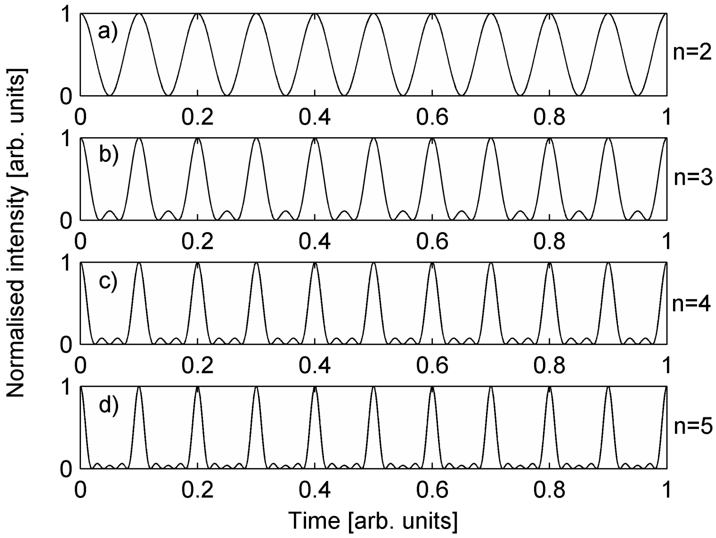

Figure 3.1: Pulse train synthesis from a number of sinusoidal waves. Plots a), b), c) and d) represent the intensities of electromagnetic fields corresponding to superposition of 2, 3, 4 and 5 axial laser modes respectively.

where $\vec{E}_k$ represents the electromagnetic (EM) field associated with each k-th mode as follows:

$$\vec{E}_k(t) = A_k(t)exp(-j(\omega_k t - \phi_k(t))\vec{\mu} \qquad (3.2)$$

with amplitude A_k, angular frequency $\omega_k = 2\pi\nu_k$ with the linear frequency ν_k being an integer multiple of the FSR, ϕ_k its instantaneous phase fluctuations, and $\vec{\mu}$ the polarization vector. Spatial dependence of the electromagnetic field is neglected in Equation 3.2, and further analysis. For the simulation results shown in Fig. 3.1 a fixed phase between contributing optical modes is introduced equal to the free spectral range between them without any random phase fluctuations ($\phi_k(t) = 0$), which resembles the 'perfect' mode-locking condition.The increase of the number of contributing optical modes broadens the spectral content, however this results in shorter pulse duration. Examples of the intensities of the fields resulting from different number of contributing longitudinal modes are shown in parts a, b, c and d of Fig. 3.1.

Fixed phase relationship between frequency components assures a constructive superposition of all electric fields at regular temporal intervals, as depicted in Fig. 3.2 (a). A signal resulting from the same frequency components with the same amplitude but with limited correlation of the phase fluctuations (randomness of the phase in the extent of $\pi/2$ by setting the value of the $\phi_k(t)$ within such limits with a Gaussian distribution) is shown in Fig. 3.2 (b), and scenario with completely uncorrelated phases is presented in Fig. 3.2 (c).

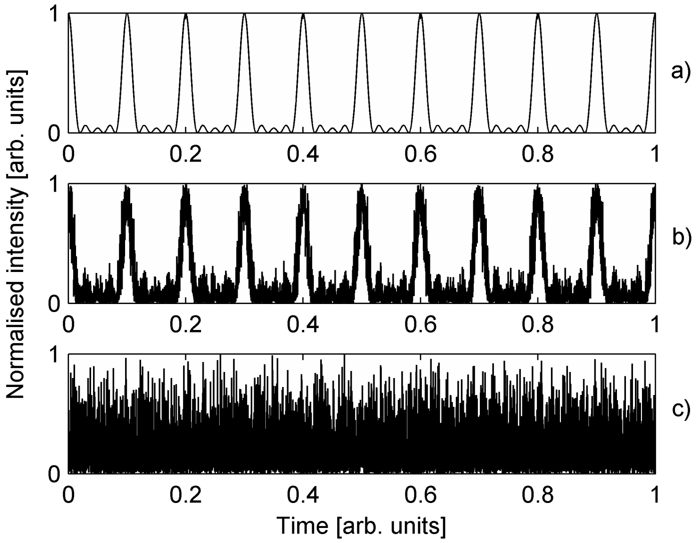

Figure 3.2: Electric field in laser cavity resulting from the same frequency components: for mode-locked case (a) and random phase relations (b, c).

Therefore the phase synchronization between the electromagnetic fields corresponding to the optical longitudinal modes present in the laser cavity is a key factor for a mode-locking process.

3.2 Mode-locking techniques

3.2.1 Active mode-locking

Active mode-locking can be achieved by periodic modulation of cavity losses or of the round-trip phase changes synchronized with resonator round-trips [3, 6, 7]. This can lead to the generation of ultra short pulses usually in the order of picoseconds pulse duration. The modulation can be realized with use of a semiconductor electro-absorption modulator, an acousto-optic or electro-optic modulator or a Mach-Zehnder integrated optic modulator

[8] placed inside the laser cavity. With active mode-locking, it is compulsory to precisely synchronize the modulating signal with the round-trip time of the resonator or a multiple integer of such, in order to achieve stable operation. A modulator must provide minimum losses (be in 'open' state) at the time when pulses are passing through it. Even slight frequency detuning between modulator and pulse train can lead to large jittering or chaotic behavior. Precise tunning can be achieved by acurate and stable laser setup alignment or by a feedback circuit adjusting modulation frequency or cavity length accordingly. Regenerative feedback can be used in means of synchronization that uses detected intensity modulation of the original pulse train, to produce a modulating signal. Harmonic mode-locking can be achieved by setting the modulation frequency at integer multiples of the round-trip cavity time in order to achieve pulse trains with higher frequencies than would be allowed by the cavity length.

3.2.2 Passive mode-locking

Passive mode-locking (PML) techniques, allow for the generation of optical pulses in the order of femtoseconds in solid state lasers, and are based on Kerr lens effect [8–12]. These techniques for semiconductor lasers are based on the nonlinear response of a semiconductor element - typically saturable absorber (SA), which is able to modulate the resonator losses faster than a modulator driven by electronic means: the shorter the pulse becomes, the faster the loss modulation has to be. This is limited by the semiconductor element recovery time. The pulse duration can be well below this recovery time [13]. The most common way to achieve PML is by introduction of a saturable absorber (SA) into the laser cavity. The steady state is considered, when a short pulse is already circulating in the laser resonator. For simplicity, it is assumed that there is a single pulse circulating, and a fast absorber. Each time the pulse hits the saturable absorber, it saturates the absorption, thus temporarily reducing the losses.The absorber can thus suppress any satellite pulses in addition to any continuous background light. Additionally, it constantly attenuates particularly the leading edge of the circulating pulse; the trailing edge may also be suppressed if the absorber can recover sufficiently fast. The absorption element thus results in a decrease of the pulse duration; in the steady state this effect balances other effects (e.g. chromatic dispersion) which tend to lengthen the pulses [13, 14]. In the picoseconds regime of pulse durations, chromatic dispersion usually has only a weak effect. Nonlinearities, in particular the Kerr effect, can be significant, depending on parameters such as the length and material of the laser crystal, the mode area at that place, and the pulse energy and duration.

3.2.3 Hybrid mode-locking

Hybrid mode-locking applies to the laser system which incorporates a combination of active and passive mode-locking techniques simultaneously. This type of mode-locking is common in the applications where the passively mode-locked laser is synchronized with an external periodical signal [15–17].

3.3 Monolithic cavity mode-locked semiconductor lasers

Mode-locked semiconductor laser components can be realized as an integrated monolithic semiconductor chip. Active, passive and hybrid mode-locking mechanisms can be implemented this way. Incorporation of a saturable absorber and the external cavity as a semiconductor waveguide allows to achieve very small devices without any of the drawbacks of the mechanical instabilities produced by optical component in an external cavity. Separated contacts at the top of uniform waveguide along the entire device length provide a variety of electrical bias configurations to different sections of the device underneath. Devices of this type offer repetition rates from few GHz up to $350\ GHz$ [4]. The device based on a multi quantum well (MQW) with hybrid mode-locking mechanisms was able to produce $2.1\ ps$ pulses with repetition rate of $500\ GHz$ and pulse energy of $0.04\ pJ$ [18].

3.4 VECSEL mode-locked laser diodes

Passively mode-locked vertical-external-cavity surface-emitting semiconductor lasers (VECSEL) allow for pico- and femtosecond pulse generation with high power outputs that can compete with conventional solid state lasers [19]. The semiconductor device may contain only a single semiconductor Bragg mirror and the active region with typically several quantum wells (QW). The semiconductor structure typically has a total thickness of only a few micrometers, and is mounted on a heat sink. The laser resonator is completed with an external mirror, typically at a distance of between a few millimeters and some tens of centimeters. The laser mode size in the semiconductor chip is essentially defined by the external resonator setup. The external resonator may be closed with additional flat or curved mirrors and may contain additional optical elements, such as an optical filter for single-frequency operation and/or wavelength tuning, a nonlinear crystal for intra-cavity frequency doubling, or a saturable absorber for passive mode-locking [20]. It is also possible to make a monolithic resonator with a micro-lens, in contact with the gain chip on one side, and having an output coupler mirror coating on the other side [20]. Electrical pumping is the preferred approach in semiconductor lasers, since otherwise an additional pump laser is required. The VECSELs have a gain structure where a ring electrode around the active area injects carriers into that region, therefore it is difficult to pump large areas uniformly in this way, avoiding a weakly pumped region at the centre of the active area. Powers achievable with such devices appear to be limited to the order of $1\ W$ [21]. Optical pumping avoids this limitation; it is easy in this way to pump arbitrarily large active areas uniformly. Furthermore, the design of the gain structure is very much simplified, since doped regions for carrying the current are not required, nor apertures to direct the current flow. The pump light is typically taken from a high-brightness broad-area laser diode or from a diode bar. Due to the very short absorption length of the semiconductor gain structure the beam quality of the pump light is not very important; a poor beam quality only requires working with a strongly converging pump beam, which requires more space and can in some cases make it more difficult to arrange the intra-cavity elements. It is possible, however, to achieve tens of watts of output power, when pumping is realized with a diode bar [22]. The external cavities of VECSELs also allow for mode-locked operation with pulse repetition rates of typically a few gigahertz, but in some cases below $1\ GHz$ or far above $10\ GHz$. Particularly with passive mode-locking of optically pumped VECSELs, utilizing a laser diode as pump source and a semiconductor saturable absorber mirror (SESAM) in the external resonator for mode-locking, tremendous progress has been achieved since the year 2000. This lead to average output powers well exceeding 1 W, i.e., being orders of magnitude higher than achievable with any other mode-locked semiconductor laser. Typical pulse durations are in the lower picoseconds range, although durations below 1 ps have also been demonstrated [23, 24]. The pulses are sometimes close to transform limited, but strongly chirped in other cases, depending on details of chromatic dispersion and other issues. It has been demonstrated that passive mode-locking is possible with a saturable absorber integrated into the gain structure [19]. Such integrated structures are difficult to grow and are so far subject to serious performance limitations. However, in the future they may allow the construction of very compact and potentially cost efficient mode-locked lasers.

3.5 Passive mode-locking mechanisms in a Fabry-Pérot semiconductor laser

Although a saturable absorber is the most common element associated with passively mode-locked lasers, the nonlinear response of an optically active semiconductor material (active region of a laser diode) can be sufficient to provide mechanisms for mode-locking [25]. Such behavior is strongly improved when the active region in a laser diode consists of quantum structures, where optical fields intensities inside such region and mutual coupling between them are increased due to better optical confinement and smaller active cross section dimensions. An optical field generated in a laser cavity can be expressed as a monochromatic wave with slowly varying amplitude as previously defined by Equation 3.2. In the case of a laser with M longitudinal modes, a mode beating occurs leading to a quadratic temporal average of a total electric field with the following expression [26]:

$$\langle |E_T|^2 \rangle = \sum_{k=1}^{M} \langle |E_k|^2 \rangle + \sum_{k=1}^{M} \sum_{j \neq k} 2 \langle E_k E_j cos(\Omega_{kj} t + (\phi_j(t) - \phi_k(t))) \rangle \qquad (3.3)$$

where Ω_{kj} is defined as $(\omega_j - \omega_k)$ beating between any two modes. Consequently in Equation 3.3 after Equation 3.2 spatial dependency of the electromagnetic fields is ignored, so it is in the following analysis. The consequence of this beating is a signal generated at the frequency $\Omega_{jk}/2\pi$ inducing a modulation of the active medium through third order nonlinear effects. This results in modulation sidebands generated around the optical modes and a process called four wave mixing (FWM) [27]. Interactions between the optical modes inside a semiconductor laser cavity through the FWM are schematically expressed in Fig. 3.3. For

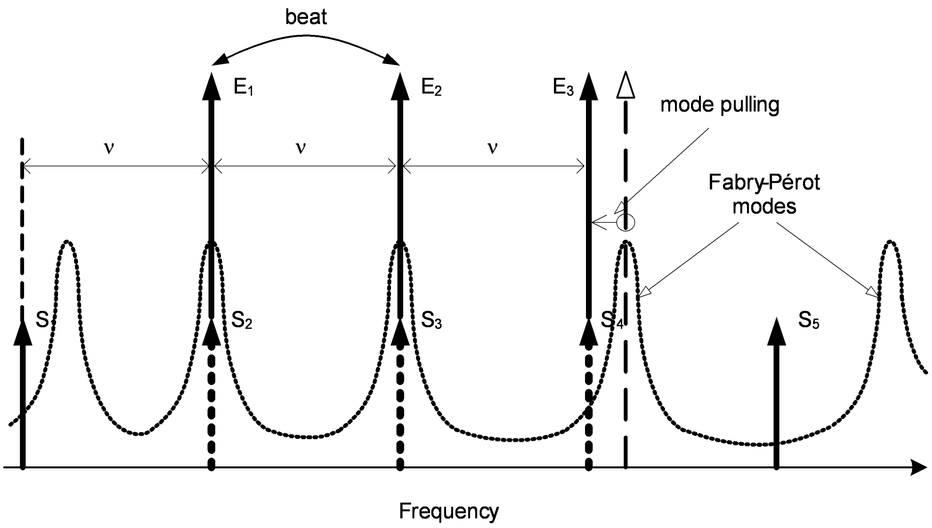

Figure 3.3: Schematic representation of the optical modes interactions inside semiconductor laser via their order nonlinear effects. E_1, E_2, E_3 represent lasing modes and S_1 to S_5 sidebands resulting from FWM effect.

the sake of simplicity the beating between modes E_1 and E_2 is considered and in this example can be considered as an origin of mode-locking. This beating results in a modulation of the gain with the frequency corresponding to the difference frequency between contributing optical modes $\nu = (\omega_2 - \omega_1)/2\pi$. Such modulation generates equidistant (in the frequency domain) side-bands S_1, S_3 and S_2, S_4 around the modes E_1 and E_2 respectively, which can be expressed by following equations:

$$S_1 = \alpha_1 \cdot E_1 \cdot E_1 \cdot \bar{E}_2 = \alpha_1 \cdot E_1^2 \cdot \bar{E}_2 \tag{3.4}$$

$$S_2 = \alpha_2 \cdot E_1 \cdot \bar{E}_1 \cdot \bar{E}_2 \tag{3.5}$$

$$S_3 = \alpha_3 \cdot E_2 \cdot \bar{E}_1 \cdot \bar{E}_2 \tag{3.6}$$

$$S_4 = \alpha_4 \cdot \bar{E}_1 \cdot E_2 \cdot E_2 = \alpha_4 \cdot \bar{E}_1 \cdot E_2^2 \tag{3.7}$$

where the α_k are coupling efficiency factors, and $\bar{E}_k$ are complex conjugates of respective fields E_k. Sideband S_4 whose amplitude and phase are related to both modes E_1 and E_2, result in pulling the mode E_3 from the Fabry-Pérot resonant position (FP resonant ripples are represented with dotted line, taking in account dispersive nature of the semiconductor) and correlate the phase of the mode E_3 with two other modes. Similar processes result from beating between modes E_2 and E_3 and transfer the phase information to the mode E_1, and this could be further extended to larger number of optical modes.

Some of these sidebands can potentially lead to mutual injection among the axial laser modes supported by the material gain, which in advance provide a mechanism for a phase information exchange between optical fields, and allow for their phase fluctuations (phase noise) synchronization. The beat signal at the frequency ν can be observed using a photo-mixing element. The assumption that the phase of each mode is uncorrelated with contributing modes implies that the second term in the right hand side of Equation 3.3 is equal to zero and so the linewidth of the generated beat signal is equal to the sum of the linewidths of the optical modes. However, if the modes are phase correlated, this term is non-zero and the resulting linewidth of the beat signal should be smaller than the summary linewidth of the optical modes [28], and as a result a hypothesis can be formulated: The beat tone generated by a multimode laser output experiences a reduction of the spectral width when compared to the summary linewidth of the optical modes contributing to that beat, when their phases are interacting in correlated manner or in other words their phase noise is reduced and therefore the laser is mode-locked. These can be expressed with the following criterion:

$$\Delta\nu_{beat} << \Delta\nu_{opt} \tag{3.8}$$

where $\Delta\nu_{beat}$ and $\Delta\nu_{opt}$ are the beat tone linewidth and the summary optical linewidth respectively. In the case of a semiconductor laser the correlation of the phases of the optical modes can occur through the four wave mixing process resulting from material nonlinearities [26, 29, 30] and result in passive mode-locking. This phase correlation of the longitudinal modes occurs through FWM process resulting from the third order nonlinear effects present in semiconductor lasers. There are five effects that can result with four wave mixing in semiconductor devices: carrier density modulation (CDM), carrier heating (CH), spectral hole burning (SHB), two-photon absorption (TPA) and the Kerr effect [26]. Dominance of some of these effects among the others is related to the separation frequency between optical modes. With the free spectral range between the modes involved on the order of below $100\ GHz$, the CDM effect is dominant and so the others maybe neglected. For frequencies beyond $100\ GHz$ up to $2.5\ THz$, CH plays the main role, and above $2.5\ THz$ it is SHB.

3.6 Summary

The mode-locking results in correlation between optical modes present in the laser cavity. Such correlation leads to high coherency between the phases of these optical modes. Superposition of the electrical fields associated with the modes generates an optical pulse stream, characterized with high repetition rate, low pulse durations and low timing jitter. There are several techniques used in order to achieve the mode-locking in different types of semiconductor laser structures. Most of these methods require a number of advanced optoelectronic devices to be integrated in order to achieve active mode-locking, or in the passive case a device comprising at least an active and a saturable absorption sections has to be used. All of those require significant efforts to be put in order to maintain stable operation. However the edge emitting devices, where the passive mode-locking can be achieved by means of mutual injection of optical modes via nonlinearities provided by gain section of the laser, can be successful counterparts in some applications, as for a stable operation they only require DC bias and temperature stabilization.

Modern semiconductor devices based on quantum structures allow producing broad spectral output and providing nonlinearities sufficient to support strong mode-locking in passive means, so it is possible to achieve the passive mode-locking within a simple single section structures as Fabry-Pérot laser diodes.Additionally they can be supported by some longitudinal mode discrimination scheme (DFB, DBR or slotted FP) in order to achieve desired spectral output in terms of number of modes and free spectral range between them.

It has been proposed that passive mode-locking can be achieved in multimode laser via four wave mixing effect. In the following chapter, some experimental evidences of passive mode-locking in various multimode lasers will be presented.

Bibliography

[1] W. E. Lamb, "Theory of an optical maser," *Physical Review*, vol. 134, p. A1429, June 1964. Copyright (C) 2009 The American Physical Society.

[2] K. Sato, "100 GHz optical pulse generation using Fabry-Perot laser under continuous wave operation," *Electronics Letters*, vol. 37, no. 12, pp. 763–764, 2001.

[3] L. E. Hargrove, R. L. Fork, and M. A. Pollack, "Locking of he-ne laser modes induced by synchronous intracavity modulation," *Applied Physics Letters*, vol. 5, pp. 4–5, July 1964.

[4] K. Merghem, A. Akrout, A. Martinez, G. Aubin, A. Ramdane, F. Lelarge, and G. Duan, "Pulse generation at 346 GHz using a passively mode locked quantum-dash-based laser at 1.55 μm," *Applied Physics Letters*, vol. 94, pp. 021107–3, Jan. 2009.

[5] K. Wilcox, A. Quarterman, H. Beere, D. Ritchie, and A. Tropper, "High peak power femtosecond pulse passively mode-locked vertical-external-cavity surface-emitting laser," *Photonics Technology Letters, IEEE*, vol. 22, pp. 1021 –1023, jul. 2010.

[6] J. DiDomenico, "Small-Signal analysis of internal (Coupling-Type) modulation of lasers," *Journal of Applied Physics*, vol. 35, pp. 2870–2876, Oct. 1964.

[7] D. Kuizenga and A. Siegman, "FM and AM mode locking of the homogeneous laser– Part i: Theory," *Quantum Electronics, IEEE Journal of*, vol. 6, no. 11, pp. 694–708, 1970.

[8] L. Schares, R. Paschotta, L. Occhi, and G. Guekos, “40-GHz Mode-Locked Fiber-Ring laser using a Mach-Zehnder interferometer with integrated SOAs,” *Journal of Lightwave Technology*, vol. 22, p. 859, Mar. 2004.

[9] C. Shank, E. Ippen, and A. Dienes, “Passive mode locking of the CW dye laser,” *Quantum Electronics, IEEE Journal of*, vol. 8, no. 6, p. 525, 1972.

[10] B. K. Garside and T. K. Lim, “Laser mode locking using saturable absorbers,” *Journal of Applied Physics*, vol. 44, pp. 2335–2342, May 1973.

[11] H. Haus, “Mode-locking of lasers,” *Selected Topics in Quantum Electronics, IEEE Journal of*, vol. 6, no. 6, pp. 1173–1185, 2000.

[12] Y. Barbarin, E. Bente, M. Heck, Y. Oei, R. Notzel, and M. Smit, “Passively mode-locked 20 and 40 GHz bulk InGaAsP lasers,” vol. 3, pp. 673 – 674 vol.3, sep. 2005.

[13] J. A. Valdmanis, R. L. Fork, and J. P. Gordon, “Generation of optical pulses as short as 27 femtoseconds directly from a laser balancing self-phase modulation, group-velocity dispersion, saturable absorption, and saturable gain,” *Optics Letters*, vol. 10, pp. 131–133, Mar. 1985.

[14] R. Paschotta and U. Keller, “Passive mode locking with slow saturable absorbers,” *Applied Physics B: Lasers and Optics*, vol. 73, pp. 653–662, Nov. 2001.

[15] G. Duan, “Optical signal processing using InP-based quantum-dot semiconductor mode-locked lasers,” in *Lasers and Electro-Optics, 2008 and 2008 Conference on Quantum Electronics and Laser Science. CLEO/QELS 2008. Conference on*, pp. 1–2, 2008.

[16] S. Latkowski, F. Surre, P. Landais, and G. Duan, “All-optical synchronization of a 40 GHz self-pulsating distributed Bragg reflector laser to return-to-zero 10, 20 and 40 gbit/s data streams,” *Optics Communications*, vol. 282, pp. 2053–2058, May 2009.

[17] S. Latkowski, F. Surre, and P. Landais, "Passively phase-locked semiconductor lasers for clock recovery and terahertz generation," *IET Conference Publications*, vol. 2008, pp. 661–664, Jan. 2008.

[18] D. Derickson, R. Helkey, A. Mar, J. Karin, J. Wasserbauer, and J. Bowers, "Short pulse generation using multisegment mode-locked semiconductor lasers," *Quantum Electronics, IEEE Journal of*, vol. 28, no. 10, pp. 2186–2202, 1992.

[19] U. Keller and A. C. Tropper, "Passively modelocked surface-emitting semiconductor lasers," *Physics Reports*, vol. 429, pp. 67–120, June 2006.

[20] N. Laurand, C. L. Lee, E. Gu, J. E. Hastie, S. Calvez, and M. D. Dawson, "Microlensed microchip VECSEL," *Optics Express*, vol. 15, pp. 9341–9346, July 2007.

[21] J. G. McInerney, A. Mooradian, A. Lewis, A. V. Shchegrov, E. M. Strzelecka, D. Lee, J. P. Watson, M. K. Liebman, G. P. Carey, A. Umbrasas, C. A. Amsden, B. D. Cantos, W. R. Hitchens, D. L. Heald, V. Doan, C. Lei, and S. P. Kilcoyne, "Novel 980-nm and 490-nm light sources using vertical-cavity lasers with extended coupled cavities," in *Vertical-Cavity Surface-Emitting Lasers VII*, vol. 4994, (San Jose, CA, USA), pp. 21–31, SPIE, June 2003.

[22] J. L. A. Chilla, S. D. Butterworth, A. Zeitschel, J. P. Charles, A. L. Caprara, M. K. Reed, L. Spinelli, R. Scheps, and H. J. Hoffman, "High-power optically pumped semiconductor lasers," in *Solid State Lasers XIII: Technology and Devices*, vol. 5332, (San Jose, Ca, USA), pp. 143–150, SPIE, July 2004.

[23] A. Garnache, S. Hoogland, A. Tropper, I. Sagnes, G. Saint-Girons, and J. Roberts, "Sub-500-fs soliton-like pulse in a passively mode-locked broadband surface-emitting laser with 100-mW average power," in *Indium Phosphide and Related Materials Conference, 2002. IPRM. 14th*, pp. 689–692, 2002.

[24] P. Klopp, F. Saas, M. Zorn, M. Weyers, and U. Griebner, "290-fs pulses from a semiconductor disk laser," *Optics Express*, vol. 16, pp. 5770–5775, Apr. 2008.

[25] J. Renaudier, G. Duan, P. Landais, and P. Gallion, “Phase correlation and linewidth reduction of 40 GHz self-pulsation in distributed Bragg reflector semiconductor lasers,” *Quantum Electronics, IEEE Journal of*, vol. 43, no. 2, pp. 147–156, 2007.

[26] G. P. Agrawal and N. K. Dutta, *Long wavelength semiconductor lasers*. United States: Van Nostrand Reinhold Co. Inc.,New York, NY, 1986.

[27] S. Latkowski, F. Surre, R. Maldonado-Basilio, and P. Landais, “Investigation on the origin of terahertz waves generated by dc-biased multimode semiconductor lasers at room temperature,” *Applied Physics Letters*, vol. 93, pp. 241110–3, Dec. 2008.

[28] S. Latkowski, F. Surre, E. Degirmenci, and P. Landais, “Passively phase-locked multimode semiconductor laser: From millimetre to terahertz wave generation,” in *Lasers and Electro-Optics, 2008 and 2008 Conference on Quantum Electronics and Laser Science. CLEO/QELS 2008. Conference on*, pp. 1–2, 2008.

[29] N. Usechak and G. Agrawal, “Semi-analytic technique for analyzing mode-locked lasers,” *Optics Express*, vol. 13, pp. 2075–2081, Mar. 2005.

[30] J. Renaudier, G. H. Duan, P. Landais, and P. Gallion, “Semiconductor Lasers-Phase correlation and linewidth reduction of 40 GHz Self-Pulsation in distributed bragg reflector semiconductor lasers,” *IEEE Journal of Quantum Electronics*, vol. 43, no. 1-2, pp. 147–156, 2007.

Chapter 4

RF signal generation by passively mode-locked laser diodes

4.1 Introduction

Generation of radio frequency (RF) and microwave signals by photonic means have many potential applications, not only in telecommunications where stable multi-gigahertz signal sources are crucial, but also in future electronic integrated circuits where signals distribution with frequencies above 3 GHz becomes an issue due to thermal limits imposed by copper based interconnects [1]. In this chapter three kinds of laser diode structures are introduced and their static optical and electrical characterizations are performed. Optical spectra and spectral width of their longitudinal components are investigated. The RF beat tones are generated by directing the infrared (IR) optical output of the lasers onto fast photodiodes and the produced electrical signals are analyzed. The collected experimental results allow for evaluation of the quality of the generated RF signals. Furthermore, an identification of passive mode-locking mechanisms for each of the examined laser structures is performed and the hypothesis claimed in Chapter 3 supported by Equation 3.8 is experimentally verified.

4.2 Distributed Bragg reflector laser diode

4.2.1 Laser under test - structure description

The investigated distributed Bragg reflector (DBR) laser diode consists of three sections. A 200 μm Bragg section is used to select the emission spectrum, at such length for the Bragg mirror multi longitudinal mode output can be provided. The 790 μm long active section consists of bulk quaternary material ($InGaAsP$). Its quasi-rectangular transverse dimensions (0.4 $\mu m \times 0.6$ μm) ensure a low polarization-sensitivity of modal gain and a single transverse mode of the electric field. The 130 μm long phase section is designed to adapt the optical modes between the active and the passive optical waveguides. Its waveguide width is expanding linearly up to the 1.8 μm at the Bragg section [2, 3]. Structure of the device is schematically shown in Fig. 4.1. The different sections are electrically isolated (~ 3.7 $k\Omega$) by ion implantation. The device was designed and fabricated by III-V Labs Alcatel-Lucent, France.

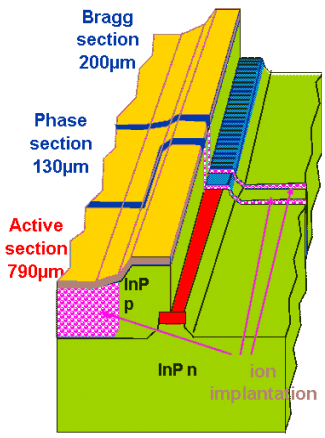

Figure 4.1: Distributed Bragg Reflector laser structure [4].

4.2.2 Steady state characterizations

Behavior of tested device under DC bias conditions was investigated by measuring its optical and electrical parameters as a function of injected current. In order to improve accuracy (in terms of precise temperature and current control) and efficiency of that process is supported by a number of programs created in the LabView© environment. In this section only steady state under DC bias conditions is investigated. The lasers operate at 25 $°C$ unless stated otherwise.

4.2.2.1 Voltage vs bias current and optical power vs bias current characterizations

Voltage versus bias current (VI) and optical power versus bias current (LI) characteristics depicted in Fig. 4.2 laser are measured for a bias current applied to the active section I_g ranging from 0 mA to 300 mA and from 300 mA to 0 mA with step of 1 mA. Both Bragg and phase sections are kept unbiased (not connected). The LI characteristic shows clear

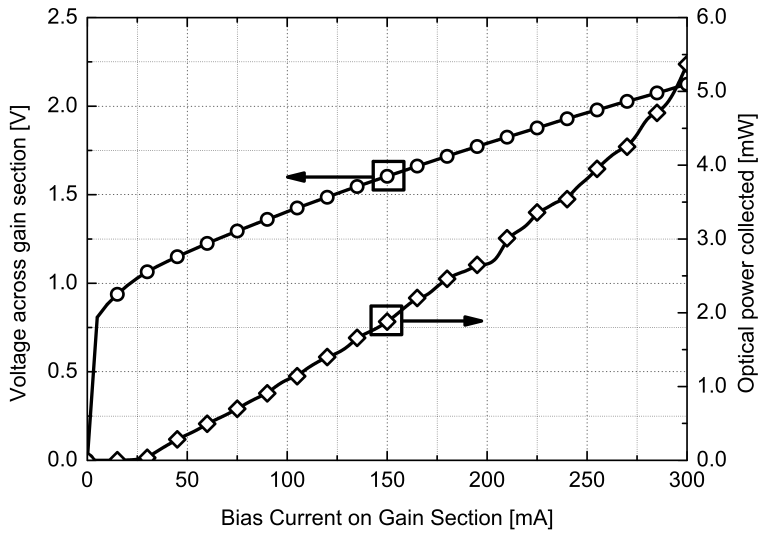

Figure 4.2: The VI and LI curves are marked with circles (○) and diamonds (◇) respectively - number of data points presented is reduced. Bragg and phase sections are unbiased and the laser diode is temperature stabilized at 25 $°C$.

threshold point at $I_{th} = 40$ mA. It was recorded two ways: by increasing and decreasing the bias current. Both curves are overlapping each other; this demonstrates that there is no unbiased part of the laser acting as a saturable absorber. The VI curve corresponds to the electrical characteristic of the used semiconductor components, dynamic impedance across the active section is between 26 Ω and 7 Ω for provided bias currents between 50 mA and 300 mA [4].

4.2.2.2 Optical spectrum - multimode output

With the adjustment of the Bragg section current I_B in range between 0 and 50 mA, it was possible to achieve single mode and multimode operation of the laser. An example of an optical spectrum collected with optical spectrum analyzer with resolution of 0.05 nm is shown in Fig. 4.3. Emission peaks are centered at 1.583 μm with side mode suppression ratio (SMSR) between three dominant modes lower than 20 dB. The free spectral range between the optical modes at 39.7 GHz corresponds to the total length of the laser at 1120 μm as detailed previously [3, 4].

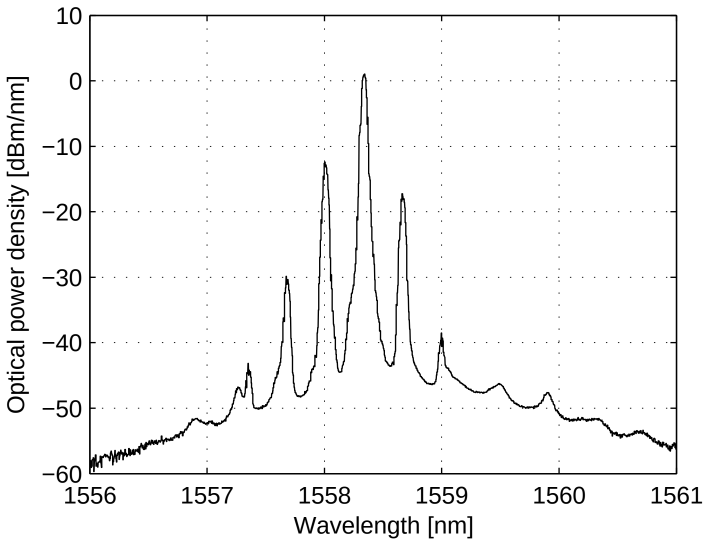

Figure 4.3: Multimode output from DBR laser diode: optical spectrum recorded for bias levels: $I_g = 88.87$ mA, $I_B = 15.4$ mA, and phase section unconnected, at room temperature conditions.

4.2.2.3 Optical linewidth - high resolution optical spectrum analysis

With use of a 'BOSA' high resolution optical spectrum analyzer provided by Aragon Photonics© it is possible to collect optical spectra with resolution of 0.025 pm (10 MHz), as shown in Fig. 4.4.

Data recorded with such level of precision allows the estimation of the linewidth of each optical mode present in the spectrum. For bias conditions of the active section set as

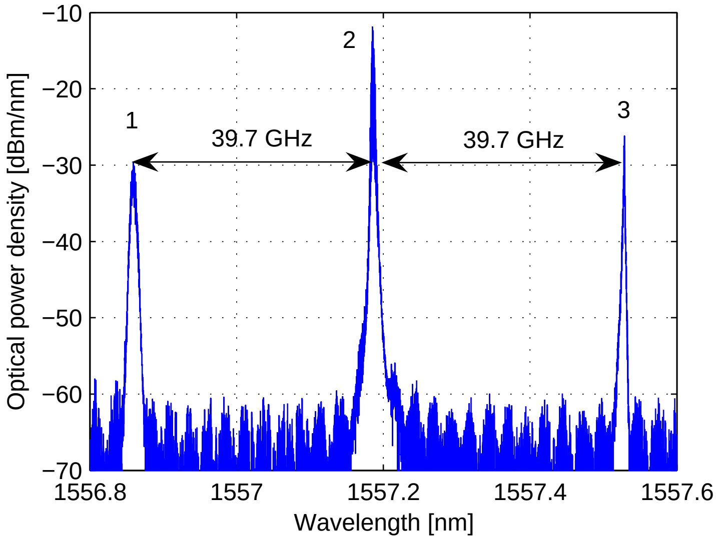

Figure 4.4: High resolution optical spectrum recorded for bias currents: $I_g = 88.87\ mA$ and $I_B = 1.75\ mA$, phase section unconnected, at room temperature conditions.

$I_g = 88.87\ mA$ and Bragg section $I_B = 1.75\ mA$ the spectrum presented in Fig. 4.4 is recorded. Linewidth measured for each mode at 3 dB drop from its peak was at 224 MHz, 74 MHz and 81 MHz for modes 1, 2 and 3 respectively, resulting with the sum of the optical linewidths at 380 MHz. Linewidth of optical modes measured with use of high resolution optical spectrum analyzer can be compared with RF beat signal produced on photodetector and recorded with electrical spectrum analyzer.

4.2.3 The RF domain investigation - experimental setup and results

It was demonstrated in an earlier paragraph that DBR laser under certain bias conditions is able to emit a multimode optical signal with free spectral range around 0.3 nm which corresponds to the frequency of 39.7 GHz. Experimental setup presented in Fig. 4.5 is used to observe if there is any output at this frequency range.

Laser is biased with I_g and I_B set at 88.87 mA and 1.75 mA respectively. An optical isolator (ISO) is used to avoid any reflections which may disturb the laser behavior. Electrical spectrum produced on a 50 GHz photodiode (PD) is collected by 40 GHz electrical spectrum analyzer (ESA) operating at 3 MHz of resolution and video bandwidths, and is

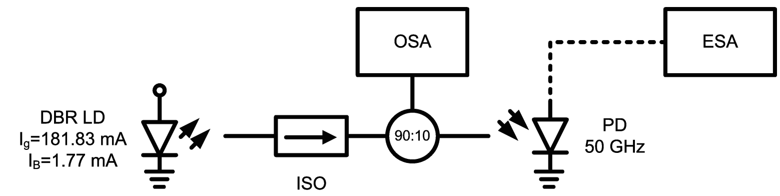

Figure 4.5: Experimental setup for optical and RF beat spectra investigation, laser is temperature controlled at $25\ ^{\circ}C$.

depicted in Fig.4.6. At the bias conditions given above a peak at 39.7 GHz is recorded, with the linewidth of 30 MHz measured at full width at half maximum (FWHM). These parameters result in Q-factor of 1333, which is calculated with following formula:

$$Q = \frac{\Delta f_{FWHM}}{f} \tag{4.1}$$

where Δf is a FWHM linewidth of the RF signal at central frequency f of the oscillator. The optical oscillator with such Q factor has a potential application in clock recovery.

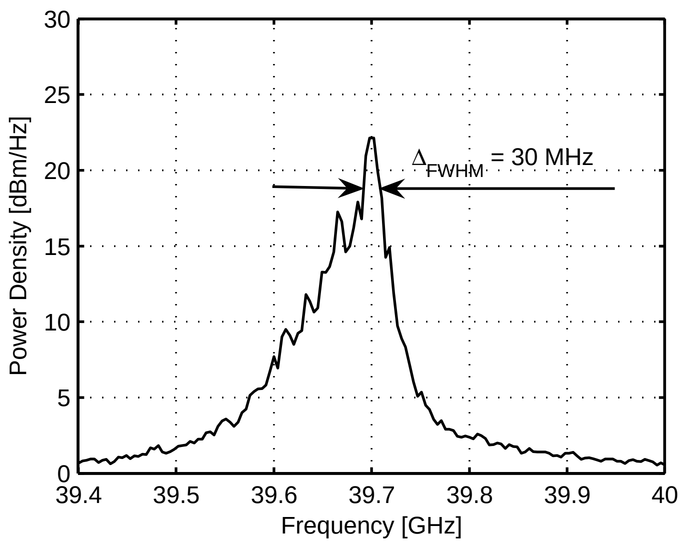

Figure 4.6: RF signal recorded at 39.7 GHz with bias conditions being $I_g = 88.87\ mA$ and $I_B = 1.75\ mA$.

The linewidth of the recorded RF beat tone at 30 MHz is smaller than summary linewidth of the contributing optical modes which implies that the modes inside the laser are passively mode-locked. Mechanism of the mode-locking originates from FWM nonlinearities provided by semiconductor material in the gain section, through which all optical modes are linked (inside the laser cavity). Separation between longitudinal optical modes is around $40\ GHz$, and for frequencies below $100\ GHz$ FWM benefits mostly from carrier density modulation (CDM) [5]. Generation of an RF signal by optical means, with DC biased DBR laser, where no direct or external modulation is applied to the laser has been demonstrated. In the following section, a simpler single section laser structure, with only one DC bias current required will be investigated.

4.3 Slotted Fabry-Pérot laser diode

The laser presented in this section is a standard Fabry-Pérot (FP) laser diode (LD) with a grating introduced at the top of the waveguide acting as an optical filter. This results in a spectrum that can be engineered according to the pattern of the grating.

4.3.1 Device structure

A single cavity semiconductor device based on multi quantum well (MQW) structure formed of five quantum wells is shown in Fig.4.7. The wells are $6\ nm$ thick and based on $AlGaAsIn$ compound and interleaved with the barriers which are $10\ nm$ thick. The device is $1050\ \mu m$ long, with $2.5\ \mu m$ wide slotted ridge waveguide. Slots are implemented as shallow etched grooves at the top of the ridge. They do not reach active region, however they are able to cause a change in the value of the refractive index underneath. Each slot is approximately $1\ \mu m$ deep (to reach a half of the ridge's heigth) and $1\ \mu m$ long while it spans across the ridge, an example of such slotted laser diode is presented in Fig. 2.17 in Chapter 2. The device was manufactured by Eblana Photonics, Ireland. Active core was designed by the manufacturer while the slots pattern follows custom design.

The profile of the slots from the top plane can be rectangular, however different shapes can be used (i.e trapezoidal) in order to graduate (smoothen) the step of the refractive index introduced by such slot. This allows to reduce the impact of inaccurate positioning during manufacturing process in particular etching of the slots [6]. Positioning of the slots allows

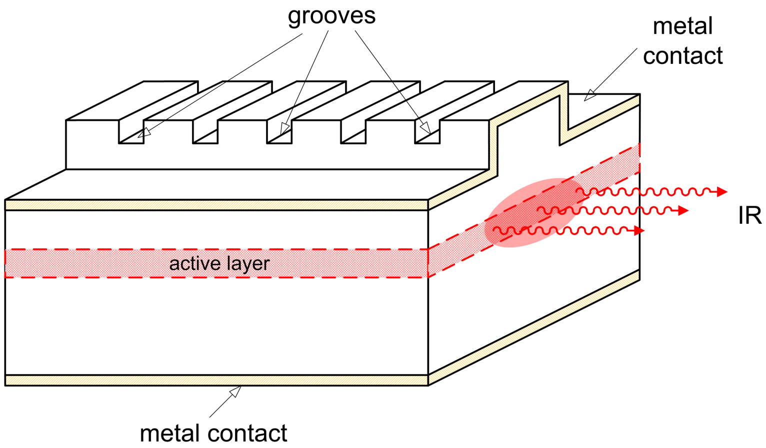

Figure 4.7: Schematic picture of a Slotted Fabry-Pérot laser diode. The laser's cavity is $1050\ \mu m$ long. Scale of th edrawing is not maintained.

the laser to operate in a stable multimode regime when operating under DC bias conditions with the longitudinal mode separation in the order of $41\ GHz$ [7].

4.3.2 Steady state characterizations

It this paragraph static characterizations of the slotted FP laser diode are performed. The semiconductor wafer containing a number of the lasers in parallel is placed on the probe station and temperature stabilized at $25\ °C$. Bias current is provided to selected laser by single DC probe and optical output is coupled to a lensed fibre mounted in micro-positioner.

4.3.2.1 Voltage vs bias current and optical power vs bias current characterizations

The voltage versus bias current and optical power versus bias current characteristics depicted in Fig.4.8 of the slotted FP device were collected for bias current applied to the active section ranging from $0\ mA$ to $100\ mA$ and from $100\ mA$ to $0\ mA$ with step of $1\ mA$.

The threshold point at bias level $I_{th} = 24\ mA$ is read clearly from LI characteristic. No hysteresis exist between LI curves collected with increase and decrease of the bias current, both curves are overlapping each other what proves that no absorber region exists in the device. The VI characteristic allows to find the impedance of the junction from $36.7\ \Omega$ at

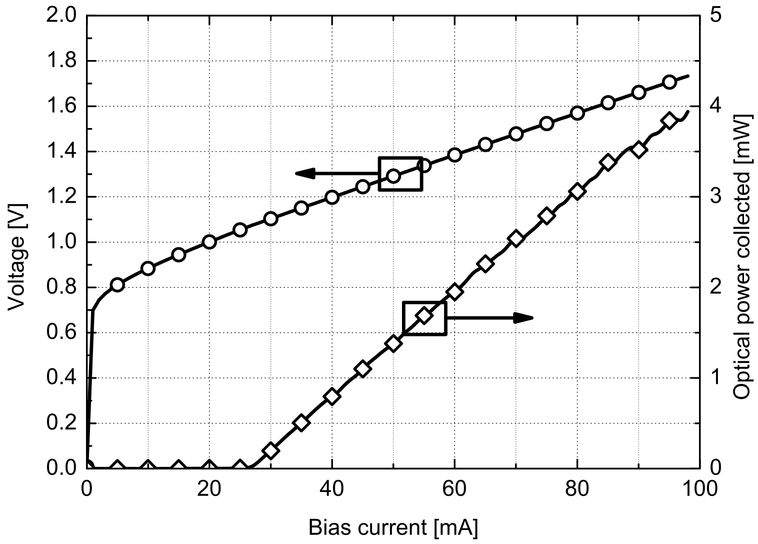

Figure 4.8: The VI and LI curves marked with circles and diamonds respectively. Device was temperature stabilized at 25 $^{\circ}C$.

30 mA to 16 Ω at bias at 100 mA.

4.3.2.2 Optical spectrum analysis - multimode operation

With an adjustment of a bias current in range between 0 mA and 100 mA it is possible to achieve stable multimode operation of the laser with optical modes separated by 41 GHz. Optical spectrum collected with standard optical spectrum analyzer providing 0.05 nm is shown in Fig. 4.9. For bias condition set at 85.2 mA multimode output is centered at 1557 nm with 11 longitudinal modes present in 10 dB window measured from the maximum of the dominant mode, and provides with an average output power of 3.4 mW. This allows to consider such a laser diode as a potential candidate for the RF generation.

4.3.2.3 Self heterodyning technique for optical linewidth measurement

Optical linewidth measurement setup based on self heterodyning approach, as shown in Fig. 4.10 is utilized in order to assess the optical linewidth corresponding to each of the laser axial modes. Use the high resolution optical spectrum analyzer with resolution of 10 MHz would impose significant error on the results as the linewidth of the optical modes from such type of the device is expected to be in the order of several megahertz. Optical output

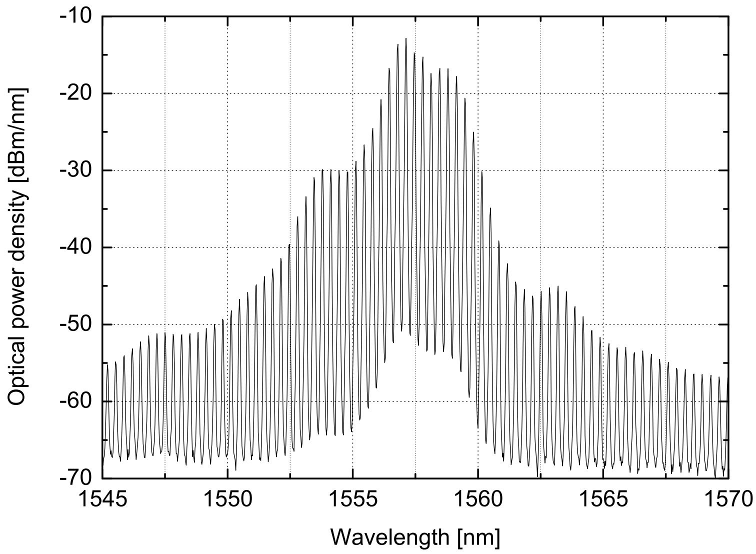

Figure 4.9: Multimode output produced by slotted FP laser diode: optical spectrum recorded for bias condition $I = 85.20\ mA$ in a room temperature.

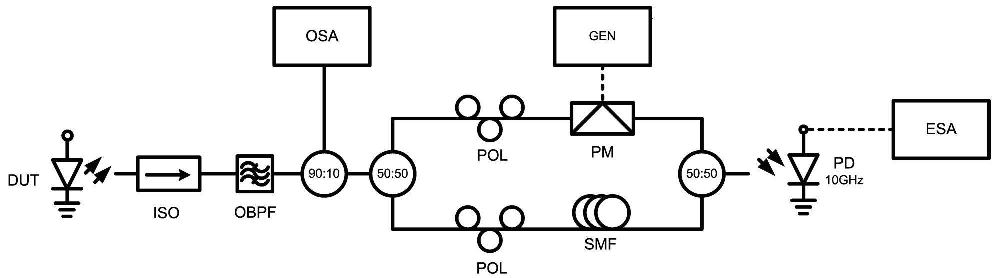

Figure 4.10: Self heterodyning setup for optical linewidth measurement.

of the slotted FP laser diode is collected with a precise lensed fibre featuring focal length of $3.5\ \mu m$ and minimum spot size of $2\ \mu m$. An optical isolator (ISO) prevents back-reflections from other elements of the setup which could disturb operation of the investigated laser. Tunable optical band-pass filter (OBPF) with a fixed $3\ dB$ bandwidth of $27\ GHz$ allows for selection of individual longitudinal modes, with at least $27\ dB$ of SMSR to neighboring ones. Signal generator (GEN) and phase modulator (PM) introduce frequency shift, which allows for observation of a beat tone at lower RF frequency of $2\ GHz$. The $12\ km$ of single mode fibre (SMF) allows to bring the signal in this branch beyond the coherence length (inversely proportional to the signal linewidth) and achieve the minimum measurable linewidth at $17\ kHz$. The FWHM linewidth $\Delta\nu_{FWHM}$ is estimated by width measurement at 10 dB drop from the peak value denoted with $\Delta\nu_{10dB}$ by use of the following formula [8]:

$$\Delta\nu_{FWHM} = \frac{\Delta\nu_{10dB}}{2\sqrt{10}} \tag{4.2}$$

The average linewidth corresponding to a single isolated optical mode with Lorentzian shape fitting in the 3 dB bandwidth is estimated to be at 50 MHz with an error of 0.1 MHz. Comparison of the summary linewidth of optical modes with a linewidth of the RF signal will determine if there are mode-locking mechanisms engaged [4, 9].

4.3.3 The RF domain analysis - experimental setup and results

Device under test (DUT) emits identical multimode spectra for wide range of bias currents. Consecutive longitudinal modes are separated by frequency around 41 GHz. The experimental setup presented in Fig. 4.11 is used to investigate the RF domain if there is any signal at this frequency range emitted. Electrical spectrum collected by 40 GHz

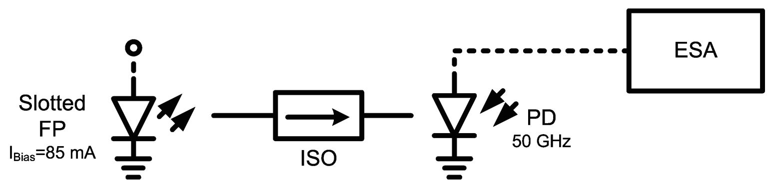

Figure 4.11: Experimental setup for RF investigation, tested laser is temperature controlled at 25 $°C$.

spectrum analyzer (ESA) with radio and video resolutions set at 30 kHz combined with bandwidth expanding external mixer (40 to 50 GHz) from 50 GHz photodetector is depicted in Fig. 4.12. Laser is biased with 85.00 mA and temperature stabilized at 25 $°C$. At such conditions an RF peak at 41.37 GHz is recorded and fitted with Lorentzian curve. The FWHM linewidth is measured at 10 dB drop from the peak value estimated to be at 900 kHz and results with a Q factor of 45966.

The linewidth of the recorded RF signal is smaller by two orders than summary linewidth of the contributing optical modes which implies that the device is passively mode-locked. The mechanism of the mode-locking originates from four wave mixing nonlinearities provided by semiconductor material, through which all optical modes are linked inside the

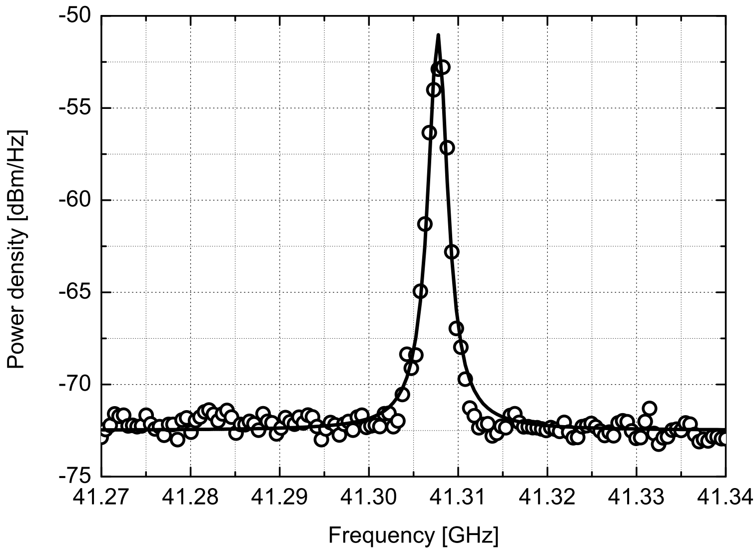

Figure 4.12: RF signal recorded at $41.3\ GHz$ with bias condition being $I_{bias} = 85.00\ mA$ and temperature controlled at $25\ °C$. The circles (○) represent the experimental data, dashed line fitted Lorentzian curve.

laser cavity. Separation between longitudinal optical modes is around $40\ GHz$, therefore the main contribution comes from carrier density modulation (CDM) effect [5].

Similarly to previous section the RF signal corresponding to the FSR between optical modes is produced however the increased number of the optical modes resulted in reduced linewidth of the RF signal and improved value of Q factor. In the following part a laser diode featuring 40 modes in $3\ dB$ bandwidth.

4.4 Quantum dash Fabry-Pérot laser diode

4.4.1 Device description

The quantum dash (QDash) based heterostructure is grown by gas source molecular beam epitaxy (GS-MBE) on S-doped InP wafer [10]. The active core consists of 6 layers of $InAs$ QDashes enclosed within $40\ nm$ thick $InGaAsP$ barriers, Fig.4.13. The whole active structure is sandwiched within two $80\ nm$ thick separate confinement heterostructure (SCH) layers . Both SCH and barriers are un-doped. Typical dimension along the growth axis and width of the QDash to achieve emission at $1.55\ \mu m$ are $2\ nm$ and $20\ nm$ respectively. The density of dots per layer is $2 \times 10^{10} cm^{-2}$. The laser under test is 1010 μm long, single-section device, without phase or saturable absorber sections [11]. The device was designed and manufactured by III-V Labs Alcatel-Lucent, France.

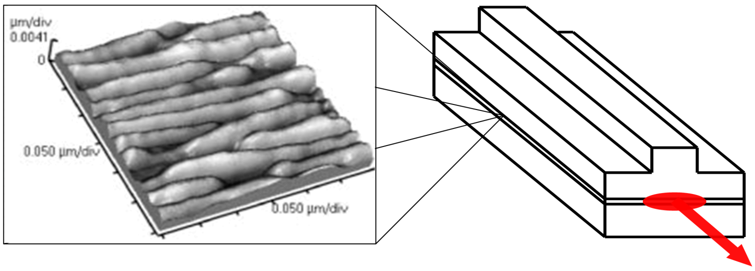

Figure 4.13: QDash Fabry-Pérot semiconductor laser structure with structure of one active layer. The dashes are elongated in the transverse direction to the beam propagation inside the laser cavity. QDash layer image after [10].

4.4.2 Steady state characterizations

The tested device is a pre-cut wafer-bar, mounted and wire-bonded to the electrodes on a ceramic sub-mount. The whole sample is placed on probe station and connected with two individual DC probes for bias and ground connections. The temperature is stabilized at 25 $^{\circ}C$ unless otherwise stated. Behavior of tested laser under DC bias conditions is investigated in optical and electrical domains as a function of injected current.

4.4.2.1 Voltage vs bias current and optical power vs bias current characterizations

The voltage versus bias current (VI) and optical power versus bias current (LI) characteristics depicted in Fig. 4.14 of the QDash FP LD were collected for bias current applied to the active section ranging from 0 mA to 400 mA and from 400 mA to 0 mA with a step of 1 mA.

LI characteristic shows clear threshold point at $I_{th} = 18\ mA$. It was recorded both ways by increasing and decreasing the bias current, both curves are overlapping each other - there is no memory effect - which proves that no absorber region exists in the device. Roll-off at the higher bias levels results from the thermal effects - increase of the current increases thermal noise but does not contribute to the laser emission. Dynamic impedance

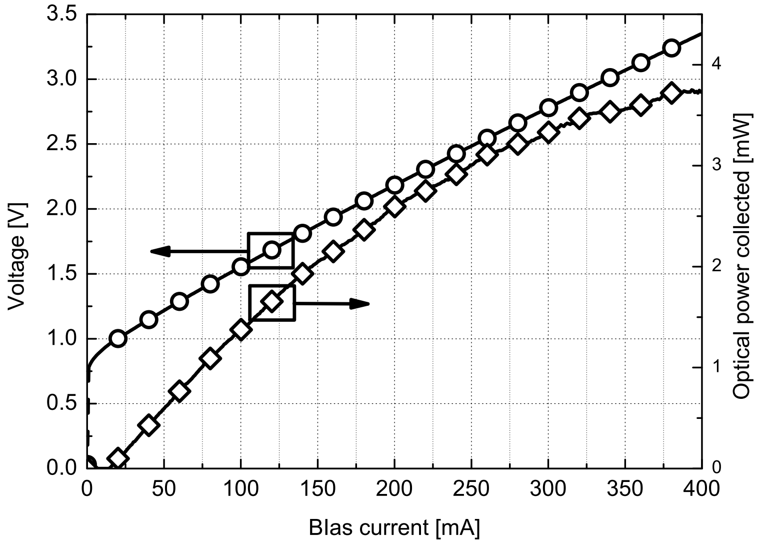

Figure 4.14: The VI and LI curves obtained from QDash FP laser diode, marked with circles (○) and diamonds (◇) respectively.

across the lasers junction varies from $52\ \Omega$ at the threshold up to $9\ \Omega$ at $400\ mA$ of the bias level.

4.4.2.2 Optical spectrum analysis - multimode operation

For all currents exceeding the threshold value, optical spectra emitted by the QDash FP laser feature a multimode structure with a nearly flat envelope. Increase of bias current leads to the increase of the number of optical modes present in the $3\ dB$ bandwidth. Example for the optical spectrum recorded with device biased at $350\ mA$ and temperature controlled at $25\ °C$ if presented in Fig 4.15. Optical spectrum is centered at $1525\ nm$ and for bias level set at $350\ mA$, spans $12\ nm$ across the $3\ dB$ bandwidth. The longitudinal optical modes present in the spectrum are separated by free spectral range (FSR) of $0.3\ nm$, which corresponds to the frequency of $40\ GHz$ approximately.

4.4.2.3 Optical linewidth measurement

Optical linewidth measurement setup based on self heterodyning approach, as presented previously in Fig. 4.10 is utilized in order to assess the optical linewidth corresponding to each of the laser's axial modes. Their values follow linear trend, with the maximum around

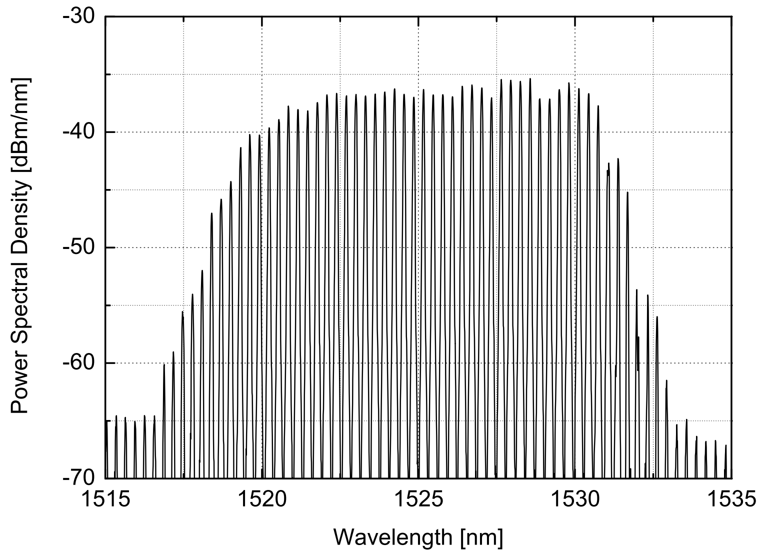

Figure 4.15: Multimode output with no external modulation applied: optical spectrum recorded for bias condition $I_{bias} = 350\ mA$ with temperature controlled at $25\ °C$.

$50\ MHz$ for shorter wavelengths and minimum around $10\ MHz$ at longer wavelengths side. Optical linewidths corresponding to each longitudinal mode for four different bias conditions applied to the QDash LD plotted in Fig. 4.18 in the next section.

Comparison of the summary linewidth of optical modes with a linewidth of the RF beat signal produced by these modes while directed on fast PD will determine if there are mode-locking mechanisms engaged [4, 9].

4.4.3 RF signal generation - experimental setup and results

It is demonstrated that tested QDash FP LD emits a number of longitudinal modes simultaneously, while being DC biased. For bias level set at $350\ mA$, there are 40 optical modes present at the output of the device in a $3\ dB$ bandwidth window. Separation between consecutive modes is around $40\ GHz$. Investigation of the signal produced by beating of these modes on fast ($50\ GHz$) photodetector is performed with use of electrical spectrum analyzer (ESA) featuring $40\ GHz$ bandwidth. Optical power collected by lensed fibre is around $2.5\ dBm$, so further amplification is not necessary. Experimental setup is presented in Fig. 4.16. Electrical spectrum collected by $40\ GHz$ spectrum analyzer and fast photo-

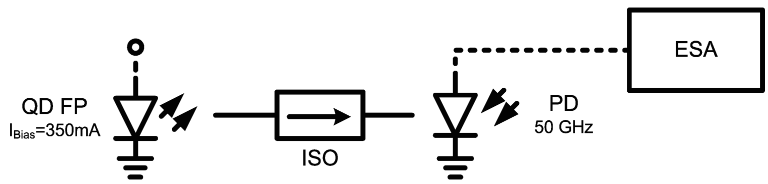

Figure 4.16: Experimental setup for RF investigation, the tested laser is temperature controlled at 25 $°C$.

diode is depicted in Fig. 4.17. Laser is biased with I_{bias} set at 350 mA and temperature

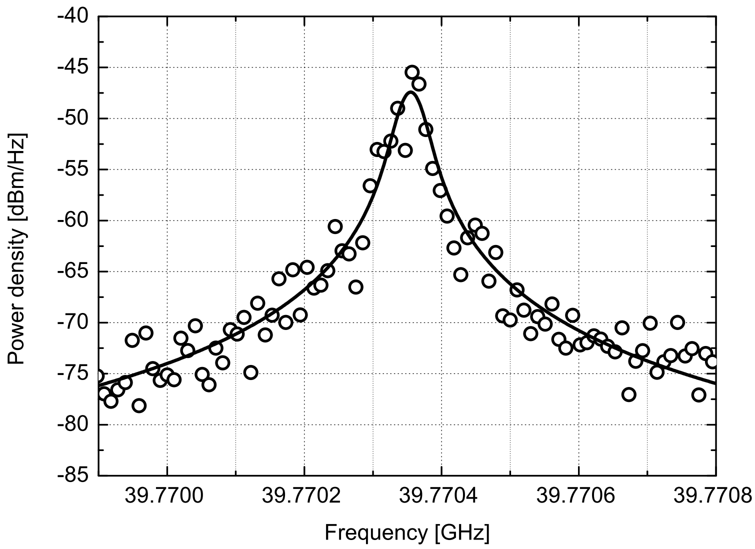

Figure 4.17: RF signal recorded at 39.77 GHz with bias condition $I_{bias} = 350\ mA$ and temperature stabilized at 25 $°C$. Measured data marked with open circles (○) and its Lorentzian fit with solid line.

stabilized at 25 $°C$. At such bias conditions, a peak at 39.7 GHz is recorded. Measured data points are fitted with Lorentzian shape, and the FWHM linewidth at 18 kHz is estimated as a width of the fitted curve at 10 dB drop from the maximum value following Equation 4.2 [7, 12, 13].

The RF beat linewidth is about three orders of magnitude lower than the sum of the optical linewidths associated with longitudinal modes produced by the laser and contributing to that beat signal. Such a difference can be attributed to high correlation between the optical modes involved - mode-locking, which results in reduction of the noise of the beat signal. Correlation between the modes is not introduced by any external means in this case,

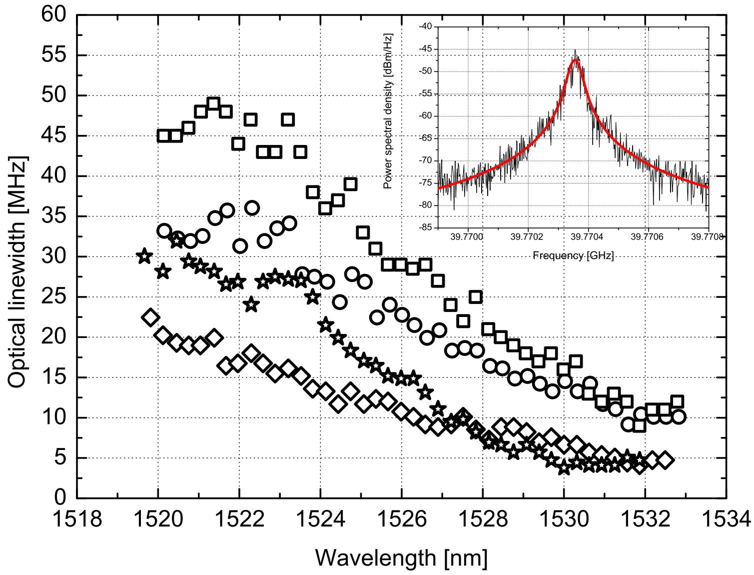

Figure 4.18: Linewidths associated with each optical mode present in a 3 dB window of the optical spectrum. The laser is temperature stabilized at 25 $°C$ and measurements are repeated for different bias levels: 150 mA ($\star$), 250 mA ($\diamond$), 350 mA ($\square$), and 450 mA ($\circ$). On inset the RF signal produced by all optical modes simultaneously at the bias provided at 350 mA.

so the mechanisms governing this behavior are passive. The resulting value of the Q factor in this case is around 220000, this supports the observation of the improvement of the generated RF signal with the increase of the number of the optical modes contributing to it. The values of FWHM optical linewidths associated with each optical mode present at the output of the laser diode biased at four different current levels are depicted in Fig. 4.18.The trend observed on the optical linewidths allows us to conclude that stronger mode-locking effects are affecting the longer wavelengths emitted by the laser. This may result from stronger linewidth enhancement factor (and inter-modal coupling efficiency) at the longer wavelengths part of the spectrum.

4.5 Summary

Generation of RF signals by DC-biased multimode semiconductor lasers is demonstrated with three different types of laser diodes: DBR, Slotted FP and FP whose active sections are based respectively on bulk, quantum well, and quantum dash semiconductor materials.

In all cases the devices were sufficient to produce stable multimode output, and generate beat signals corresponding to the free spectral range between the longitudinal optical components at their outputs. All investigated structures are able to produce RF signals with frequencies around $40\ GHz$ which falls into the microwave band.

Analysis of the results achieved in optical and electrical spectral domains gives support to the hypothesis presented in Chapter 3. The reduction of the spectral width of the generated RF beat tone when compared to the summary linewidth of the optical modes contributing to this beat signal is observed. A signature of passive mode-locking can be concluded in all presented semiconductor lasers. As a consequence of PML the optical pulse formation at the output of such laser should occur, which is experimentally investigated in following chapter.

Increase of the value of the Q factor with the increase of the number of optical modes produced by a laser should be noted. Along with improved signal quality one can conclude that quality of mode-locking in terms of inter-modal phase synchronization is improved with a larger number of modes.

The frequency of the generated signal is directly related to the free spectral range at the output of the particular laser diode. The FSR can be expanded in a single laser diode to reach the terahertz frequencies. Generation of signals within this band by multimode laser diodes will be studied in Chapter 7.

Bibliography

[1] M. Bohr, "Interconnect scaling-the real limiter to high performance ulsi," in *Electron Devices Meeting, 1995., International*, pp. 241 –244, Dec. 1995.

[2] B. Lavigne, J. Renaudier, F. Lelarge, O. Legouezigou, H. Gariah, and G.-H. Duan, "Polarization-insensitive low timing jitter and highly optical noise tolerant all-optical 40-ghz clock recovery using a bulk and a quantum-dots-based self-pulsating laser cascade," *Lightwave Technology, Journal of*, vol. 25, pp. 170 –176, jan. 2007.

[3] S. Latkowski, F. Surre, P. Landais, and G. Duan, "All-optical synchronization of a 40 GHz self-pulsating distributed Bragg reflector laser to return-to-zero 10, 20 and 40 gbit/s data streams," *Optics Communications*, vol. 282, pp. 2053–2058, May 2009.

[4] J. Renaudier, G. Duan, P. Landais, and P. Gallion, "Phase correlation and linewidth reduction of 40 GHz self-pulsation in distributed Bragg reflector semiconductor lasers," *Quantum Electronics, IEEE Journal of*, vol. 43, no. 2, pp. 147–156, 2007.

[5] S. Latkowski, F. Surre, and P. Landais, "Passively mode-locked semiconductor lasers and their applications," in *Transparent Optical Networks, 2008. ICTON 2008. 10th Anniversary International Conference on*, vol. 2, pp. 110–113, 2008.

[6] J. A. Patchell, B. Kelly, and J. J. C. O'Gorman, "Semiconductor laser and method of manufacture," Patent US 7672348, 02 2010.

[7] R. Maldonado-Basilio, S. Latkowski, F. Surre, and P. Landais, "Linewidth analysis of

40-GHz passively mode-locked multi-mode semiconductor lasers," *Optics Communications*, vol. 283, pp. 299–303, Jan. 2010.

[8] D. Derickson, J. Vobis, L. Stokes, P. Hernday, V. McOmber, D. M. Barney, W. V. Sorin, J. Beller, C. M. Miller, S. W. Hinch, and C. Hentschel, *Fiber Optic Test and Measurement*. Prentice Hall PTR, Nova Jersey, 1998.

[9] S. Latkowski, F. Surre, E. Degirmenci, and P. Landais, "Passively phase-locked multimode semiconductor laser: From millimetre to terahertz wave generation," in *Lasers and Electro-Optics, 2008 and 2008 Conference on Quantum Electronics and Laser Science. CLEO/QELS 2008. Conference on*, pp. 1–2, 2008.

[10] F. Lelarge, B. Dagens, J. Renaudier, R. Brenot, A. Accard, F. van Dijk, D. Make, O. L. Gouezigou, J. Provost, F. Poingt, J. Landreau, O. Drisse, E. Derouin, B. Rousseau, F. Pommereau, and G. Duan, "Recent advances on InAs/InP quantum dash based semiconductor lasers and optical amplifiers operating at 1.55 μm," *Selected Topics in Quantum Electronics, IEEE Journal of*, vol. 13, no. 1, pp. 111–124, 2007.

[11] A. Shen, J. G. Provost, A. Akrout, B. Rousseau, F. Lelarge, O. Legouezigou, F. Pommereau, F. Poingt, L. Legouezigou, G. H. Duan, *et al.*, "Low confinement factor quantum dash (QD) mode-locked Fabry-Perot (FP) laser diode for tunable pulse generation," in *Optical Fiber communication/National Fiber Optic Engineers Conference, 2008. OFC/NFOEC 2008. Conference on*, p. 13, 2008.

[12] R. Maldonado-Basilio, S. Latkowski, F. Surre, and P. Landais, "Linewidth study of 40-GHz passively mode-locked multimode semiconductor lasers," in *CLEO/Europe - EQEC 2009 - European Conference on Lasers and Electro-Optics and the European Quantum Electronics Conference*, (Munich, Germany), pp. 1–1, 2009.

[13] R. Maldonado-Basilio, J. Parra-Cetina, S. Latkowski, and P. Landais, "Timing-jitter, optical, and mode-beating linewidths analysis on subpicosecond optical pulses generated by a quantum-dash passively mode-locked semiconductor laser," *Optics Letters*, vol. 35, pp. 1184–1186, Apr. 2010.

Chapter 5

Optical pulse generation by passively mode-locked laser diodes

5.1 Introduction

Modern optical networks require solutions based on all-optical approaches in many cases dependent on the sources of short optical pulses. There are a number of techniques for the generation of short optical pulses like: pulse carving, gain switching, Q-switching and mode-locking. In this chapter a short review of these techniques will be provided, along with some modern methods of characterization of optical pulses. Experimental demonstration of very short optical pulse generation, with use of three different types of passively mode-locked laser diodes is carried out. Due to their parameters, they can be featured as 'green' - power efficient, small size, relatively cheap to manufacture - pulse sources, in high speed optical networks. Additional possible applications in all optical data treatment schemes will also be presented.

5.2 Pulse generation techniques

5.2.1 Pulse carving

Generation of optical pulses can be performed by modulation of initially continuous light with a fast modulator, allowing the light to pass for only a short period of time. This method has however large drawbacks: the pulse duration is in this method limited by bandwidth of the modulator; a large part of the optical energy is lost on the modulator when it is in a ‘closed’ state. Despite these, there have been efforts made to utilize CW source and optical modulators, and multi-gigahertz repetition-rates with picoseconds pulse durations have been reported [1, 2]. There are a few pulse generation techniques that are mostly used nowadays, which can offer much shorter pulses with higher power and repetition rates.

5.2.2 Q switching

The technique is based on modulation of the losses of the laser cavity (modulation of the Q factor of the resonator). Intra-cavity losses are initially kept on high level, so the lasing action cannot occur, but the pump energy is being accumulated in gain medium. The sudden reduction of the losses initiates the laser action; radiation energy builds up within hundreds or thousands of cavity round-trips. Once the power in the cavity reaches the saturation energy of the gain medium, the gain starts to saturate. The peak of the emitted pulse is reached when the gain is equal to given low losses. After this point the stored energy depletion continues due to high intra-cavity power [3].

The modulation of the losses can be achieved by active (active Q switching) or passive (passive Q switching) way. In the active Q switching, the losses are modulated with an active control element, which usually takes the form of an optical modulator triggered by an electrical signal. It can be also triggered by a mechanical element like a rotating end mirror. In either case, generated pulse energy depends on stored energy in the gain medium and pulse repetition rate [4]. For the passive Q switching, a saturable absorber introduced into the laser cavity is used in order to modulate the losses. The pulse is being generated automatically, as soon as the stored energy level in the gain medium is sufficient to decrease the losses of the saturable absorber. In such a system, the pulse energy and duration are fixed (by saturable absorber and gain recovery times), and changes of the pump power result in change of repetition rate [4]. Passive Q switching allows for higher repetition rates than those offered by active Q switching techniques; however the pulse energies are usually lower [4, 5]. Lasers which use the Q switching technique generate periodical pulse-trains, with repetition rates from kilohertz to megahertz, and pulse durations from below $1\ ns$ to a few nanoseconds. Pulse energies vary between millijoules for small laser chips to kilojoules for large laser systems. The emitted peak power can be orders of magnitude higher, when compared to that obtained in CW operation.

5.2.3 Gain switching

Gain switching is a pulse generation technique, which involves the modulation of the gain by the pump power. If high pump power is applied to the laser for a short period of time, the laser emission starts with a delay (necessary for the amplification of initial spontaneous emission). This allows for the energy accumulation in a gain medium, which is then emitted in the form of a pulse. The pulse duration can be shorter than the pump duration and shorter than the upper state lifetime [6]. The pump power can be switched off between the pulse generations or can be kept at a level below the threshold.

In semiconductor lasers, gain switching can be achieved by application of the short electrical pulses or consciously modulated signal [7]. Pulse trains with repetition rates up to several gigahertz can be obtained with pulse durations between nano and picoseconds, which can be exploited for telecommunication applications [8–11]. The advantage of the gain switched lasers compared to Q switched and mode-locked devices, is an easily tunable repetition rate, which does not require modifications of the laser's cavity.

5.2.4 Mode-locking

The mode-locking techniques which are described in Chapter 4, allow for generation of ultra-short optical pulses with high repetition rates. Pulse durations can be in order of femtoseconds, and repetition rates can reach hundreds of gigahertz [5, 12, 13]. Pulse generation with passively mode-locked semiconductor laser is studied experimentally in following sections of this chapter.

5.3 Pulse characterization techniques

Variety of measurement techniques can be used in order to characterize optical pulses. Temporal information about optical pulses can be retrieved with use of fast photodetector connected to the digital sampling oscilloscope. Bandwidths at 80 GHz and temporal resolution in order of picoseconds are achievable but only for repetitive signals with good trigger. Information about repetition rate, pulse duration and its temporal shape, and timing jitter can be measured in the limits of bandwidth and temporal resolution. For shorter pulse durations intensity autocorrelation techniques can be utilized in order to retrieve the information about temporal pulse-shape; however in order to fully recover optical pulse in both time and spectral domains, frequency resolved optical gating (FROG) can be used.

5.3.1 Intensity autocorrelation

The intensity autocorrelation allows for the estimation of the duration of ultrashort optical pulses [14–17]. In order to investigate input optical field $E(t)$, with intensity $I(t) = |E(t)|^2$, two parallel optical beams, with variable optical delay are generated, and combined on second harmonic generation (SHG) crystal, in order to generate a signal proportional to $|E(t) + E(t-\tau)|^2$. Beams propagating along the optical axis, proportional to the cross product appearing with expression $|E(t) \times E(t-\tau)|$, are collected by a slow response photodetector, as depicted in Fig. 5.1. The recorded signal can be expressed as:

$$I_M(\tau) = \int_{-\infty}^{+\infty} |I(t)I(t-\tau)|dt \tag{5.1}$$

where $I_M(\tau)$ is an intensity autocorrelation of the pulse. The width of the intensity autocorrelation is related to the duration of the original pulse. When the shape of the original pulse is known or can be assumed, the deconvolution factor can be used to obtain the original pulse-width from intensity autocorrelation trace. Table 5.1 shows the values of the deconvolution factors for common pulse shapes.

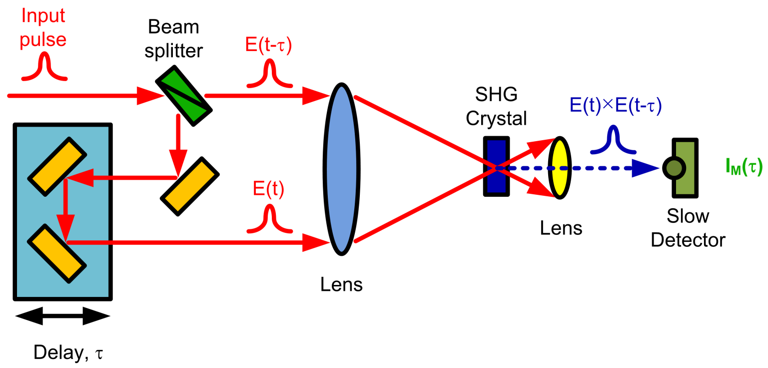

Figure 5.1: Schematic diagram of an intensity autocorrelator based on SHG crystal.

Although the pulse duration can be measured from the intensity autocorrelation, it is not possible to obtain information about the phase. Moreover an autocorrelation is symmetrical and the autocorrelation function is even, so: $I_M(-\tau) = I_M(\tau)$. This property leads to an uncertainty in the time axis and consequently of the temporal amplitude profile of the pulse.

Table 5.1: Scaling factors for autocorrelation traces of common pulse shapes.

Pulse shape	**Scaling factor**
Gaussian	1.414
Hyperbolic secant	1.543

5.3.2 Frequency resolved optical gating - FROG

Second harmonic generation (SHG) frequency resolved optical gating (FROG) is a pulse characterization scheme, which allows to fully resolve ultrashort optical pulses [18–20]. In construction it is similar to the intensity autocorrelator, but instead of using a slow detection to record the signal, the second harmonic signal is resolved spectrally by an spectrometer (frequency resolved), as presented in Fig. 5.2. The recorded two dimensional data, called

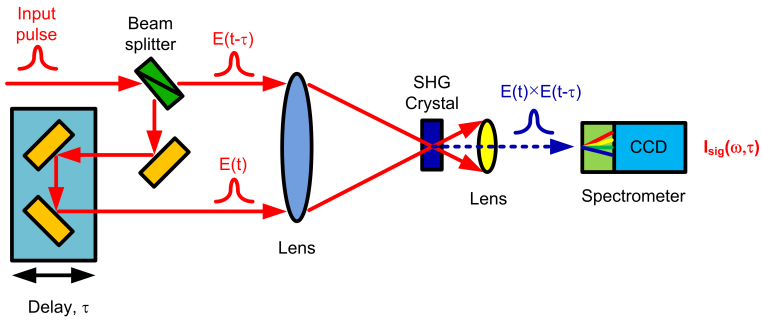

Figure 5.2: Schematic diagram of an SHG FROG system.

a spectrogram, represents an autocorrelation intensity as a function of time and angular frequency $I(t, \omega)$, and allows for the retrieval of the intensity and the phase of the input pulse.

$$I_{sig}(\omega, \tau) = |\int_{-\infty}^{+\infty} P(t)G(t-\tau)\exp(-i\omega t)dt|^2 \tag{5.2}$$

where $P(t)$ is a probe pulse, and $G(t)$ is a gate pulse, both are determined by nonlinear interaction function, such as SHG for the FROG. They both take a form of $E(t)$, so Equation 5.2 becomes:

$$I_{sig}(\omega, \tau) = |\int_{-\infty}^{+\infty} E(t)E(t-\tau)\exp(-i\omega t)dt|^2 \tag{5.3}$$

The FROG system has no information about $E(t)$, it uses an iterative algorithm, which takes into account the recorded spectrogram and form of the nonlinearity, to achieve the best match between real recorded spectrogram and a generated one from $E(t)$ with matching phase and amplitude profiles.

5.4 Generation of 10 ps optical pulses at 40 GHz repetition rate by PML DBR laser diode

The first device under test is a DBR laser previously presented in Chapter 4. It has been demonstrated to operate in a multimode regime with signature of passive mode-locking.

5.4.1 Experimental setup

The experimental setup presented in Fig. 5.3 consists of the DBR laser placed on probe station and temperature stabilized at 25 $°C$. The optical spectrum analyzer (OSA) and the FROG system are used to provide detailed information about the optical output. The optical output from the DBR laser is coupled with a lensed fibre with focal length of 3.5 μm. An average optical power of 2.5 mW is collected, with gain and Bragg sections biased at 200 mA and 14.3 mA respectively. The optical amplifier (EDFA 1) is followed by a 5 nm optical bandpass filter (OBPF). The polarization controller (POL) and high power optical amplifier (EDFA 2) are elements of the FROG system necessary for conditioning the input signal for maximal second harmonic generation.

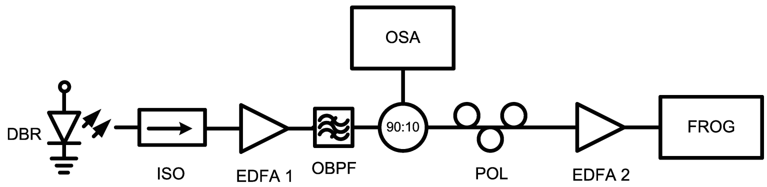

Figure 5.3: Experimental setup used for optical output characterization from DBR laser.

Optical spectrum analyzer provides information about spectral shape of the signal produced by tested device after pre-amplification stage, and the FROG system allows for retrieval of the detailed information about pulsed nature of this output, if any. The lengths of fibre links between the components of the setup are minimized - total length of SMF patch-cords in this setup is less than 4 m - in order to reduce the fibre induced dispersion and its impact on the recorded pulse profile. However, additional impact of the dispersion related effects introduced by a fibre present in optical amplifiers (approximately 11 m in each EDFA) should to be taken into consideration for recorded pulses.

5.4.2 Results

The DBR LD biased on gain and Bragg sections respectively with I_g set at 200 mA, and I_B set at 14.3 mA, with phase section unbiased (not connected) and temperature stabilized at 25 $°C$, gives an output spectrum presented in Fig. 5.4. The optical spectrum features eight

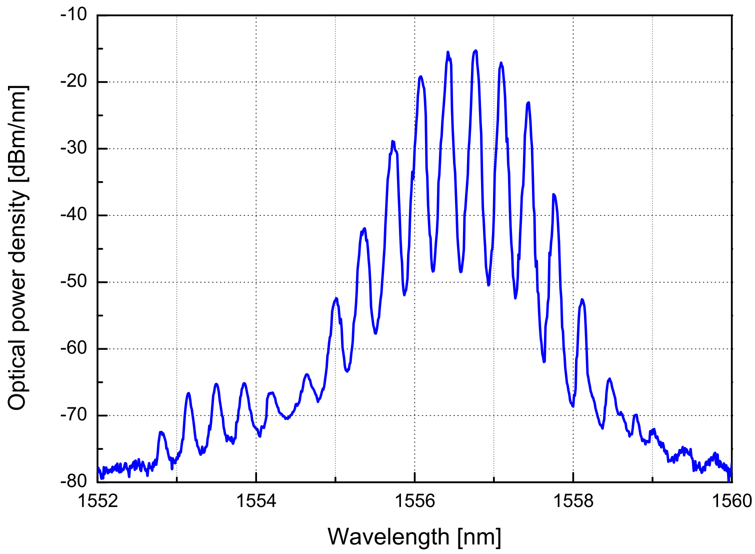

Figure 5.4: Optical spectrum recorded from DBR LD, DC biased with currents I_g and I_B being set at 200 mA and 14.3 mA respectively. Temperature controlled at 25 $°C$.

modes in 30 dB bandwidth with FSR of 39.7 GHz, centered at 1556.6 nm. The FROG system for these given bias conditions presents a spectrogram shown in Fig. 5.5a.

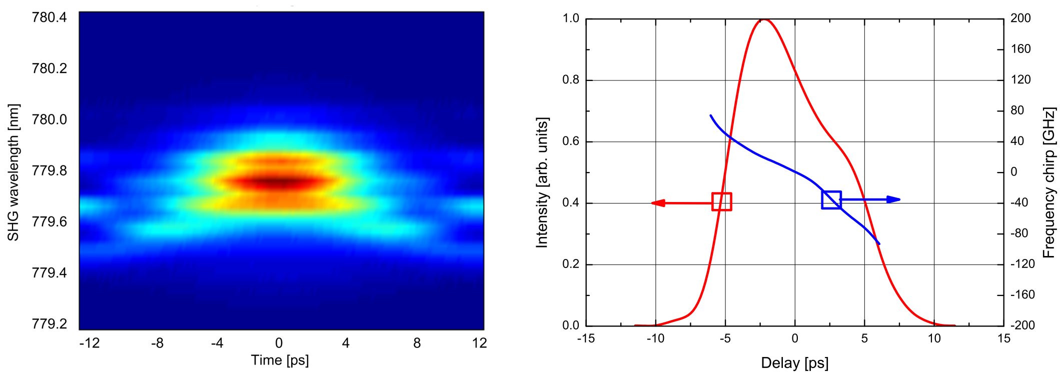

(a) Recorded spectrogram.

(b) Resolved optical pulse.

Figure 5.5: Spectrogram recorded from DBR LD and corresponding optical pulse resolved with FROG. The DBR LD is DC biased with currents I_g and I_B being set at 200 mA and 14.3 mA respectively and temperature stabilized at 25 $°C$.

A tested DBR laser under DC bias conditions, generates an optical pulse stream with repetition rate of 39.7 GHz. The emitted pulses are characterized by a pulse duration of 9.34 ps measured at full width at half maximum and linear chirp across the pulse-width, with magnitude of 150 GHz and negative slope. The peak power of the pulses can be estimated to be around $6.7\ mW$ taking into account average power collected from the laser diode, repetition rate and assuming simple pulse profile (square for a given value).

It has been demonstrated that passively mode-locked DBR LD featuring multimode output with three longitudinal modes in the $3\ dB$ bandwidth can produce optical pulses with a repetition rate related to the free spectral range between these modes. In the following section a different type of passively mode-locked laser diode which output spectrum consists of 40 longitudinal modes is going to be investigated, and the impact of the number of modes on the generated pulses will be examined.

5.5 Generation of 2.5 ps optical pulses at 40 GHz by QDash Fabry-Pérot laser diode

The experimental analyses of the quantum dashed Fabry-Pérot laser diode performed in Chapter 4 indicate that this laser is passively mode-locked. This QDash FP LD, features multimode spectrum consisting of 40 longitudinal modes with a nearly flat envelope. The large difference between the linewidth of the RF beat signal produced on a fast photodetector and the sum of the optical linewidths of the modes contributing to that beat signal proves the strong mode-locking effect. Many longitudinal modes present at the output of the laser suggests formation of very short optical pulses.

5.5.1 Experimental setup

The intensity and spectral time evolution of this laser is investigated according to the setup depicted in Fig 5.6. The tested laser (QDash FP) is mounted on ceramic sub-mount,and DC biased on a probe station. The temperature is stabilized at $25\ ^{\circ}C$. Average optical power coupled to the fibre is at $4\ mW$, for a bias level of $350\ mA$. An optical isolator (ISO) is introduced in order to prevent back-reflections to the tested LD which could disturb the PML process. Optical amplifier EFDA 1 provides pre-amplification of the signal. A tunable optical bandpass filter (OBPF) centered at wavelength of $1530\ nm$ allows to investigate the performance of the laser when its output is subjected to an external optical filtering at

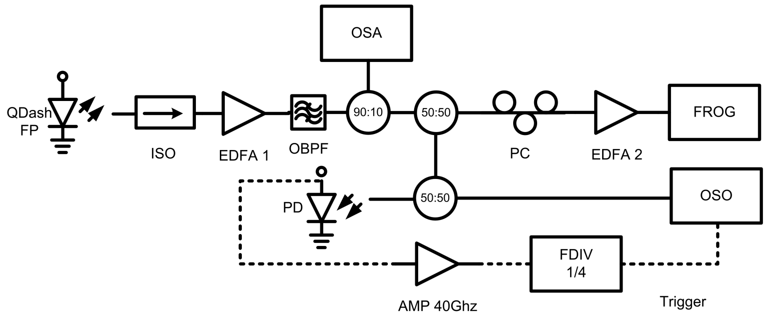

Figure 5.6: Experimental setup for investigation of the output of QDash FP laser under DC bias conditions. Temperature is stabilized at $25\ °C$.

various filter bandwidths. A number of optical couplers are used to distribute the optical signal among the experimental equipment. An optical spectrum analyzer (OSA) monitors spectral content of the signal at the input of the pulse characterization equipment. The polarization controller (PC) and the high power optical amplifier (EDFA 2) are imposed by the FROG system. Additionally, optical output is observed with $500\ GHz$ bandwidth optical sampling oscilloscope (OSO) offering a $0.83\ ps$ temporal resolution. An electrical trigger was retrieved from the optical input path via $50\ GHz$ photodetector, low noise broadband RF amplifier (AMP) and 1:4 frequency divider (FDIV), to support the OSO measurements.

5.5.2 Temporal analysis

From the device biased at $350\ mA$ and temperature stabilized at $25\ °C$, pulse stream with repetition rate of $39.8\ GHz$ is recorded with the optical sampling oscilloscope, as presented in Fig. 5.7, when no filtering scheme is applied. No quantitative measurements can be retrieved from this temporal trace due to a number of factors: the temporal resolution of the OSO is close to the expected (below $1\ ps$) pulse duration, and its sensitivity to limited quality trigger of a trigger line.

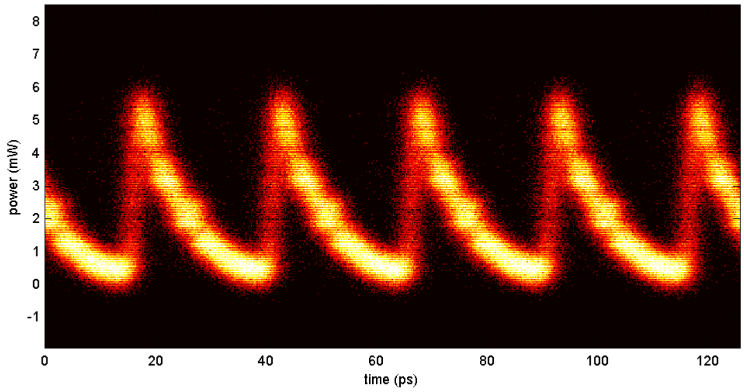

Figure 5.7: Optical sampling oscilloscope trace. Device under test biased at $350\ mA$, and temperature stabilized at $25\ ^{\circ}C$.

However some observations regarding the pulse-shape can be concluded:

- The rising edge of the pulses is shorter than the trailing one.
- There are features on the trailing part of the pulses.
- The peak power is $6\ mW$ (the average optical power at the input of OSO at $3\ dBm$).

Due to the limitations imposed by used optical sampling oscilloscope, full recovery of the pulses is performed with the FROG system. Results are presented in Fig. 5.8, where pulses characterized with pulse durations of $2.6\ ps$, $2.9\ ps$ and $6\ ps$ are recorded with the optical bandpass filter set at $1530\ nm$ with $6\ nm$, $3\ nm$ and $1\ nm$ bandwidths respectively. Therefore the pulse duration dependancy on the spectral bandwidth can be concluded.

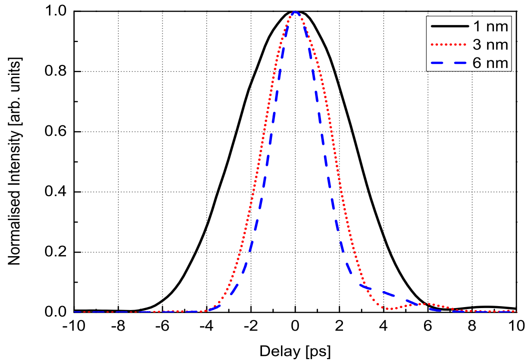

(a) Intensity profile of the optical pulses.

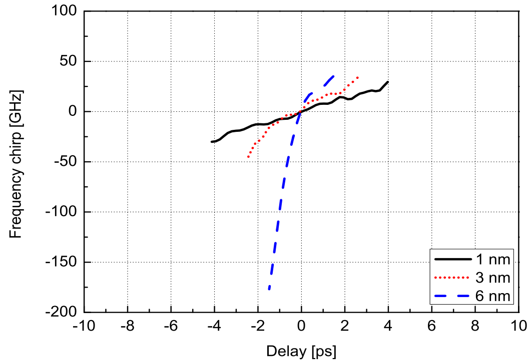

(b) Frequency chirp associated with the optical pulses.

Figure 5.8: Optical pulses generated from PML QDash FP laser diode resolved with FROG system for filter bandwidths at 1, 3 and 6 nm denoted in black, red and blue colour respectively.

The pulse duration is reduced with an increase of the optical filter bandwidth. The measured pulse-widths are ranging between 2.2 ps when no filtering scheme is used up to 6 ps for the 1 nm filter bandwidth. The slope of the chirp for all filtering conditions is positive while its magnitude increases with the increase of the filter bandwidth. With the constant average power (4 mW) collected by a lensed fibre from the laser diode, the peak powers associated with the pulses can be estimated betwen 16.7 mW and 39 mW for given filter presets, and at 46 mW when the optical filter is not in use (for simplicity a square pulse shape is assumed in this estimation) [12, 21, 22].

The positive slope associated with the pulses emitted by QDash FP LD is an interesting feature. It allows to introduce simple compression scheme based on group velocity dispersion in standard single mode fibre, which will be exploited in the following section for short pulse generation.

5.6 Sub-picosecond optical pulses generated from QDash FP laser diode with fibre based compression scheme

Pulses recorded from QDash FP LD in the previous section are characterized with a chirp of positive slope, regardless of applied filtering condition. However the magnitude of the chirp increases with the increase of the filter bandwidth. The large value of positive chirp imposed on the pulses allows introducing pulse compression scheme, based on group velocity dispersion (GVD) in a standard single mode fibre (SMF) [23]. For wavelengths around $1530\ nm$ standard SMF operates in anomalous dispersion regime, which allows in combination with proper fibre length to compensate for the initial positive chirp associated with a pulse at the input of the fibre.

5.6.1 Experimental setup and results

The SMF of $450\ m$ in length is introduced into the setup used in the former section as presented in Fig. 5.9.

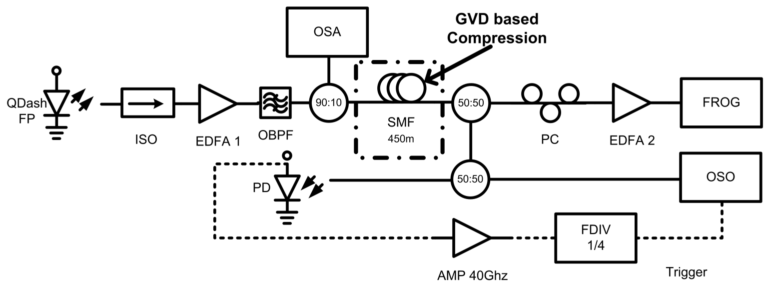

Figure 5.9: Experimental setup for investigation of the output of QDash FP laser under DC bias conditions. The $450\ m$ of SMF is introduced in order to compensate for initial chirp. Temperature is stabilized at $25\ °C$.

Optical sampling oscilloscope recorded data once again that provides with just a brief view of the pulse shape, as depicted in Fig. 5.10, however significant reduction of the pulse-width and increase of peak power from $6\ mW$ to $18\ mW$ (similarly to previous experiment the average optical power at the input of the OSO is maintained at $3\ dBm$) can be observed. Repetition rate remained unchanged at $39.8\ GHz$.

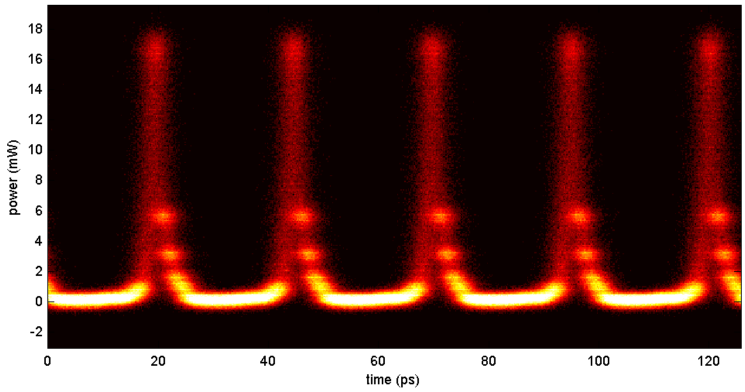

Figure 5.10: Optical sampling oscilloscope trace. Device under test biased at 350 mA, and temperature stabilized at 25 $°C$. Compression scheme based on introduction of 450 m long SMF.

In order to fully characterize the pulse parameters it is necessary to use the FROG system. Data recovered with a FROG system reveal pulse duration reduction down to 1.3 ps, for the same bias, temperature and filtering conditions (3 nm), as presented in Fig. 5.11. The magnitude of the chirp for these conditions is reduced to 20 GHz, however the slope

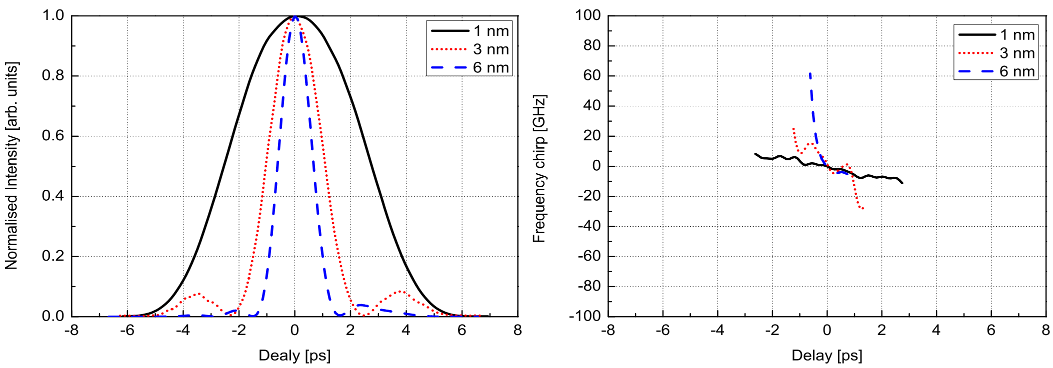

(a) Intensity profile of the optical pulses.

(b) Frequency chirp associated with the optical pulses.

Figure 5.11: Optical pulses generated from PML QDash FP LD with compression scheme engaged, resolved with the FROG system for filter bandwidths at 1, 3 and 6 nm denoted in black, red and blue colour respectively.

of the chirp is changed to negative. This suggests that the length of the SMF fibre is not fully optimized (too long in this case). This measurement was duplicated for various filter bandwidths as plotted in Fig. 5.12. Pulses of durations from 5.2 ps to as low as 700 fs are recorded for different filtering configurations. Results for the filter bandwidth at 12 nm

correspond to the setup without filtering.

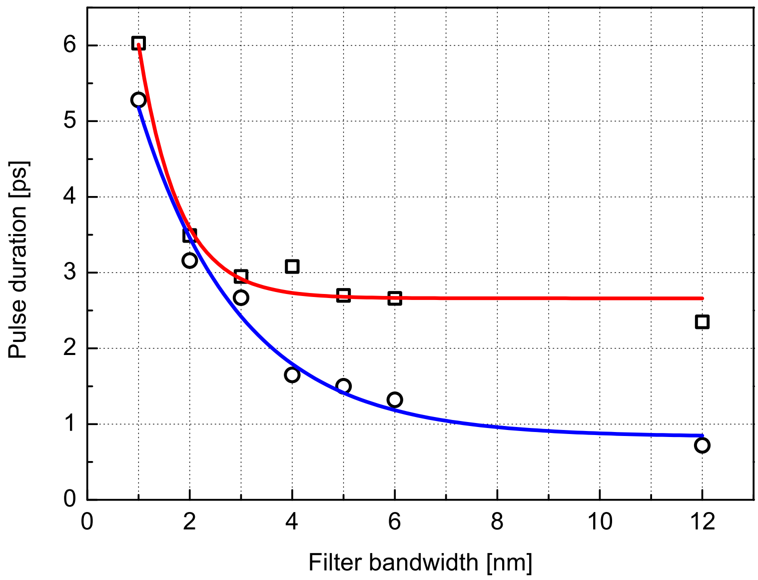

Figure 5.12: Pulse duration dependency on the bandwidth of the optical filter. Scenarios with compression scheme engaged (blue) and without (red), data points marked by circles and squares respectively. Exponential curves fitted on both datasets.

The peak powers estimated for produced pulses are in range from 19 mW for optical filter preset at 1 nm to 143 mW for unfiltered condition [12, 22].

5.7 Summary

This chapter provided the experimental evidences that basic semiconductor structures, in which signature of passive mode-locking was demonstrated previously, can serve as very short optical pulse sources, even though they require only DC bias and temperature stabilization at room conditions. By the introduction of the standard SMF fibre, opposite slopes of the fibre GVD and the input pulses chirp are exploited in order to compensate one by another. The chirp compensation results in the pulse duration reduction. A pulse-width of around 700 fs is achieved with such a compression scheme [12, 21, 22, 24].

Bibliography

[1] Y. Takita, F. Futami, M. Doi, and S. Watanabe, "Highly stable ultra-short pulse generation by filtering out flat optical frequency components," in *Lasers and Electro-Optics, 2004, Conference on*, vol. 1, p. 4 pp. vol.1, may. 2004.

[2] T. Sakamoto, T. Kawanishi, and M. Izutsu, "Widely wavelength-tunable ultra-flat frequency comb generation using conventional dual-drive Mach-Zehnder modulator," *Electronics Letters*, vol. 43, pp. 1039 –1040, sep. 2007.

[3] W. G. Wagner and B. A. Lengyel, "Evolution of the giant pulse in a laser," *Journal of Applied Physics*, vol. 34, pp. 2040 –2046, jul. 1963.

[4] J. Degnan, "Optimization of passively q-switched lasers," *Quantum Electronics, IEEE Journal of*, vol. 31, pp. 1890 –1901, nov. 1995.

[5] R. Paschotta, *Field Guide to Laser Pulse Generation*, vol. FG14. SPIE Press, August 2008.

[6] P. Ho, L. A. Glasser, E. P. Ippen, and H. A. Haus, "Picosecond pulse generation with a cw gaalas laser diode," *Applied Physics Letters*, vol. 33, pp. 241 –242, aug. 1978.

[7] G. Aspin and J. Carroll, "Gain-switched pulse generation with semiconductor lasers," *Solid-State and Electron Devices, IEE Proceedings I*, vol. 129, pp. 283 –290, dec. 1982.

[8] P. Anandarajah, C. Guignard, A. Clarke, D. Reid, M. Rensing, L. Barry, G. Edvell, and J. Harvey, "Optimized pulse source employing an externally injected gain-switched

laser diode in conjunction with a nonlinearly chirped grating," *Selected Topics in Quantum Electronics, IEEE Journal of*, vol. 12, pp. 255 – 264, mar. 2006.

[9] A. Clarke, P. Anandarajah, and L. Barry, "Generation of widely tunable picosecond pulses with large smsr by externally injecting a gain-switched dual laser source," *Photonics Technology Letters, IEEE*, vol. 16, pp. 2344 –2346, oct. 2004.

[10] R. Maher, P. Anandarajah, and L. Barry, "Generation and characterisation of 40 GHz picosecond optical pulses generated using an EAM," vol. 4, pp. 201 –204, jun. 2006.

[11] R. Maher, P. M. Anandarajah, A. D. Ellis, D. Reid, and L. P. Barry, "Optimization of a 42.7 Gb/s wavelength tunable RZ transmitter using a linear spectrogram technique," *Opt. Express*, vol. 16, no. 15, pp. 11281–11288, 2008.

[12] S. Latkowski, R. Maldonado-Basilio, and P. Landais, "Sub-picosecond pulse generation by 40-GHz passively mode-locked quantum-dash 1-mm-long Fabry-Prot laser diode," *Optics Express*, vol. 17, pp. 19166–19172, Oct. 2009.

[13] K. Merghem, A. Akrout, A. Martinez, G. Aubin, A. Ramdane, F. Lelarge, and G. Duan, "Pulse generation at 346 GHz using a passively mode locked quantum-dash-based laser at 1.55 μm," *Applied Physics Letters*, vol. 94, pp. 021107–3, Jan. 2009.

[14] J. A. Armstrong, "Measurement of picosecond laser pulse widths," *Applied Physics Letters*, vol. 10, no. 1, pp. 16–18, 1967.

[15] R. K. Jain, J. E. Brown, and W. P. Robinson, "Simple distortion-free real-time optical pulse correlator," *Appl. Opt.*, vol. 21, no. 22, pp. 4073–4076, 1982.

[16] L. Barry, P. Bollond, J. Dudley, J. Harvey, and R. Leonhardt, "Autocorrelation of ultrashort pulses at 1.5 μm based on nonlinear response of silicon photodiodes," *Electronics Letters*, vol. 32, pp. 1922 –1923, sep. 1996.

[17] K. Sala, G. Kenney-Wallace, and G. Hall, "CW autocorrelation measurements of picosecond laser pulses," *Quantum Electronics, IEEE Journal of*, vol. 16, pp. 990 – 996, sep. 1980.

[18] R. Trebino, K. W. DeLong, D. N. Fittinghoff, J. N. Sweetser, M. A. Krumbügel, B. A. Richman, and D. J. Kane, "Measuring ultrashort laser pulses in the time-frequency domain using frequency-resolved optical gating," *Review of Scientific Instruments*, vol. 68, no. 9, pp. 3277–3295, 1997.

[19] J. Dudley, L. Barry, J. Harvey, M. Thomson, B. Thomsen, P. Bollond, and R. Leonhardt, "Complete characterization of ultrashort pulse sources at 1550 nm," *Quantum Electronics, IEEE Journal of*, vol. 35, pp. 441 –450, apr. 1999.

[20] D. T. Reid, P. Loza-Alvarez, C. T. A. Brown, T. Beddard, and W. Sibbett, "Amplitude and phase measurement of mid-infrared femtosecond pulses by using cross-correlation frequency-resolved optical gating," *Opt. Lett.*, vol. 25, no. 19, pp. 1478–1480, 2000.

[21] S. Latkowski, R. Maldonado-Basilio, and P. Landais, "Short pulse generation with 40 GHz passively-mode locked Q-Dashed Fabry-Pérot laser," in *Transparent Optical Networks, 2009. ICTON '09. 11th International Conference on*, pp. 1–4, 2009.

[22] R. Maldonado-Basilio, J. Parra-Cetina, S. Latkowski, and P. Landais, "Timing-jitter, optical, and mode-beating linewidths analysis on subpicosecond optical pulses generated by a quantum-dash passively mode-locked semiconductor laser," *Optics Letters*, vol. 35, pp. 1184–1186, Apr. 2010.

[23] G. P. Agrawal, *Nonlinear fiber optics*. Academic Press, 2007.

[24] R. Maldonado-Basilio, S. Latkowski, and P. Landais, "720-fs pulse generation with 40 GHz passively-mode locked quantum-dash Fabry-Pérot laser," in *Optical Communication, 2009. ECOC '09. 35th European Conference on*, pp. 1–2, 2009.

Chapter 6

Synchronization of passively mode-locked laser diodes

6.1 Introduction

In order to improve the transmission distance, capacity, transparency, and speed of optical networks, all-optical data signal treatment techniques and systems have to be employed [1, 2], and implementation of so called 3R (re-amplification, re-timing, reshaping) regeneration functionalities by all-optical means is highly desirable [3, 4]. All-optical clock extraction is fundamental for efficient implementation of the technologies mentioned above.

The properties of passively mode-locked semiconductor lasers demonstrated in former chapters allow to find many applications for these type of devices. They can serve as opto-electronic signal generators, optical pulse sources, and can be used in electronic circuits for clock generation, etc.

In this chapter the response of the semiconductor lasers previously demonstrated to operate in passive mode-locking regime is studied. On this basis a clock extraction scheme on an all-optical basis is proposed with use of two different semiconductor laser structures.

6.2 Synchronization of the DBR LD with optical signals at 10, 20 and 40 GHz

The first device under test is the DBR laser discussed in Chapters 4 and 5 in the context of RF signal and optical pulse generation. The laser diode is mounted on a sub-carrier and placed on the probe station, bias currents to the gain and Bragg sections are supplied with two DC probes while the ground is contacted by substrate. The laser is temperature stabilized at $25\ ^{\circ}C$.

6.2.1 Experimental setup and results

The experimental setup presented in Fig. 6.1 is built in order to investigate the response of the DBR laser operating in its multimode regime to an injected optical pulse train. The external signal has a frequency close to the DBR LD free running frequency or its sub-harmonic.

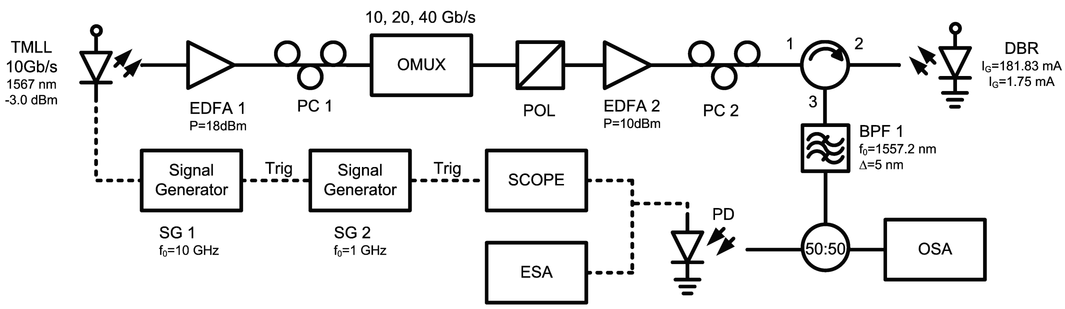

Figure 6.1: RF signal recorded at $39.7\ GHz$ with bias conditions being $I_g = 88.87\ mA$ and $I_B = 1.75\ mA$.

The $10\ Gb/s$ pulse train is generated with a tunable mode-locked laser (TMLL) source. The TMLL laser is actively locked to the reference signal from an electrical signal generator (SG 1) at the frequency of $9.98538\ GHz$. The optical spectrum of that signal and its temporal amplitude and chirp profiles are shown in Fig. 6.2.

The optical spectrum exhibits ripples separated by $10\ GHz$ with a peak located around $1567\ nm$ which is set $10\ nm$ away from the optical signal emitted by laser under test. Optical pulse streams corresponding to $40\ Gb/s$ ($39.82\ GHz$) and also its sub harmonics at

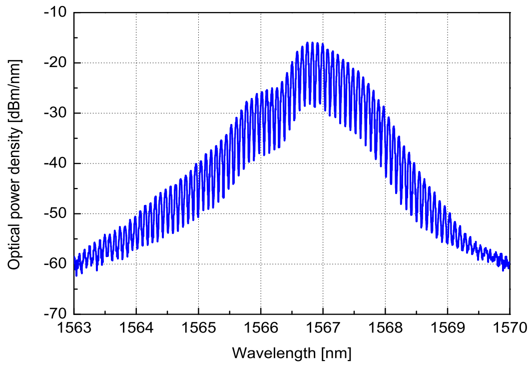

(a) Optical spectrum.

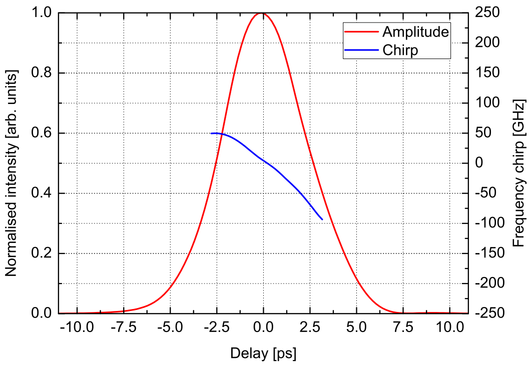

(b) Temporlal intensity and chirp profiles.

Figure 6.2: Optical pulses generated by TMLL at 10 GHz activelly locked to an external signal generator SG 1.

20 Gb/s and 10 Gb/s are generated with an optical multiplexer (OMUX) and injected into the laser under test via an optical circulator. The DBR LD is biased at conditions for which it presents multimode output and exhibits pulsation with the RF frequency at 39.7 GHz. It was demonstrated in previous chapters that such behavior in case of this laser results from a passive mode-locking process [5]. The optical spectrum from the tested laser when in free running condition is presented in Fig. 4.4. The average power injected into the tested laser is estimated to be 0 dBm after taking into account coupling losses. The optical signal from the third port of the circulator is filtered by 5 nm tunable optical band pass filter (BPF 1) and directed to the optical spectrum analyzer and 50 GHz photodetector (PD). An electrical signal from the photodetector is then observed with 50 GHz digital sampling oscilloscope (SCOPE) and 40 GHz electrical spectrum analyzer (ESA). An additional electrical signal generator (SG 2) triggered by SG 1 provides an electrical trigger signal at 1 GHz to the SCOPE. Two optical Erbium doped fibre amplifiers, EDFA 1 and EDFA 2, are used in order to boost the signal before OMUX and injection respectively. Polarization controller PC 1 and an optical polarizer (POL) are required for proper alignment and operation of OMUX and to assure uniform polarization along the produced pulse-train. Polarization controller PC 2 is used to match the injected signal polarization with a waveguide of the laser. Temporal traces of injected optical signals at different bit-rates are shown in Fig. 6.3a.

It maybe noted that all injected optical signals can be considered as an equivalent of

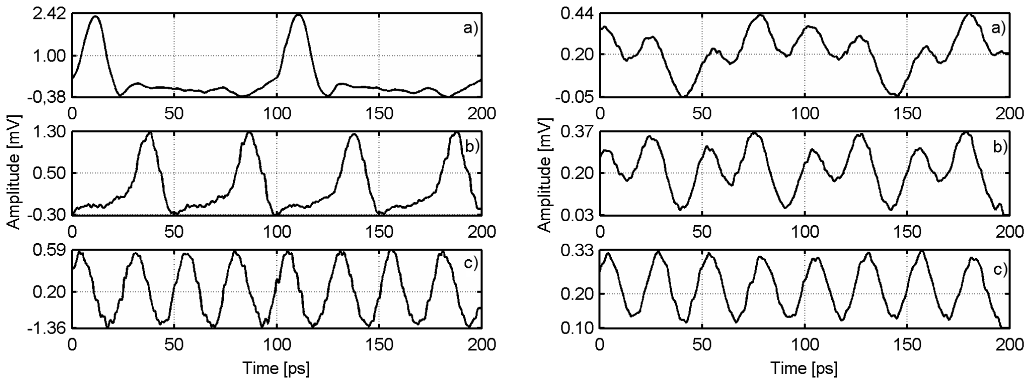

(a) Optical pulses injected into DBR LD. (b) Response of DBR LD to the injected signal.

Figure 6.3: Optical pulse trains with 10, 20 40 Gb/s repetition rates marked a, b and c respectively injected into the DBR LD and its response for these. All traces shown with offset of $2\ mV$.

40 Gb/s return to zero (RZ) data stream constructed of different data patterns in the following way:

- 10 Gb/s (a) equivalent to 40Gb/s 1000 pattern.
- 20 Gb/s (b) equivalent to 40Gb/s 10 pattern.
- 40 Gb/s (c) equivalent to 40Gb/s 1 pattern.

In the Table 6.1 the extinction ratios for 10, 20 and 40 Gb/s bit-rates are given. The extinction ratio was calculated from temporal traces retrieved with the FROG system. The

Table 6.1: Extinction ratio of source signals for variety of used bit-rates, calculated from FROG measurement data.

	Bit-rate		
	10 Gb/s	*20 Gb/s*	*40 Gb/s*
ER (dB)	34	32	32

response of the DBR LD for all injected pulse-trains recorded with the sampling oscilloscope are shown in Fig. 6.3b. The temporal traces are optically filtered at the output of the circulator. Waveforms are recorded with a scope being triggered by the original clock signal used to lock the pulse source.

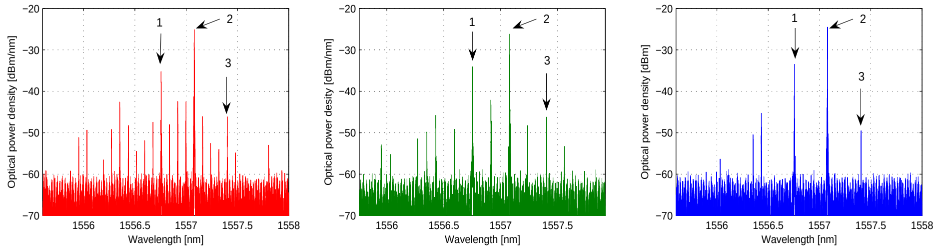

(a) 10 Gb/s. (b) 20 Gb/s. (c) 40 Gb/s.

Figure 6.4: High resolution optical spectra of the DBR laser diode output signal biased at $I_g = 150\ mA$, $I_B = 18.82\ mA$ for 0 dBm of average injected power at various bit-rates.

The spectral distribution of the DBR infrared signal is changed as depicted on Fig. 6.4. The spectra presented are recorded with a high resolution optical spectrum analyzer offering spectral resolution of 80 fm. Additional spectral components are visible along original modes marked 1,2 and 3 on all figures. The free spectral range between those modes corresponds to the clock frequency of the injected data stream.

It is worth remembering, that the injected signal has a peak at 1567 nm , hence it is separated from the DBR emission by 10 nm. In Fig. 6.4a three additional modes appear between modes 1,2 and 3. The FSR between those modes corresponds to 10 GHz, matching the bit-rate of injected signal. In Fig. 6.4b only one extra mode appears between original laser spectra, and the FSR of 20 GHz corresponds to 20 Gb/s. In Fig. 6.4c no extra modes are present, which corresponds to 40 Gb/s, however, in this case modification of the spectrum can be observed by means of the change in the power distribution among the modes and the FSR between them to 39.82 GHz. The signal injected at 1567 nm leads to alteration of the free running frequency frequency of the DBR LD according to the bit-rate injected. This proves the synchronization of the DBR LD to the bit-rate of the injected signal. Additional evidence can be concluded from the analysis of the optical linewidth of the dominant mode presented in Table 6.2. This linewidth undergoes reduction due to reduction of phase-noise associated with optical modes in result of synchronization.

Signals produced on the PD and recorded with the RF spectrum analyzer for all injected data streams and for a free running laser are presented in Fig. 6.5 for sake of comparison.

Table 6.2: Optical linewidth of the dominant mode measured for different injected data-rates at 0 dBm of average injected power.

	Free running	**Bit-rate**		
	39.7 GHz	*10 Gb/s*	*20 Gb/s*	*40 Gb/s*
Linewidth *(MHz)*	74.1	40.4	43.87	43.8

Regardless of the injected signal data rate, the DBR laser produces a spectral component

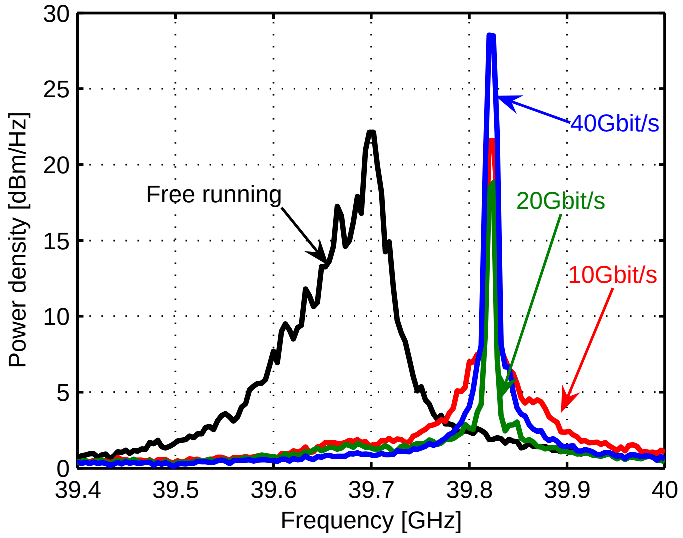

Figure 6.5: Spectral response of DBR device for injected pulse trains with 10, 20 and 40 Gb/s repetition rates marked with labeled arrows.

at frequency 39.82 GHz, with a linewidth of less than 12 MHz. By comparison with the free-running spectrum it is noticeable that the peak frequency is shifted by 120 MHz from 39.7 GHz and the FWHM linewidth is reduced by 30 MHz. The Q factor has improved from value of 1333 up to 3318. The DBR laser is synchronized by the injected optical signal for each of the bit-rates. This proves that the beat tone and the output pulse stream generated by the DBR LD is locked with original clock signal and reveals potential of this type of a laser for clock recovery at 40 Gb/s in all optical fashion from incoming data signals at 10 Gb/s, 20 Gb/s and 40 Gb/s.

The feasibility of the passively mode-locked DBR laser diode for clock extraction from various bit-streams with repetition rates corresponding to its free running frequency and its sub-harmonics have been demonstrated. In the following paragraph PML QDash LD is studied for the injection of the optical data signal with repetition rate equal to the higher order harmonic of its natural modulation frequency [6].

6.3 All optical clock recovery at 40 Gb/s with PML QDash laser diode from 160 Gb/s RZ optical data stream

The response of the QDash FP laser diode described in Chapter 4 for the injection of the optical data stream at 160 Gb/s is studied in this section. The tested laser is set on the ceramic sub-mount and placed on the probe station with two DC probes in order to provide bias and ground connections. Temperature is controlled at 25 $°C$. The optical output of the laser is coupled with lensed fibre with focal length of 3.5 μm. The response of the device is investigated in terms of feasibility for all-optical clock extraction.

6.3.1 Experimental setup and results

The experimental setup that was built in order to optically inject with data and investigate the response of the QDash FP LD is depicted in Fig. 6.6. It consists of four sections: 10 Gb/s PRBS source, bit-rate multiplication, clock extraction, and detection. The 10 Gb/s

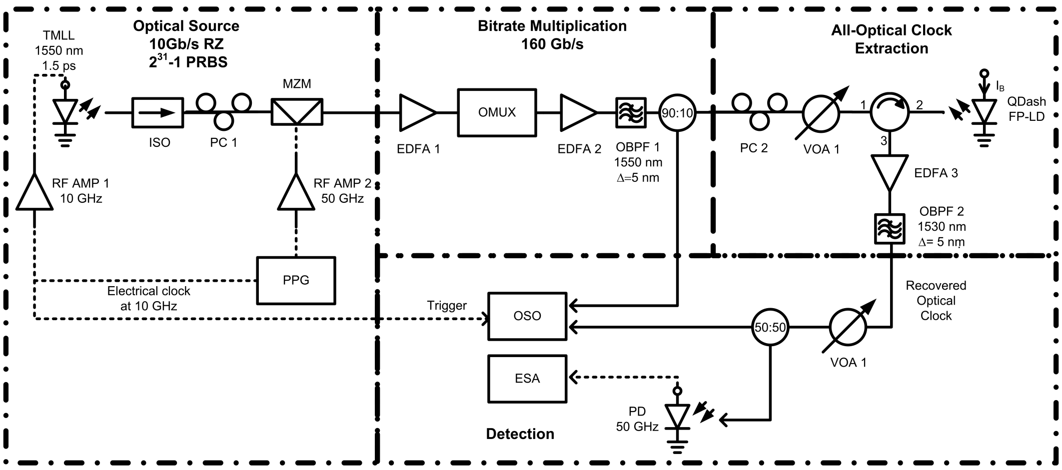

Figure 6.6: Experimental setup for demonstration of all-optical clock recovery, performed by MLLD subjected to an optical injection with a 160 Gb/s RZ ($2^{31}-1$) long data stream.

source features 10 Gb/s pulse pattern generator (PPG), which drives Mach-Zehnder optical modulator (MZM) with a data output and locks the tunable mode-locked laser (TMLL) with a 9.98 GHz clock signal. The TMLL is set to produce 1.5 ps long pulses with 10 Gb/s repetition rate. Optical isolator (ISO) secures the TMLL from back-reflections. Polarization controller allows adjusting the input signal to the MZM. At the output of this section an error-free 10 GB/s return to zero (RZ) optical data with ($2^{31} - 1$) long pseudo random bit sequence (PRBS) is provided. Additionally the electrical trigger from the PPG clock output is connected to the trigger input of the optical sampling oscilloscope (OSO). Bit-rate multiplication section consists of two Erbium doped fibre optical amplifiers (EDFA 1 and EDFA 2), optical bit-rate multiplier (OMUX), and an optical bandpass filter with 6 nm bandwidth used to suppress the amplified noise. The signal at the output of this stage at 160 Gb/s is distributed to the detection stage for monitoring of the quality of the multiplexed data, and to the clock recovery module. In the latter the signal is being injected to the QDash LD via optical circulator. A polarization controller (PC 2) and variable optical attenuator are used to optimize the polarization and the power of the signal injected into the laser diode. The QDash LD operates at bias level of 111 mA and is temperature stabilized at 25 $°C$. The output of the laser is transferred to the third port of the circulator and filtered out spectrally from the injected data signal with 5 nm optical bandpass filter centered at 1532 nm. Output of the filter is passed to the detection section where it is amplified with EDFA 3 and distributed to 500 GHz bandwidth OSO with a resolution of 0.8 ps, and 50 GHz photodetector connected to the 40 GHz electrical spectrum analyzer (ESA). The optical 160 Gb/s RZ signal at the output of the multiplication is shown in Fig. 6.7. It features a $Q_{S/N}$ factor of 5.7 dB which assures that the signal is error-free [7] after the multiplication stage. It has to be mentioned that in the context of this section the $Q_{S/N}$ factor is equivalent to signal to noise (S/N) parameter for data modulated signal and is expressed by [7]:

$$Q_{S/N} = \frac{P_1 - P_0}{\delta_0 + \delta_1} \tag{6.1}$$

with P_1, P_0 and δ_1, δ_0 being 1 and 0 levels and their standard deviations respectively.

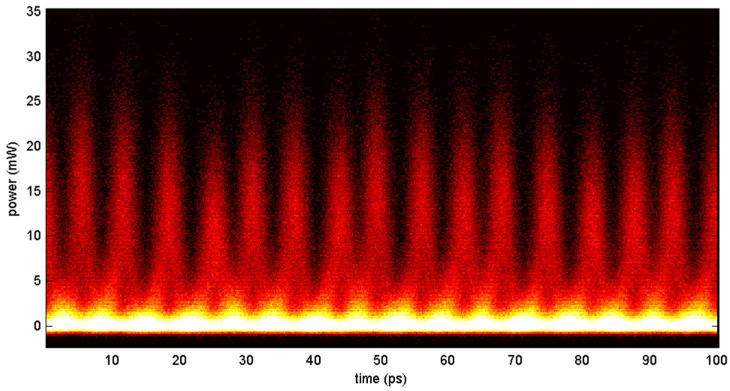

Figure 6.7: 160 Gb/s RZ Eye diagram recorded with OSO with resolution of $0.8\ ps$. The eyes feature $Q_{S/N}$ factor measured directly at $5.7\ dB$.

This optical bit stream is injected to the QDash LD with a power of $10\ dBm$ measured at the VOA - this does not include the losses on the circulator and coupling losses estimated to be at least of $6\ dB$. Electrical spectrum recorded as a response of the tested device for given injection is presented in Fig. 6.8. For the sake of comparison the spectrum under injection is overlapped with a spectrum when the device is free running - no optical injection - at the same bias and temperature conditions.

The RF signal shift can be noticed from $39.805\ GHz$ to $39.813\ GHz$ with large decrease of the FWHM linewidth, which is highlighted by a single side band (SSB) spectral noise with respect to the carrier frequency plots in Fig. 6.8b. A more detailed view of the RF peaks produced on the photodetector is shown in Fig. 6.9. The data is recorded with a resolution of $10\ kHz$ in case of the free running laser, and $10\ Hz$ for externally locked case. Reduction of the FWHM linewidth from $50\ kHz$ (measured as FWHM of a Lorentzian curve fit to the presented data) in free running condition to $8\ Hz$ when device is subjected to the injection of an external optical data stream. These results show the change of the fundamental frequency of the beat tone to a new one enforced by the external optical signal four times higher bit-rate, and large phase noise reduction due to improved inter-modal synchronization. To confirm the synchronization with the data and original clock at PPG,

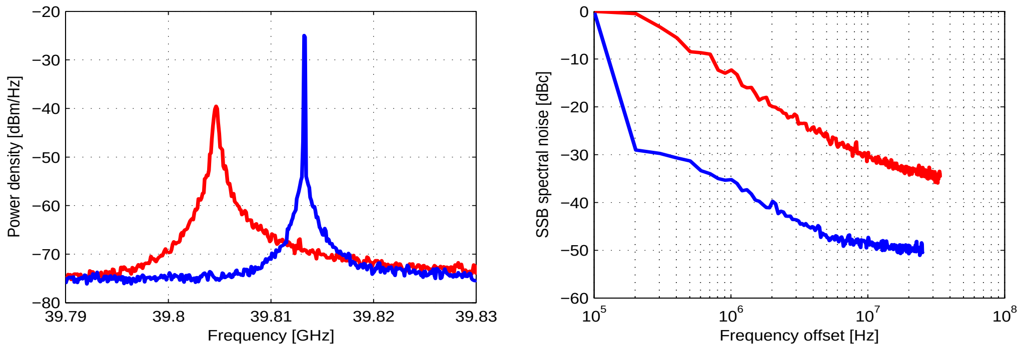

(a) RF spectra.

(b) SSB spectral noise.

Figure 6.8: RF spectra and single side band spectral noise for: free running QDash laser (red) and its response for injected pulse train at 160 Gb/s (blue). In both cases LD operates under DC-bias at 111 mA.

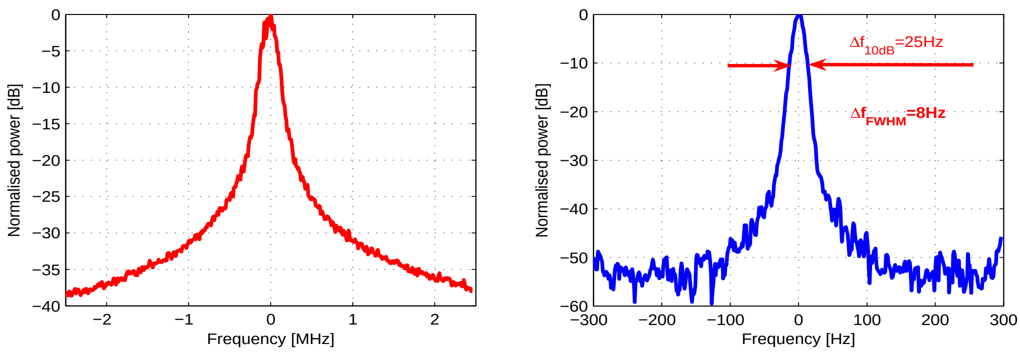

(a) Free running.

(b) Under injection.

Figure 6.9: RF spectra for: free running QDash laser (red) at 5 MHz span, and its response for injected pulse train at 160 Gb/s (blue) recorded at 600 Hz span.

the optical signal is analyzed with the OSO which uses the original electrical trigger from the PPG. The stable waveform recorded at the filtered output from the QDashed laser is depicted in Fig. 6.10. The recorded $40\ GHz$ waveform is synchronized with the original clock from the PPG. It features a $Q_{S/N}$ factor of more than $6dB$. The clock is recovered in all-optical meaning from the incoming $160\ Gb/s$ RZ data stream. Clock signal extracted in this fashion can be utilized for example in high bit-rate time division demultiplexing approaches.

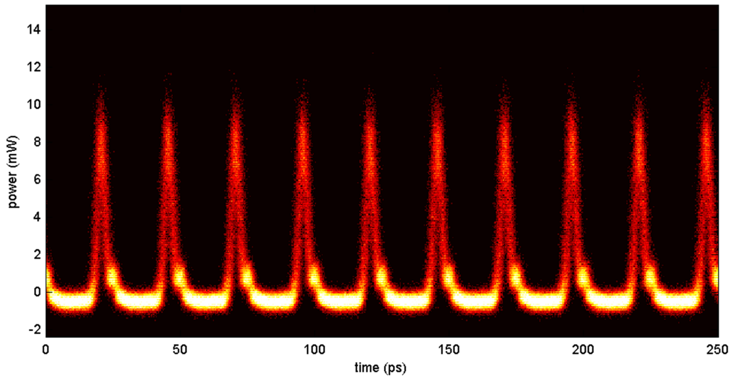

Figure 6.10: Waveform corresponding to the $40\ Gb/s$ recovered clock triggered by original electrical clock signal from PPG.

6.4 Summary

Two semiconductor lasers previously demonstrated to have a signature of passive mode-locking successfully synchronized their free running frequency to the one of the injected optical bit stream. The DBR laser can be synchronized with various bit-rates corresponding to the fundamental free running frequency of the tested laser and its sub-harmonics. The QDash FP laser employed into $160\ Gb/s$ data transmission system locks to its clock and produces the output at $40\ Gb/s$. These prove the potential of passively mode- locked laser diodes to serve as an all optical clock extraction elements, which can be further utilized in all-optical data processing schemes at high data rates.

The frequencies at which presented devices were operating so far were in the RF band

and able to respond for signal reaching the millimeter range. It is possible however, to achieve a passively mode-locked laser diodes with free spectral range within the terahertz band. This could result in generation and response for such frequencies by simple semiconductor lasers. This will be investigated in the next chapter.

Bibliography

[1] M. O'Mahony, D. Simeonidou, D. Hunter, and A. Tzanakaki, "The application of optical packet switching in future communication networks," *Communications Magazine, IEEE*, vol. 39, pp. 128 –135, mar. 2001.

[2] A. Jourdan, D. Chiaroni, E. Dotaro, G. Eilenberger, F. Masetti, and M. Renaud, "The perspective of optical packet switching in ip dominant backbone and metropolitan networks," *Communications Magazine, IEEE*, vol. 39, pp. 136 –141, mar. 2001.

[3] B. Lavigne, O. Leclerc, P. Brindel, D. Chiaroni, B. Dany, P. Guerber, D. Rouvillain, and A. Alcatel, "All-optical 3R regeneration," in *Lasers and Electro-Optics Society 2000 Annual Meeting. LEOS 2000. 13th Annual Meeting. IEEE*, vol. 2, pp. 407 –408 vol.2, 2000.

[4] B. Lavigne, P. Guerber, P. Brindel, E. Balmefrezol, and B. Dagens, "Cascade of 100 optical 3R regenerators at 40 Gbit/s based on all-active Mach Zehnder interferometers," in *Optical Communication, 2001. ECOC '01. 27th European Conference on*, vol. 3, pp. 290 – 291 vol.3, 2001.

[5] J. Renaudier, G. Duan, P. Landais, and P. Gallion, "Phase correlation and linewidth reduction of 40 GHz self-pulsation in distributed Bragg reflector semiconductor lasers," *Quantum Electronics, IEEE Journal of*, vol. 43, no. 2, pp. 147–156, 2007.

[6] S. Latkowski, F. Surre, P. Landais, and G. Duan, "All-optical synchronization of a 40 GHz self-pulsating distributed Bragg reflector laser to return-to-zero 10, 20 and 40 gbit/s data streams," *Optics Communications*, vol. 282, pp. 2053–2058, May 2009.

[7] G. Bosco, A. Carena, V. Curri, R. Gaudino, P. Poggiolini, and S. Benedetto, "A novel analytical approach to the evaluation of the impact of fiber parametric gain on the bit error rate," *IEEE Transactions on Communications*, vol. 49, no. 12, pp. 2154–2163, 2001.

Chapter 7

Terahertz signals generation by passively mode-locked laser diode

7.1 Overview and motivations

The multimode semiconductor lasers presented in previous chapters allow for the generation of signals with repetition rates related to the free spectral range (FSR) among the longitudinal optical modes present at their optical output. The bandwidth of the material gain provided by optically active semiconductor material is sufficient to support optical modes separated by a frequency of several gigahertz. Would the dynamics of the gain in semiconductor suffice to respond at the detuning of a few THz? With an appropriate longitudinal mode selection mechanism a laser diode should provide a discrete mode output with FSR in terahertz band. However, would it be possible to observe a THz signal and passive mode-locking? Such questions will be answered in this chapter.

The following sections discuss briefly terahertz technology, and its importance in various disciplines of science is stressed. The slotted Fabry-Pérot laser diode operating in multimode regime with terahertz separation frequency is demonstrated. Generation of a THz beat tone on an ultra fast photomixing element, along with a direct emission of such radiation by these type of semiconductor lasers will be studied.

7.2 Introduction: Terahertz technology

The term *terahertz* was firstly used in 1970 to describe the frequency range of the emission of a $HeNe$ laser. Nowadays, the terahertz term refers to the submillimeter-wave energy that falls into the wavelength range between 30 μm and 1000 μm that corresponds to frequencies of 300 GHz to 10 THz, as presented in Fig. 7.1. This range fills the gap in the electromagnetic spectrum between microwaves and far infrared. While the bottom limit with millimeter-wave band is quite precisely defined by components with upper operating frequency reaching 300 GHz, the top border is not well defined and can vary in publications from 3 THz to 10 THz [1].

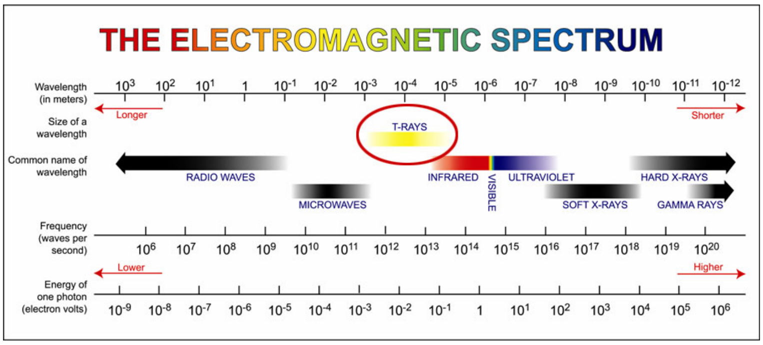

Figure 7.1: The terahertz band in a view of broad electromagnetic spectrum. Source: *www.advancedphotonix.com*.

For many years the terahertz band, despite being of interest to scientists since 1920, has remained nearly unexplored when compared to other parts of the EM spectrum [1]. Predominantly this is due to little commercial support for terahertz systems, as signals at these frequencies have very limited atmospheric propagation compared to microwave and optical bands. The term terahertz gap is often used to highlight that fact. The only areas incorporating terahertz technology were high resolution spectroscopy and remote sensing for characterization of thermal emission lines for a variety of lightweight molecules. In such context the amount of information provided could not be matched with other parts of EM spectrum. A lot of effort of research centers have been put towards improvement of the detectors and sources covering terahertz band, and these allow for the emergence of THz technology beyond the strictly scientific areas into commercial applications i.e. medical examination, quality control or security screening systems.

7.2.1 Terahertz applications

The photon energy band between 1.2 and $12.4\ meV$, or in term of wavelengths from $1\ mm$ to $100\ \mu m$, corresponds to black body temperature between 14 and $140\ K$, below that of ambient background temperature on Earth. Spectral traces of interstellar dust clouds in that range contain a lot of spectral lines attracting the attention of astronomers and their interest in terahertz sensors. Another astronomic application for terahertz sensors is the observation of planetary and small-body (moons, asteroids and comets). Atmospheric compositions and dynamics of these bodies are useful in modeling Earth's atmosphere and gives insight into the evolution of the solar system [1]. Terahertz systems are often used in plasma fusion diagnostics. Data like electron density as a function of time and position in a plasma core, and power spectrum temperature distribution along plasma radius can be retrieved with different measurement techniques. Sub-millimeter spectroscopy is one the oldest areas exploiting the terahertz signals. Measurements are performed with broad-band Fourier transform spectrometers with use of thermal sources and bolometric detectors [1]. Many of the following technologies like heterodyne instrumentation and more modern direct detectors originate from this field. An advantage of sub-millimeter-wave spectroscopy is that lighter molecules have very strong emission or absorption lines due to rotational and vibrational excitations which peak in the sub-millimeter band. Radar and communications applications are severely limited by the atmospheric opacity at terahertz frequencies. However, inter-satellite transmission systems can benefit from a smaller antenna size than that for radio-frequency needed to produce highly directional beams and large bandwidths offered by terahertz carriers. Stratosphere operation is advantageous for terahertz communication or radar systems because of low scattering and better penetration through the dust or clouds compared to IR and optical wavelengths [1]. Use of terahertz sources to illuminate scale sized models of large objects to simulate radars signal scattering that would be obtained at lower frequencies on objects of actual size was proposed [2]. The cost of such a system is attractive when compared to real dimensions anechoic chambers [1]. One of the most vibrant applications, especially from a commercial point of view, is terahertz time domain spectroscopy or T-ray imaging [3, 4]. This technique, by processing measurements of transmitted or reflected terahertz energy incident on the sample, reveals spectral content, time of flight and direct strength for imaging. The principle involves generation and detection of EM terahertz transients. By scanning the delay line and simultaneously gating or sampling the terahertz signals incident detector, a time domain waveform proportional to the terahertz field amplitude and containing the frequency response of the sample is produced [1]. Scanning either the generator or the sample allows the building of two dimensional images over time. T-ray imaging system are attractive tools for medical examination [5–7] and security screening [8–10]. Nowadays terahertz EM radiation is considered to be harmless, and non-destructive for probing of biological materials or electronic parts.

7.2.2 Terahertz components

Components that are used in terahertz applications fall mainly into two categories: sensors and sources. However, guiding structures, quasi optics, antennas, filters and sub-millimeter materials are also important contributors.

7.2.3 Detectors

Critical parameters for detection at terahertz frequencies are low photon energies between 1 and 10 meV that result in a need for cryostatic conditions for detector operation, long integration time radiometric techniques or both in order to reduce the effect from ambient thermal noise which naturally dominates emitted narrow-band signals. A large Airy disk diameter (hundreds of micrometers) makes it necessary to use a mode converter or antenna between signal and detector element [11]. Most common sensors are based on heterodyne detection since the dominant area for terahertz technology was high resolution spectroscopy. However this is changing and more emphasis is put towards direct detection techniques and components.

7.2.3.1 Heterodyne semiconductor detection

Signal acquisition is accomplished by signal frequency down-conversion where a signal in the THz range is converted to the RF range, and post amplification at lower frequency. A Schottky diode mixer is the preferred down converter for the terahertz range. This technique requires a local oscillator (LO) operating at terahertz frequency (narrowband terahertz source - FIR gas or more recently quantum cascade laser - in order to achieve intermediate frequency (IF) in RF range.

7.2.3.2 Heterodyne superconductor detection

High sensitivity detectors rely on cryogenic cooling for terahertz operation. Several superconducting detectors have been developed based on the Josephson effect [12], superconductor - semiconductor barriers (super Schottky) [13], and bolometric devices. However, the superconductor - insulator - superconductor (SIS) tunnel junction mixer has become an equivalent to the Schottky diode down converter in terms of operational frequencies. The current flow mechanism is based on photon-assisted tunneling [14]. Similarly to the Schottky diode, the SIS mixer relies on high nonlinear VI characteristic. The advantage of the SIS mixers is their low LO power requirement in comparison with Schottky diodes.

An alternative to the SIS mixer is the transition-edge or hot electron bolometer (HEB) mixer [15]. Modern HEB mixers are based on micro-bridges of niobium niobium-nitride, niobium-titanium-nitride and more recently aluminum and ytterbium-boride-copper-oxide ($YBCO$) based materials that respond thermally to terahertz radiation. Micrometer or even smaller sized HEB devices can operate at very high speeds through fast photon or electron cooling [16]. Required LO power is even lower than in case of SIS mixers being at 1 to 100 nW range and operation above 5 THz has been reported [17].

7.2.3.3 Direct detectors

For applications that do not require ultrahigh spectral resolution, heterodyne systems are being replaced by direct detectors, for example: Small area $GaAs$ Schottky diodes [13] used as antennas, coupled square-law detectors, conventional bolometers based on direct thermal absorption and change of resistivity, composite bolometers with thermometer or readout integrated with the radiation absorber, micro-bolometers using antenna to couple power to a small thermally absorbing region [14, 18, 19], and Golay cells. The last ones are based on thermal absorption and expansion of a gas in a sealed chamber. The changes in the volume via displacement of a mirror in an optical amplifier or an acoustic bolometer, are detected and monitor the change in pressure of heated air cell using photo-acoustic detector, and a fast calorimeter [20] based on single-mode heating of an absorber filled cavity.

7.2.4 Sources

The most difficult component to realize in sub-millimeter system is a source. There are a few reasons for such a situation. Traditional electronic solid-state devices based on semiconductor materials, i.e. oscillators and amplifiers are limited by parasitic and transit times that cause frequency roll-off and resistive loss effects become too high at such wavelengths. Tube sources suffer from physical scaling problems and they need extremely high electric and magnetic fields as well as high current densities. Optical style sources like solid-state lasers must operate at cryogenic cooling conditions to operate at low energy levels ($\sim meV$) [1]. Successful techniques for terahertz signal generation are based on frequency conversion, either up-conversion from RF signal or downconversion from optical signal. This is realized by laser to laser pumping (far-IR to sub-millimeter downconversion) or with use of Schottky diodes multiplication (up-conversion from RF band). Other approaches to achieve narrow-band terahertz power involve: optical mixing on nonlinear crystals [13, 14], photomixing [15, 19–21], picosecond laser pulsing [22, 23], laser sideband generation [24, 25], inter-sub-band and quantum cascade lasing [26, 27], direct semiconductor oscillation with resonant tunneling diodes [28–30], direct lasing gases [31], and Josephson junction oscillations [32].

7.2.4.1 Upconversion techniques

The most common technique to produce power above the microwave band is through non-linear reactive multiplication of lower frequency oscillators [1]. The most reasonable approach is to multiply and amplify from microwave frequencies (20 GHz to $40GHz$) available through voltage controlled oscillators (VCO) or dielectric-resonator oscillators (DRO) and millimeter wave up-converters. W-band (75 GHz -110 GHz) InP MMIC power amplifiers [33] are commercially available, able to achieve 300 mW to 400 mW at 100 GHz frequency. In order to convert from W-band to terahertz frequencies through solid state up-conversion, several octaves must be covered. As higher order multipliers ($> \times 4$) offer poor conversion efficiency, the most efficient solutions are based on series chains of doublers or triplers. Multiplied planar $GaAs$ Schottky barrier diodes mounted on single-mode waveguide are used in most of today sources [34]. Small electrical size and assembly constraints led to some extremely low loss device topologies [35]. In addition, for high order multiplying due to low efficiency of the power handling capacity of the first few stages of the chain [1] - a multiple of elements in series can be added to even the heat and voltage distribution. Multiplier chain driven by amplified source at 100 GHz has reached $1.2\ THz$ with 75 μW at room temperature conditions and 250 μW when operated at 130 K.

7.2.4.2 Tubes

Terahertz tube sources [36] are based on emission from bunched electrons spiraling about in strong magnetic fields: backward-wave tubes or carcinotrons offer the most power and wavelength tunability at sub-millimeter range. Bench top commercial units can reach to $1.2\ THz$ with mW levels of power, but coupling to actual antenna suffers from multimode output of the tube - power coupled can be 1/1000 compared to total output power. Available tubes operate at voltages from 2 to 6 kV, and a magnetic field around 1 T can be achieved from samarium cobalt permanent magnets. They can sweep the range over ten gigahertz at kilohertz rates. Lifetime of such devices is less than a few thousands of hours which increases their cost, however there are some efforts to refresh klystron or other tube configurations with modern monolithic fabrication techniques [36, 37].

7.2.4.3 IR-pumped gas lasers

Another commonly used source at terahertz frequencies is the IR-pumped gas laser [1]. Constructions are usually based on grating tuned CO_2 pump lasers at 20 to 100 W injected power into low-pressure flowing-gas cavities that lase to produce terahertz signals [1]. Power levels of 1 to 20 mW can be reached based on the chosen emission line - one of the strongest emission lines is from methanol at 2522.78 GHz. Not all frequencies in THz regime are covered by strong emission lines and some gases are very toxic. Nonetheless, gas lasers are used in spectroscopy and as terahertz local oscillators (LO) in receivers [38, 39].

7.2.4.4 Sideband sources

A harmonic generator driven by a laser - far infrared (FIR) gas laser - mentioned in the previous paragraph to create side band source [25, 40], offers more flexibility in tuning compared to IR-pumped gas lasers.

7.2.4.5 Quantum cascade lasers

Direct semiconductor terahertz laser sources based on inter-sub-band transitions and quantum cascade lasers [41–43] are also a source of THz radiation. Most of these lasers require temperature cooling. Most recent lasers target a frequency range around 3 THz at temperature controlled at 164 K in a pulsed mode operation and at the temperature of 117 K with CW operation. For these lasers, the temperature increase results in a large decrease of emitted power [44]. The incorporation of large second-order susceptibility into the active region of that type of lasers operating in dual-wavelength mode allows the generation of THz signals corresponding to the difference-frequency. This will eventually allow operation at room temperature conditions [45].

7.2.4.6 Optical regime downconversion

One of the most successful commercial technique to generate terahertz energy is downconversion from optical regime. Two principal methods have been exploited to produce both narrow and broad-band signals. Photomixing [15, 21, 46], uses the difference frequency of two locked CW lasers focused onto a small area of a photoconductor with very short (less than 1 ps) carrier lifetime, e.g. low temperature grown $(LTG) - GaAs$, to photo-generate carriers between less than 1 μm spaced electrodes acting as a source and a drain. These electrodes are printed on the semiconductor material. The induced photo-carriers produce a photocurrent modulated at the lasers detuning frequency. This current is coupled to an RF circuit or to the antenna that couples or radiates the terahertz energy [1]. The resulting signal is characterized by a narrow bandwidth, eventually phase-locked and tunable over the full terahertz span by shifting the optical frequency of one of the lasers. The optical to terahertz frequency conversion efficiency is less than 10^{-5} for a single device [46], and it decreases with the increase of the frequency - maximum output power of 1 μW at 1 THz drops to 0.1 μW at 3 THz. The temperature cooling and stacking of photomixers, and or improving the semiconductor materials can lead to a better conversion efficiency and maximum power. The resulting narrow-band and tunable THz signal generated with such a device, can find applications mostly in areas like radiometry and communications [47]. A second optical approach to produce the terahertz radiation is based on femtosecond ultra short optical pulses illuminating a photo-conductor such as silicon-on-sapphire or $LTG\ GaAs$ confined between two electrodes. The generated carriers are accelerated by an applied electrical field (less than 100 V). The resulting current surge, which is coupled to an antenna, has a broad frequency spectrum corresponding to the optical pulse duration, i.e. terahertz rates. Similar results can be achieved by applying short optical pulses to a crystal with strong second order susceptibility χ^2 (field induced polarization) such as zinc telluride [48]. Due to higher order susceptibility nonlinear response, this produces time varying polarization with frequency response linked to the pulse duration time, i.e. terahertz frequency. T-ray systems are based on this technique [47, 48]. Similarly to the photomixing technique, energy can be radiated from antennas printed on semiconductor antennas. Typical frequency range is between $0.2\ THz$ and $2\ THz$, or higher depending on laser pulse parameters. Average powers over the entire spectrum are very low: between nanowatts and microwatts with pulse energies in the femtojoule to nanojoule range [1].

The discussion in further parts of this chapter with respect to terahertz signal generation by passively mode-locked laser diodes, will rely on the optical regime downconversion presented in this section, regardless of particular implementation: indirect via photomixing, or direct due to intra-cavity effects.

7.3 Dual-mode slotted Fabry-Pérot laser diode with THz free spectral range

A laser diode similar in structure to the one described in Chapter 4 is investigated. It is a single cavity device featuring multimode output with a free spectral range of 372 GHz. Such frequency falls into the terahertz band. Static and dynamic characterizations of the laser diode are performed. The device is mounted in T0 packaging and settled in a temperature stabilization block, as shown in Fig.7.2. Through all testes device is operated under DC bias conditions and temperature controlled at 25 $^{\circ}C$.

7.3.1 Laser under test structure

A single cavity semiconductor device based on multi quantum well (MQW) structure formed of five quantum wells is shown in Fig.7.3. The wells are 6 nm thick and based on $AlGaAsIn$ compound and the barriers are 10 nm thick and made of $AlGaAsIn$. The device is 350 μm long, with 2.5 μm wide slotted ridge waveguide. Slots are implemented as shallow etched grooves at the top of the ridge - they do not reach the active region, however, they are able to cause a change in the value of the refractive index underneath. The introduced slot pattern allows the laser to operate in stable dual-mode regime under DC bias conditions with mode separation of 372 GHz [49]. . The laser diode was designed, and manufactured by Eblana Photonics, Ireland.

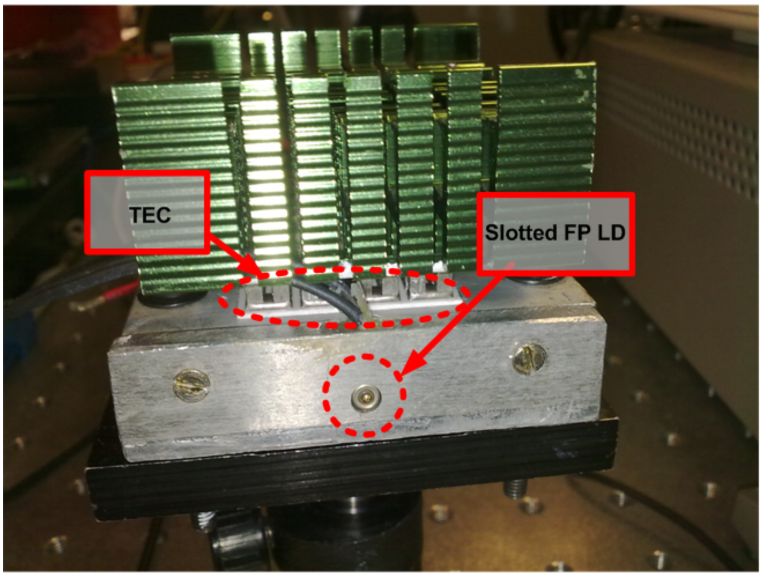

Figure 7.2: Slotted FP LD in temperature control block based on thermoelectric cooler (TEC). Through all measurements the laser is maintained at $25\ ^{\circ}C$.

7.3.2 Steady state characterizations

Initially the laser diode is characterized under continuous wave (CW) operation. Through all experiments the laser under test is supplied with a DC-bias and temperature stabilized at $25\ ^{\circ}C$. Control of current source and measurement data acquisition and presentation is supported by programs written in LabView© and Matlab© environments. Characterizations of dynamics in the laser are carried out in further sections of current chapter.

7.3.2.1 Experimental setup

The experimental setup used for steady state characterizations is shown in Fig.7.4. The tested laser is mounted in a temperature control block as shown in Fig.7.2, and temperature held at $25\ ^{\circ}C$. The optical output is coupled with a lensed optical fibre placed in a fibre holder on a three-axis micropositioning stage. An optical isolator (ISO) prevents reflections from other parts of the setup. An optical coupler distributes the collected optical signal among optical power meter (OPM) and optical spectrum analyzer (OSA). The voltage across the laser is directly read out for the current source.

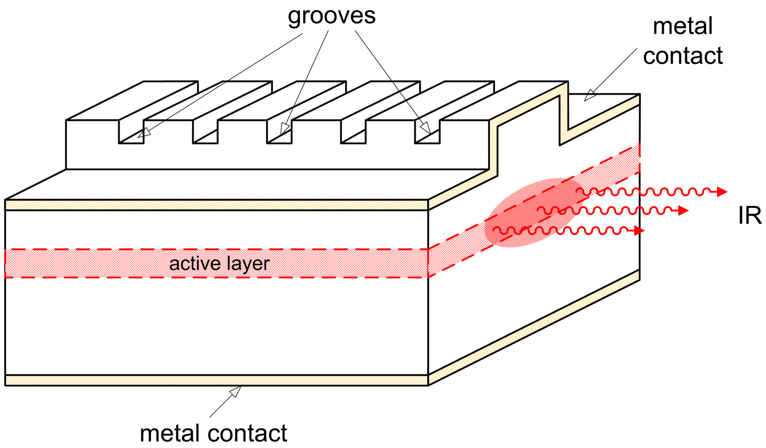

Figure 7.3: Slotted Fabry-Pérot laser schematic structure of the device, scale not maintained. The length of the laser's cavity is of 350 μm.

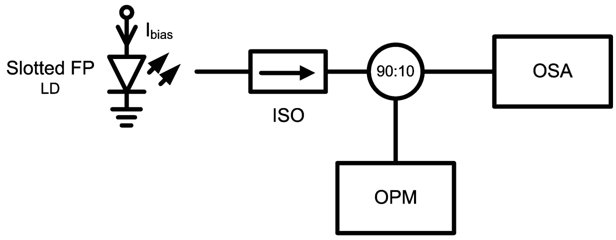

Figure 7.4: Experimental setup used for steady state characterizations of the slotted FP laser diode. Device is DC biased and temperature stabilize at 25 $°C$.

7.3.2.2 Voltage vs bias current and optical power vs bias current characteristics

With the slotted Fabry-Pérot structure the voltage across device and optical output power were measured as a function of applied DC bias current. The voltage across the laser junction versus current characteristic (VI) is presented in Fig.7.5. The voltage drop across the laser reaches a maximum value of 1.6 V at 100 mA. The impedance is ranging for 70 Ω to 18 Ω in the examined bias currents scope. The optical power versus injected current curves (LI) in Fig.7.5, indicate the threshold current at $I_{th} = 18\ mA$. The LI curves are taken by both increasing and decreasing the bias current in the range from 0 mA to 100 mA. There is an overlap between these LI curves, hence there is no spurious saturable absorber section in the device, which might be at the origin of the laser mode-locking.

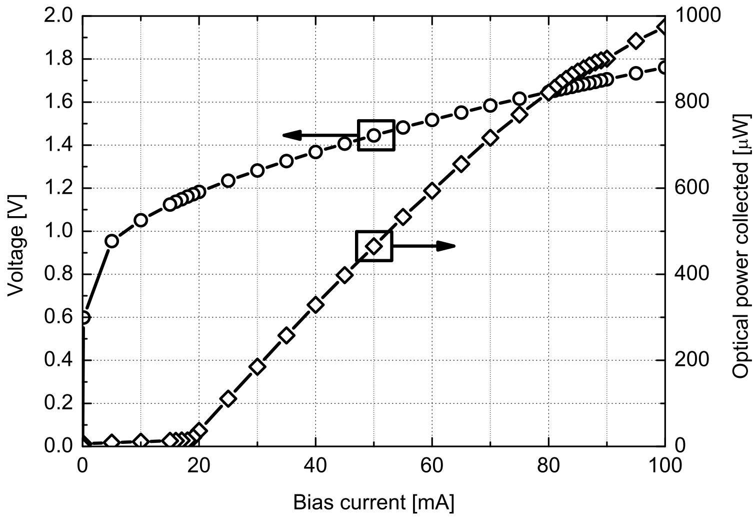

Figure 7.5: The VI and LI curves measured with temperature stabilized at 25 $°C$, marked with circles (○) and diamonds(◇) respectively.

7.3.2.3 Spectral characterization

The optical spectrum is recorded with a standard optical spectrum analyzer offering 5 GHz of optical resolution. Laser diode bias current is set at 88.7 mA and temperature is controlled at 25 $°C$ and the collected data is shown in Fig.7.6.

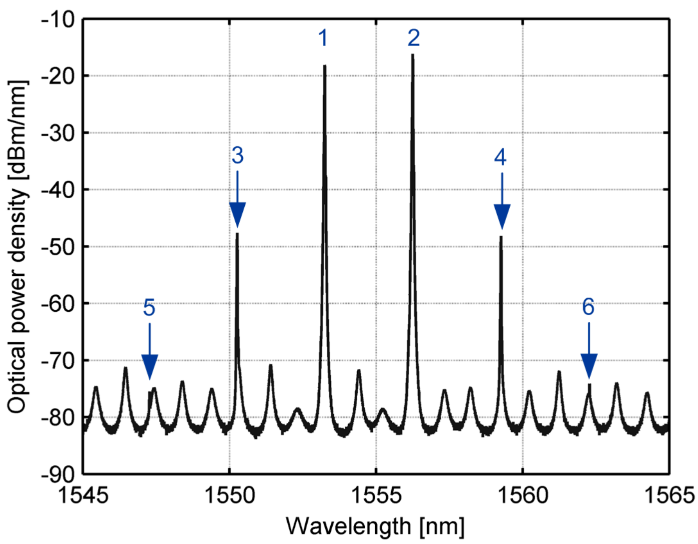

Figure 7.6: multimode operation, optical spectrum recorded for $I_{Bias} = 88.7\ mA$ at at temperature maintained at 25 $°C$.

With above bias and temperature conditions the device operates in a stable multimode regime with power distributed almost evenly among both dominant modes. The two dominant modes (denoted 1 and 2 on the figure) are localized at $1553\ nm$ and $1556\ nm$ respectively with a separation of $3\ nm$ which corresponds to the frequency of $372\ GHz$ at this wavelengths. Background ripples separated by $1\ nm$ correspond to Fabry-Pérot resonance of a $350\ \mu m$ long device with a 3.5 refractive index. Two lateral modes marked 3 and 4, on both sides of the dominant ones are pulled out of central positions of the Fabry-Pérot resonant ripples visible at the background of the spectrum. This is evidence of strong FWM nonlinearities affecting the optical signal inside the cavity, which acts as a passive mode-locking mechanism. Additional products of FWM effects numbered 5 and 6, can be seen at a further distance from the dominant modes, which is twice the free spectral range between them. These, however, are unable to initiate the lasing - these can be a result of the lack of the gain and/or suppression of these wavelengths by the slot pattern used. The separation between longitudinal modes is beyond $100\ GHz$ so FWM is dominantly benefiting from carrier heating (CH) and spectral hole burning (SHB) nonlinearities. With use of LabView© based control software precise control of the provided bias current and monitoring of the temperature conditions is accomplished. A set of optical spectra is collected as a function of bias current as presented in Fig.7.7.

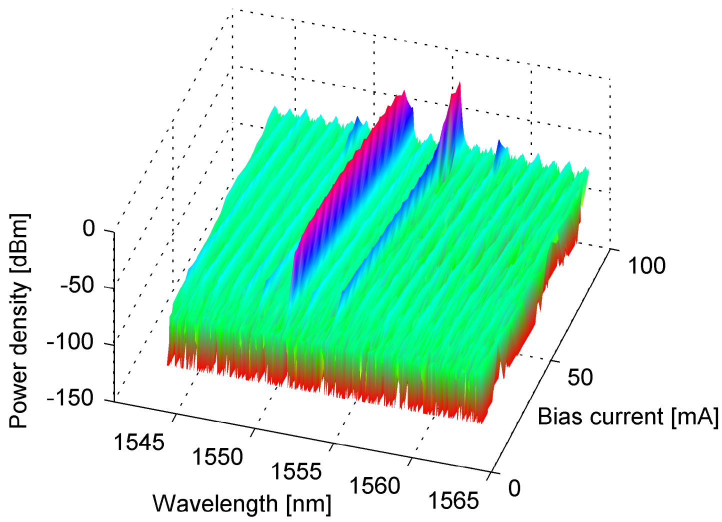

Figure 7.7: Optical spectrum evolution with increase of the bias current. Temperature stabilized at 25 $°C$

The spectral evolution of the optical output of the slotted FP LD can be observed. For all the currents above the threshold the device operates in multimode regime, for the currents ranging from 85 mA to 95 mA the power is balanced among dominant modes, the nonlinear interactions are enhanced and further lateral modes appear.

7.3.2.4 High resolution optical spectrum analysis

With a similar experimental setup where the standard optical spectrum analyzer is being replaced with a high resolution instrument - 'BOSA' by Arragon Photonics © - the spectral width of the optical modes can be measured. The optical output of the laser under test when it operates in dual-mode conditions is recorded with 10 MHz of the optical resolution, and presented in Fig.7.8.

The FSR between all optical components corresponds to a frequency of 372 GHz. The FWHM linewidths are measured directly at 3 dB drops from the maxima. They vary from 14 MHz at shorter wavelengths to 161 MHz at the longer wavelength parts of the spectrum. The summary linewidth of all optical modes is measured at $\sum \Delta\nu_{opt} = 246\ MHz$.

Measurements presented in this section show that the laser under test is able to oper-

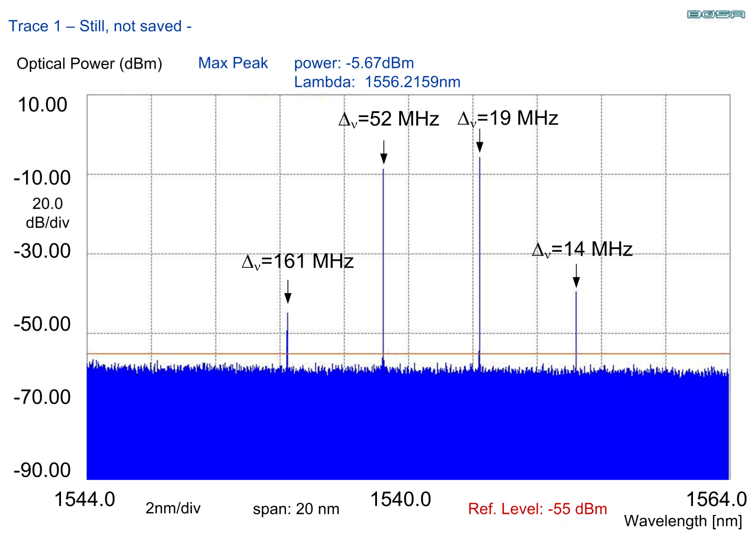

Figure 7.8: High resolution optical spectrum recorded with BOSA® system recorded at dual-mode operation conditions.

ate in a stable multimode regime for a wide range of bias currents at room temperature conditions. All longitudinal modes originate from the same optically active semiconductor medium which induces nonlinear relations between them. Optical spectra recorded for currents where the optical power is evenly distributed among the modes contain features resulting from four wave mixing nonlinearities. These are clearly visible on both sides of the dominant modes at the spacing corresponding to the integer multiples of the FSR between them. In order to investigate the impact of these nonlinear intra-cavity interactions on the optical signal emitted from such multimode laser, some dynamic characterizations are carried out in the following section.

7.4 Terahertz modulations in optically active semiconductor material

It was demonstrated in the previous section that optical modes originating from single laser diode undergo nonlinear mutual interactions inside the laser cavity. These interactions of the optical fields result in a process of four wave mixing. The FWM in optically active semiconductor material is associated with modulation of that material at the separation frequency between optical components. Dynamic characterizations of the slotted FP LD are carried out in this section in order to identify such intra-cavity modulations and their impact on the optical output of the laser.

7.4.1 Intracavity modulations in the semiconductor laser through FWM effect at 372 GHz

In order to identify the intra-cavity modulations at terahertz frequencies in the slotted FP LD introduced previously in this chapter, the CW injection scheme presented in Fig.7.9 is used. The device under test (DUT) operates at $90.25\ mA$ and is temperature stabilized at $25\ ^{\circ}C$. The optical output from the tested laser diode is coupled with lensed fibre with focal length of $3.5\ mm$ connected to the second port of optical circulator - injected CW probe beam from the tunable external cavity laser (ECL) follows the same patch but in opposite direction. The optical isolator (ISO) prevents back-reflections from the setup to the ECL. The CW signal from the ECL is provided via the optical polarization controller (PC) to the first port of the circulator. The polarization of the injected beam is adjusted to match the polarization of the laser's waveguide for optimum interaction with the optical fields inside the cavity. A standard optical spectrum analyzer working in increased sensitivity mode

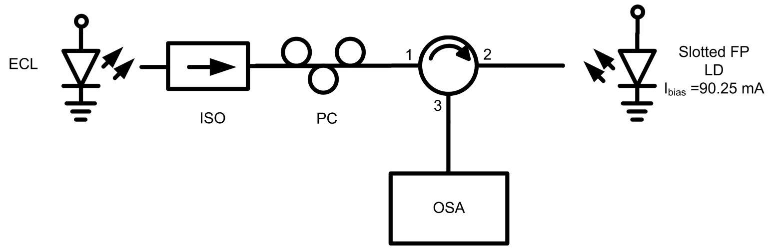

Figure 7.9: Dual-mode slotted FP LD subjected to injection of CW signal from tunable ECL source. DUT operates in stable dual-mode regime, with bias at $90.25\ mA$ and temperature stabilized at $25\ ^{\circ}C$.

with optical resolution of $0.02\ nm$ ($2.5\ GHz$ at $1550\ nm$) is used to monitor the output from the tested LD at the third port of the optical circulator. In the Fig.7.10 the optical spectrum collected from the laser under test without the CW signal injected is shown. For these bias and temperature conditions the laser operates in stable multimode condition with

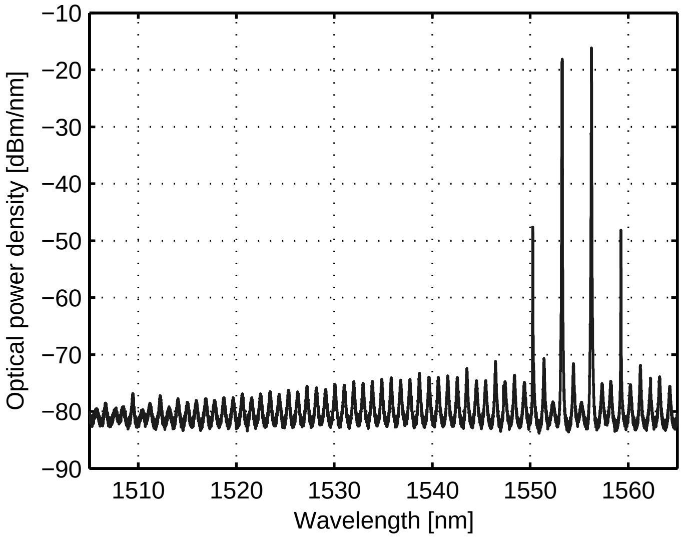

Figure 7.10: Optical spectrum collected from DUT when it is DC biased at $90.25\ mA$ and temperature controlled at $25\ °C$.

four modes clearly above the background level. The background consists of FP resonant ripples separated at around $123\ GHz$. The power distribution among the two dominant modes is slightly unbalanced, however at these conditions original emission is maintained at this part of the spectrum when the laser is subjected to the optical injection of the probe beam. The probe beam is a CW signal from the ECL at $1509\ nm$ with a nominal linewidth of 100 kHz. The wavelength of the probe beam is chosen in order to keep it sufficiently far from the emission of the tested laser, and to avoid possible additional beat components that could result from the beat between probe signal and the original modes from tested device. Injected CW signal has a power of $5.5\ dBm$ measured at the output of the ECL. Spectra recorded at these conditions are presented in Fig.7.11. After injection of the probe beam two modulation sidebands appeared in the surrounding of CW signal. They are equidistant from the probe signal at the frequency of $372\ GHz$ which is the same as the free spectral range between the two dominant modes originally present at the output of slotted FP LD. This proves the intra-cavity modulation of the optically active semiconductor material with the frequency corresponding to the detuning frequency of the longitudinal modes in the multimode semiconductor laser.

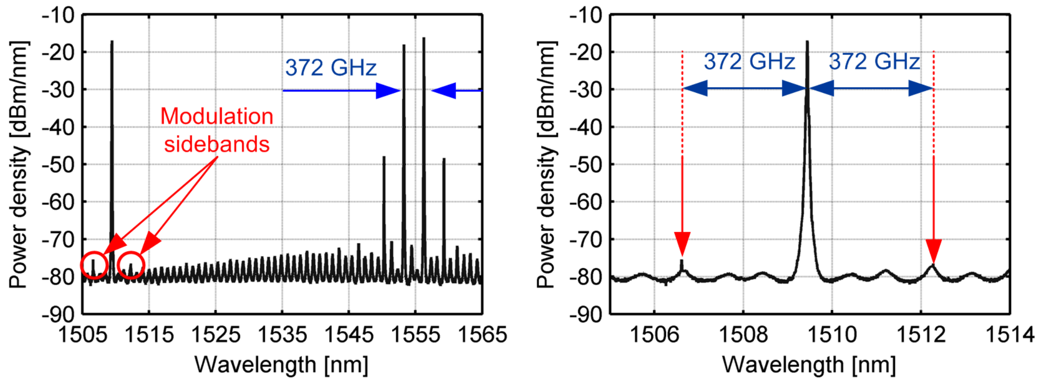

(a) Full span including original modes.

(b) Magnification of injected CW signal.

Figure 7.11: Optical spectrum collected from tested laser when subject to the injection or CW probe signal at $1509\ nm$ and $5.5\ dBm$.

In the next section a laser of similar structure with free spectral range of $1.1\ THz$ is tested in the same fashion.

7.4.2 Slotted FP laser diode with intra-cavity modulation at 1.1 THz

The slotted FP LD is structurally identical with the laser introduced and characterized in Chapter 4, except for the number and placement of the slots. The infrared output presented in Fig.7.12 is collected with a standard $5\ GHz$ optical resolution OSA. The laser diode was manufactured by Eblana Photonics, Ireland, with a customized (by author's group) waveguide slot pattern. The recorded spectrum at $67\ mA$ features two dominant modes separated by frequency of $1.1\ THz$. Additional lateral modes indicating four wave mixing interactions inside the laser cavity are clearly visible above FP resonant ripples.

The experimental scheme presented in Fig. 7.9 is used to identify if an intra-cavity modulation is generated in this laser. The CW probe beam from the ECL is positioned at wavelength of $1524\ nm$ in order to separate it spectrally from the original emission of the laser. Two optical spectra are presented in Fig.7.13 recorded from the laser diode.

The device is biased at $67\ mA$ and temperature controlled at $25\ °C$. The sideband resulting from intra-cavity modulation appears on the shorter wavelength side of the probe beam. Spectral separation of the sideband from injected CW signal is at $1.1\ THz$ and

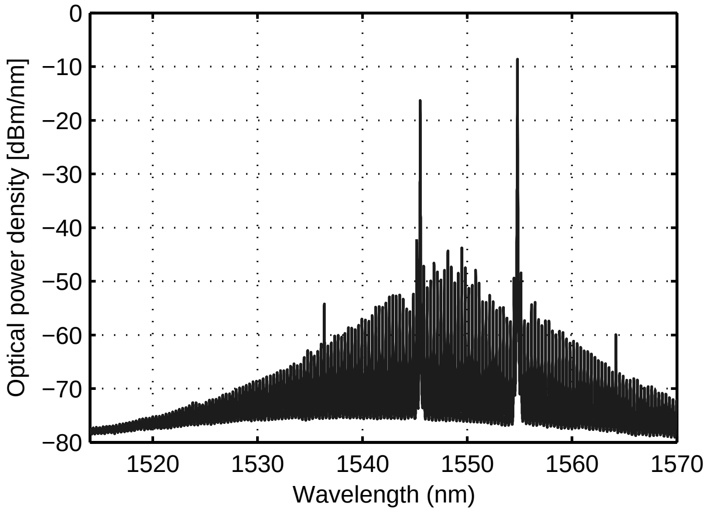

Figure 7.12: The multimode output from the slotted FP laser diode with FSR between dominant modes at $1.1\ THz$. Device is dc biased at $67\ mA$ and temperature stabilized at $25\ °C$.

equals the free spectral range between two dominant modes. It is worth noticing that on the longer wavelengths side of the spectrum, the intensity of the background FP ripples is high at the distance where the second modulation sideband is expected - it may be buried in the background.

It was demonstrated in the last two experiments that the gain of the semiconductor laser undergoes modulations resulting from the beating of the intra-cavity modes with the detuning between them in the terahertz range.

In the following section dominant modes emitted by the device with FSR at $372\ GHz$ will be examined with use of the FROG setup, and the performed experiment will allow to observe the temporal evolution of these modes affected by gain modulations.

7.4.3 Terahertz modulations on the optical carrier - frequency resolved optical gating detection

The impact of the intra-cavity modulation demonstrated in the previous section on the optical output is investigated. Temporal analysis of the dominant modes emitted from tested laser diode is performed with use of a frequency resolved optical gating (FROG) system.

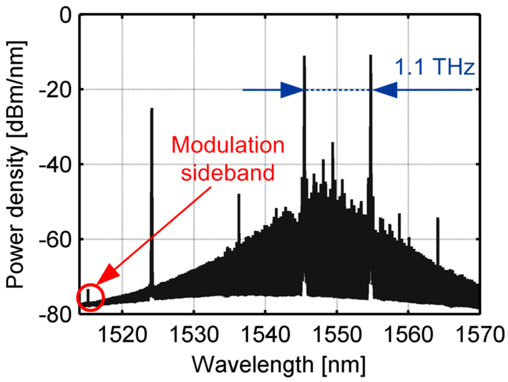

(a) Full span including original modes.

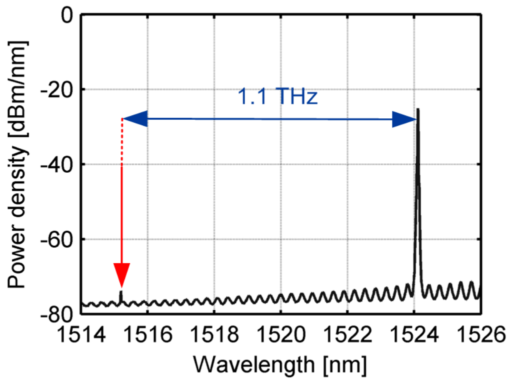

(b) Magnification of injected CW signal.

Figure 7.13: Optical spectrum collected from DUT when subject to the injection of CW signal at 1524 nm and 5.5 dBm; a) full span including original modes; b) magnification of injected signal with modulation sideband. Sideband marked with red circles.

Description of the SHG FROG system was given in Chapter 6 regarding characterization of short optical pulses. However in this experiment the FROG system will be used to observe the temporal evolution of the laser modes. Experimental setup is presented in Fig.7.14. The output from the tested laser is coupled with a lensed optical fibre with focal length of

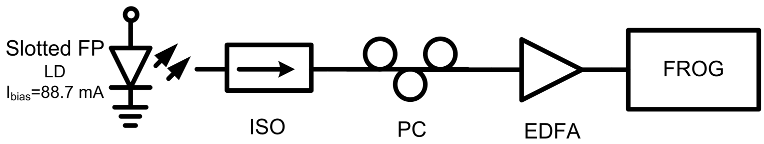

Figure 7.14: Experimental setup for temporal investigation of the output from the slotted FP LD biased at 88.7 mA and temperature stabilized at 25 $°C$.

3.5 mm. An optical isolator prevents back-reflections into the tested LD in order to assure stable operation. A polarization controller (PC) is used to achieve phase matching condition required for second harmonic generation (SHG) on the crystal in the FROG system. The high power optical amplifier (EDFA) is used in order to provide sufficient power for SHG process. The spectrogram recorded from the free running slotted FP laser biased at 88.7 mA is presented in Fig.7.15. Two outer signals denoted 1 and 2 are corresponding to the second harmonics of original modes launched into the FROG system, the third signal is an additional product equal to $\omega_1 + \omega_2$ generated on the SGH crystal inside the FROG system.

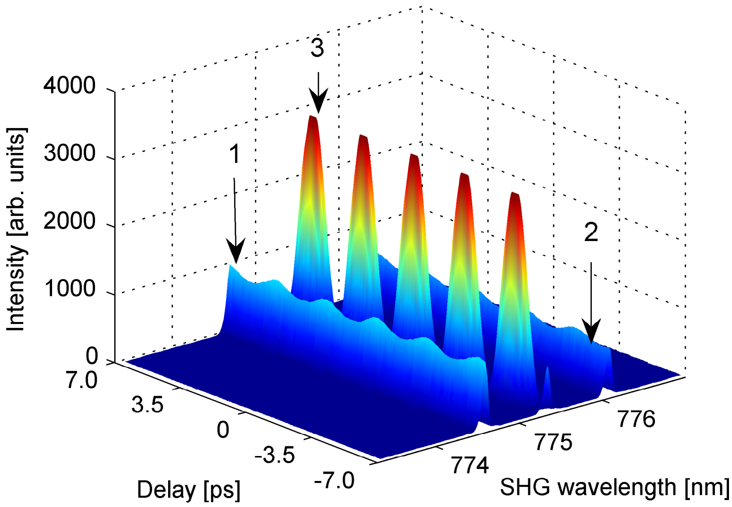

Figure 7.15: Spectrogram recorded from device under test, biased at 88.7 mA.

The time evolution of the two main modes as an autocorrelation function is shown in Fig.7.16. The autocorrelation traces are retrieved from the spectrogram by integration of the wavelengths span around two dominant modes. The two modes undergo nearly sinusoidal variations. The period of this variation translates to a frequency of 372 GHz which is the separation frequency between longitudinal optical modes emitted simultaneously by slotted FP laser. It can also be noticed that both traces are shifted by π, or in other words both modes are in counter-phase, but their phase difference remains constant in time. The latter is a proof of phase synchronization and therefore mode-locking in those type of laser diodes. Fig.7.17 and Fig.7.18 show the spectrogram, optical spectrum and time variation traces

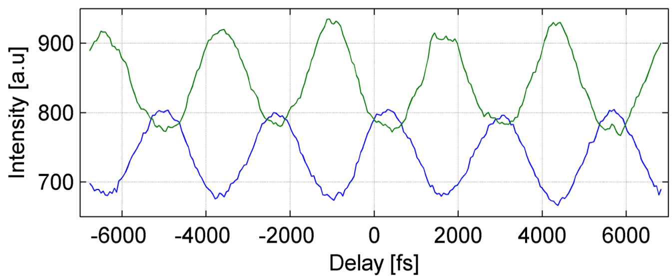

Figure 7.16: Autocorrelation traces retrieved from FROG measurement, corresponding to two modes emitted from DC biased tested laser diode.

recorded from two CW tunable laser sources. They are launched into the measurement setup with use of 50:50 optical coupler, instead of the investigated laser diode. Their output powers are set to be equal and with corresponding wavelengths $1553\ nm$ and $1556\ nm$ - separation frequency to be close to the one of the tested semiconductor laser.

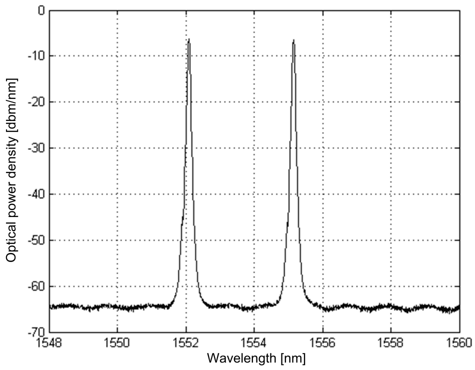

(a) Optical spectrum.

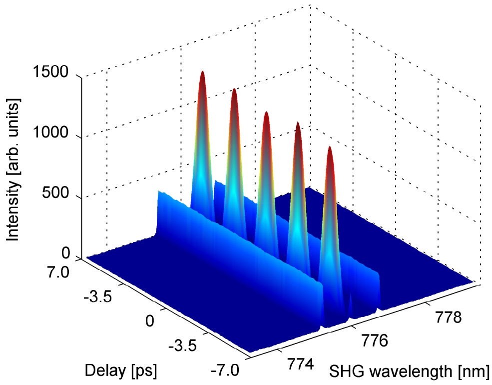

(b) Spectrogram.

Figure 7.17: Optical spectrum and spectrogram recorded from two tunable lasers coupled into the FROG system.

The autocorrelation traces retrieved in the same fashion as previously, do not undergo any organized variations, however the signal which corresponds to the sum of the signal frequency generated by SHG crystal inside FROG system can be seen on a spectrogram, however it does not exist at the input to the FROG, and should be ignored.

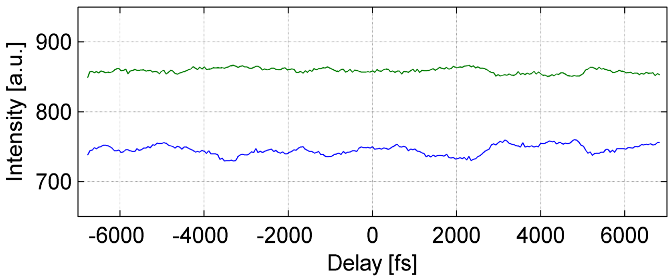

Figure 7.18: Autocorrelation traces retrieved from FROG measurement, corresponding to signals emitted from tunable sources.

Comparison of two experiments carried out with the use of the FROG system allows the assumption that optical modes traveling through semiconductor material are interacting with each other. Two modes originating from the same semiconductor laser cavity undergo periodical perturbations with constant phase shift. The origin of this oscillation lies in the nonlinear response of the semiconductor material to the optical signal passing through it resulting in four wave mixing (FWM). This completes the observations presented in the former section.

The frequency of the modulation, related to the separation frequency between optical signals, falls into the terahertz range. These intra-cavity modulations are self-initialized and sustained by the laser diode while it is provided with a single DC bias current at room temperature conditions. No external modulation in any form is applied to the devices. A very narrow (spectrally) signal is expected, as there are two optical modes strongly contributing to the intra-cavity beating [50, 51]. The linewidth of the beat signal produced by the optical output from the investigated slotted FP LD on an ultra-fast photodiode is assessed within next section.

7.5 Indirect generation of narrow-band terahertz wave by dual-mode slotted FP semiconductor laser coupled to UTC Photodiode

The terahertz signal generation at room temperature via photomixing of the multimode output of the slotted FP LD on the uni-traveling carrier photodiode (UTC-PD) will be presented. Detection scheme based on active subharmonic mixer and high bandwidth electrical spectrum analyzer allows to evaluate the linewidth the generated signal. All components used through presented experimental work operate at room temperature. The experimetnts presented in this section were carried out in collaboration with iemn research center, at University of Lille, France.

7.5.1 Experimental setup

The source laser is the slotted FP laser diode operating in multimode regime with two dominant modes separated by 372 GHz, that has been introduced and studied in previous sections of the current chapter. The uni-traveling carrier photodiode is used as a photomixing element for optical beams of two different wavelengths at the emission window around 1.5 μm. It offers a bandwidth up to 1800 GHz [52]. It is monolithically integrated with a transverse-electromagnetic-horn antenna (TEM-HA) [53] in order to efficiently couple the terahertz signal between semiconductor material and free space. A block diagram of the experimental setup used for generation and detection of the terahertz signal is presented in Fig. 7.19.

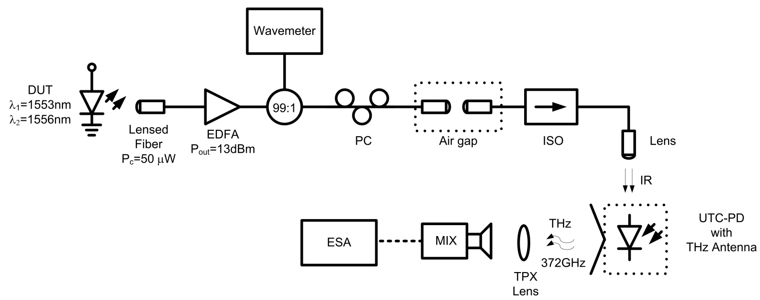

Figure 7.19: Experimental setup used for observation of terahertz signal produced by photo-mixing element (UTC-PD) from optical modes emitted from lotted FP laser diode at room temperature conditions.

The optical signal produced at the output of slotted FP-LD, biased at $88.7\ mA$ and temperature controlled at $25\ °C$ is collected by a lensed optical fiber with a power of $50\ \mu W$. An erbium doped fiber amplifier (EDFA) operating in constant optical power output mode set to 13 dBm delivers the level required for the UTC-PD to operate efficiently, after consideration of the losses introduced by other elements of the setup. For the same reason photocurrent generated on UTC-PD is monitored and kept around $300\ \mu A$. A wavemeter uses $1\ \%$ power from the optical coupler for continuous spectrum monitoring. A polarization controller (PC) allows adjusting the state of polarization of the infrared beam directed on the UTC-PD with a lensed optical fiber. An optical isolator (ISO) prevents feedback from the reflections from the surface of the photodetector. A THz signal is generated on the UTC-PD and propagated via TEM-HA. A polymethylpentene (TPX) lens with 25 mm focal length is used to collimate the radiated terahertz beam into the rectangular waveguide of an active subharmonic mixer (MIX). The intermediate frequency signal is resolved with an electrical spectrum analyzer (ESA), with a resolution bandwidth of 1 MHz and a sweep time of 20 ms, with no averaging.

7.5.2 Terahertz signal and its linewidth - results

The THz signal recorded from the slotted FP LD biased at 88.5 mA and temperature controlled at 25 $°C$. A signal recorded for such bias and temperature conditions is shown in Fig. 7.20 in linear scale. The measured data points are fitted with a Lorentzian curve. The central frequency at 371.89 GHz and the linewidth of 16.9 MHz are measured.

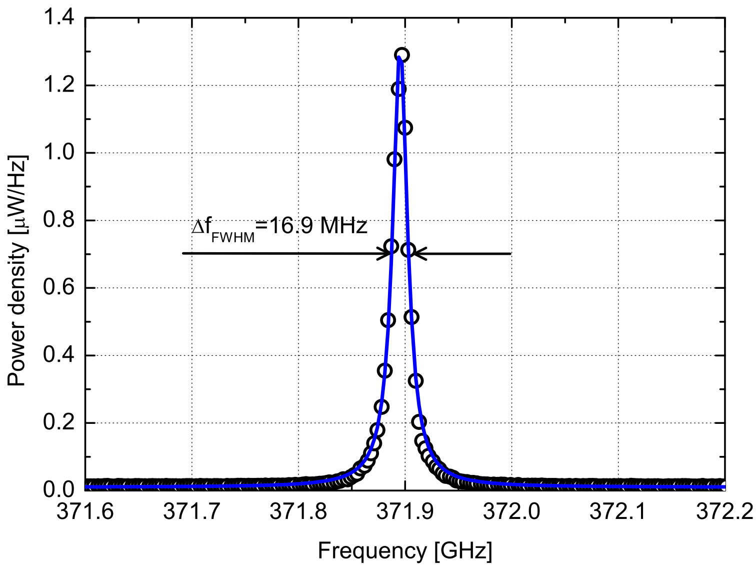

Figure 7.20: THz peak converted to linear scale and fitted with Lorentzian curve. Circles represent measured data points, solid line fitted curve. Linewidth measured at half maximum.

A central frequency change is observed with relation to the level of the bias current provided to the laser diode. Terahertz signals recorded for different bias levels are depicted in Fig. 7.21 Dependency of the central frequency on the bias condition is presented in Fig. 7.22. It shows a linear trend, where increase of the bias level provided to the slotted FP LD results in an increase of the central frequency of the terahertz signal.

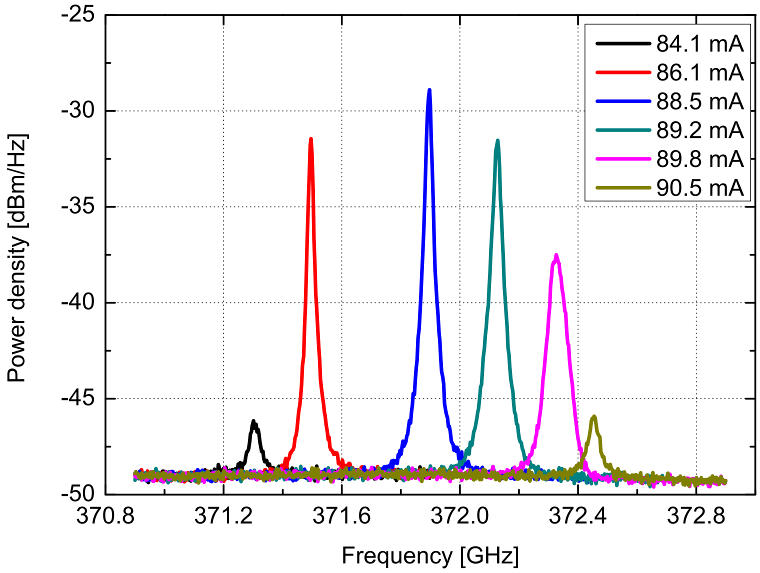

Figure 7.21: Terahertz signals recorded for different bias levels provided to slotted FP LD. Temperature maintained at 25 $^{\circ}C$.

The tunability of the generated terahertz signal in range of $1200\ MHz$ with adjustments of the bias current can be concluded. The terahertz linewidth dependence on the bias is plotted in Fig. 7.23 along with the power unbalance/side mode suppression ratio (SMSR) with respect to the same argument. Parabolic distribution of this parameter can be assumed with minimum value at $16.9\ MHz$ for a bias level on the LD at $88.5\ mA$, corresponding to even power distribution among optical modes [54].

The resolution offered by the ESA allowed for unprecedented assessment of the linewidth associated with the terahertz signal generated by dual-mode laser diode and UTC-PD. The measured linewidth of the generated teraretz signal is smaller than the summary linewidth of optical modes, however it is in the same order. One can write:

$$\Delta f_{THz} \sim \sum \Delta\nu_{opt} \tag{7.1}$$

This is insufficient to confirm the hypothesis provided by Equation 3.8, however, some future study supported experimentally should be performed in order to investigate the terahertz linewidth more precisely. The results presented in this section were collected with resolution of $1\ MHz$, however, with a long integration time of $1\ s$, which could lead to a

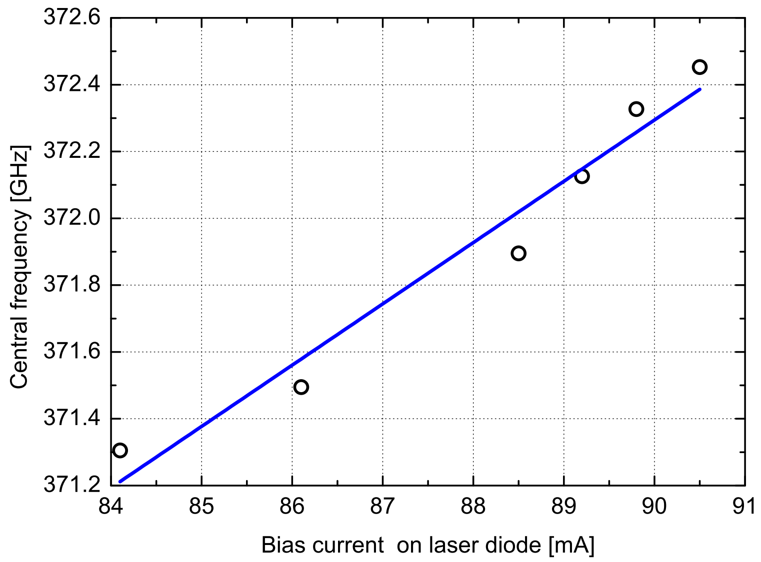

Figure 7.22: Terahertz peak frequency dependency on the level of bias current applied to the slotted FP LD. Measured data and linear fit.

considerable overestimation of the spectral width of the recorded signal.

The slotted FP LD and the UTC-PD operate at room temperature and require only single DC bias in case of laser, while no bias at all is required in the case of the photomixer. The optimization of the setup in terms of coupling efficiency would result in redundancy of the optical amplifier and allow for a compact size, battery operated THz source for applications compatible with megahertz linewidths [54].

It is demonstrated in former sections that intra-cavity modulations occur in optically active semiconductor material due to simultaneous presence of number of optical fields. Frequency of those modulations correspond to the separation frequency between these optical fields. In the next section the possibility of a direct emission of the signal by a multimode laser diode with FSR between the optical modes in terahertz range is investigated.

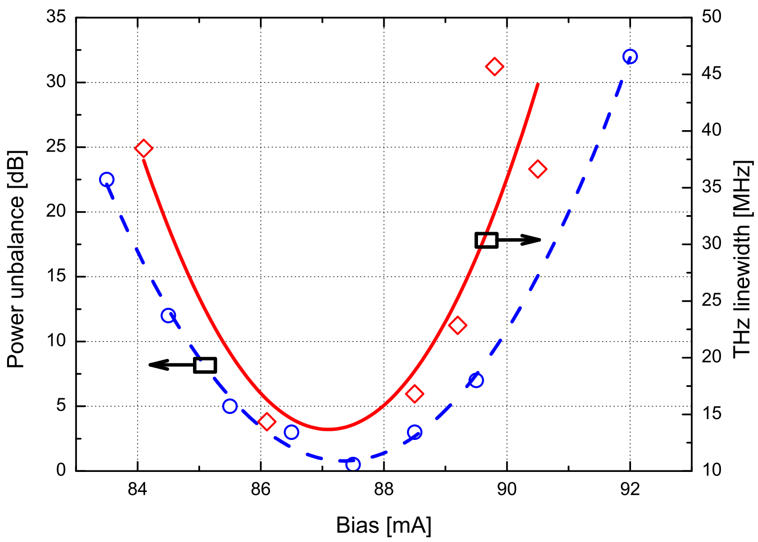

Figure 7.23: Power unbalance and terahertz linewidth dependency on the level of bias current applied to the slotted FP LD, measured data denoted with (○) and (◇) respectively. Solid and dashed lines are representing quadratic fit to experimental results.

7.6 Direct generation of terahertz signals with slotted Fabry-Pérot laser diode

The intracavity modulation at terahertz frequency resulting from the multimode operation of the semiconductor laser diode has been experimentally evidenced in previous chapters. This modulation occurs in the slotted FP laser diode when it is operating without external modulation applied by any means, with a DC-bias provided and temperature stabilized at $25\ ^{\circ}C$. A bolometer based setup allows to investigate if this modulation while affecting the optical modes inside the laser cavity is accompanied with a direct emission of an electromagnetic signal at the frequency related to this modulation. The rationale is as follows: to generate the electromagnetic (EM) field the acceleration of the charged particles (electrons) is required. This is the case, as the carriers in the multimode semiconductor laser are modulated according to the inter-modal beat frequency. The research activities presented in this section were carried out in terahertz laboratories of Cavendish Laboratory at Cambridge University, United Kingdom and Technical University of Darmstadt, Germany.

7.6.1 Terahertz detection system - Fourier transform infrared spectrometer with bolometer

The Fourier transform infrared (FT-IR) spectrometer combined with a bolometer as a detector offers the most sensitive form of known detection method of terahertz radiation, allowing to resolve detected signal spectrally.

7.6.1.1 Bolometer

A bolometer is a device for measuring the energy of incident electromagnetic radiation. It was invented in 1878 by the American astronomer Samuel Pierpont Langley. It consists of an 'absorber' connected to a heat sink (area of constant temperature) through an insulating link. The result is that any radiation absorbed by the absorber raises its temperature above that of the heat sink - the higher the energy absorbed, the higher the temperature will be. Temperature change can be measured directly or via an attached thermometer (composite design). Bolometers can be used to measure radiation energy of any frequency, however for most wavelength ranges there are other methods of detection that are more sensitive [55, 56]. For sub-millimeter wavelengths (from 200 μm to 1 mm wavelength), the bolometer is the most sensitive detector for any measurement over more than a very narrow wavelength range. In order, to achieve the best sensitivity, cryogenic conditions with cooling down to a fraction of a degree above absolute zero (typically from 50 mK to 300 mK) are necessary. An example schematic picture of a bolometer's cross-section is presented in Fig. 7.24.

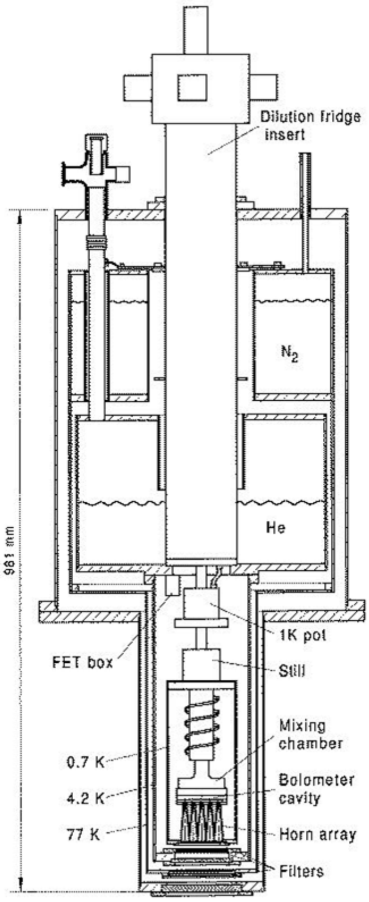

Figure 7.24: Cryostatic chamber with a bolometer [55].

7.6.1.2 Fourier transform infrared spectrometer

Fourier transform spectroscopy is a measurement technique whereby spectra are collected based on measurements of the temporal coherence of a radiative source, using time-domain measurements of the electromagnetic radiation or other type of radiation. The Michelson spectrograph relies on the same principle as the Michelson-Morley experiment. Light from the source is split into two beams by a half-silvered mirror, one is reflected off a fixed mirror and one off a moving mirror which introduces a time delay - the Fourier transform spectrometer is just a Michelson interferometer with a movable mirror. The beams interfere, allowing the temporal coherence of the light to be measured at each different time delay setting. By making measurements of the signal at many discrete positions of the moving mirror, the spectrum can be reconstructed using a Fourier transform of the temporal coherence of the light. Michelson spectrographs are capable of very high spectral resolution observations of very bright sources.

7.6.2 Experimental setup and results

It was shown in previous sections that the slotted FP laser is capable of emitting multimode optical output under DC bias and for room temperature conditions. Experimental investigation with a fast photodetector and electrical spectrum analyzer has proven that the RF signal of the frequency corresponding to separation frequency between longitudinal optical modes can be observed at the output of the DBR leaser. However, a similar experimental setup does not offer sufficient bandwidth to investigate the frequency range in which the separation frequency of the spectrum emitted by slotted FP structure falls. Separation frequency of the slotted FP laser at 372 GHz, falls into the terahertz frequency range, and therefore a limited amount of equipment exists that is able to cope with it. The experimental setup, depicted in Fig. 7.25 is used to perform tests on the slotted FP laser. It consists of two main elements: bolometer as a detector and a Fourier transform infrared (FT-IR) spectrometer as a frequency discriminator. The tested device is temperature controlled at 25 $°C$ and its output

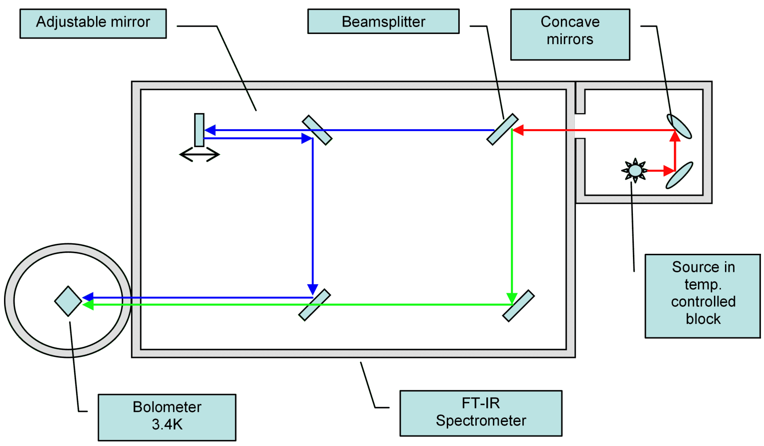

Figure 7.25: Schematic diagram of FT-IR spectrometer combined with a bolometer as a detector.

is coupled to the input window of the FT-IR spectrometer with two gold plated concaved mirrors. Inside the spectrometer the incoming signal was divided by a beam-splitter, one leg of the signal was delayed with respect to the other with an adjustable mirror and then both beams were combined on the bolometer. Interference signals as a function of the displacement of the adjustable mirror were recorded. The Fourier transformation is performed to produce the final spectrogram. The combination of the efficiency of the beam-splitter and the sensitivity of the bolometer set the measurement range between $400\ GHz$ and $1\ THz$. The interior of the FT-IR spectrometer is evacuated before measurements in order to minimize influence of water vapor on the measurement. The bolometer is cooled down to an operating temperature of $3.4\ K$. The whole setup is placed on an anti-vibration workbench in an electrostatic isolated chamber. We were able to record signals at a -frequency in the vicinity of $0.7\ THz$ for a range of bias currents applied to the laser diode. A single peak recorded for $65\ mA$ of bias current is shown in Fig. 7.26. Terahertz signal is centered around $0.7\ THz$ and it is nearly ten times stronger than background noise. This frequency

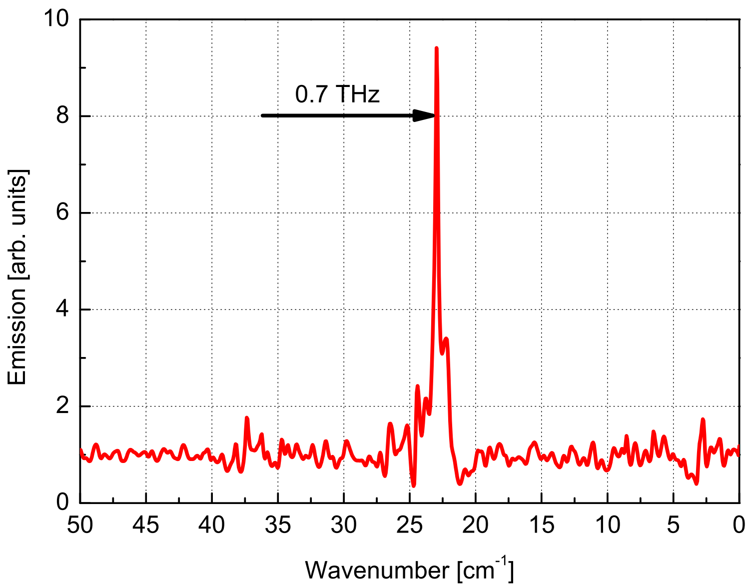

Figure 7.26: Terahertz peak at $0.7\ THz$ recorded from slotted FP LD operating in dual-mode regime under DC bias and at room temperature.

corresponds to the second harmonic of the free spectral range between longitudinal optical modes present in optical output of the laser under test. It also conforms to results retrieved from the FROG experiment. The FWHM linewidth of the recorded terahertz signal is below the spectral resolution of the FT-IR system ($1.86\ GHz$) [54, 57].

7.7 Summary

The generation of a narrow-band terahertz signal semiconductor laser device operating in multimode regime has been experimentally investigated using several techniques. It was demonstrated for the first time that the terahertz signals can be generated using a passively mode-locked semiconductor laser. Signals at $372\ GHz$ and $1.1\ THz$ were shown. The implication of the four wave mixing in the process of gain modulation and passive mode-locking at the detuning frequencies of $372\ GHz$ and $1.1\ THz$ was demonstrated. This is supported by a combination of experimental evidences. However, no definite support was directly found at terahertz frequencies for the condition formulated previously in Chapter 3 and evidenced for mmW signals in Chapters 4 and 5, which should be expressed for THz band signal as follows:

$$\Delta f_{THz} << \Delta \nu_{opt} \tag{7.2}$$

This is due to insufficient resolution of the detection schemes used in the terahertz domain. Also the power of the generated THz signals was not evaluated as the experimental arrangements utilized did not offer such measurement or were uncalibrated with a reference source.

Bibliography

[1] P. Siegel, “Terahertz technology,” *Microwave Theory and Techniques, IEEE Transactions on*, vol. 50, no. 3, pp. 910–928, 2002.

[2] T. Horgan, J. Waldman, M. J. Coulombe, W. Nixon, and G. Szatkowski, *A 524 GHZ Polarimetric Compact Range for Scale Model RCS Measurements*. Storming Media, 1999.

[3] D. D. Arnone, C. M. Ciesla, A. Corchia, S. Egusa, M. Pepper, J. M. Chamberlain, C. Bezant, E. H. Linfield, R. Clothier, and N. Khammo, “Applications of terahertz (THz) technology to medical imaging,” in *Proceedings of SPIE*, vol. 3828, p. 209, 1999.

[4] E. R. Mueller, “Terahertz radiation: Applications and sources.,” *Industrial Physicist*, vol. 9, p. 27, Aug. 2003.

[5] E. Pickwell, B. E. Cole, A. J. Fitzgerald, M. Pepper, and V. P. Wallace, “In vivo study of human skin using pulsed terahertz radiation,” *Physics in Medicine and Biology*, vol. 49, no. 9, p. 1595, 2004.

[6] W. L. Chan, J. Deibel, and D. M. Mittleman, “Imaging with terahertz radiation,” *Reports on Progress in Physics*, vol. 70, no. 8, p. 1325, 2007.

[7] G. M. Png, J. W. Choi, B. W.-H. Ng, S. P. Mickan, D. Abbott, and X.-C. Zhang, “The impact of hydration changes in fresh bio-tissue on thz spectroscopic measurements,” *Physics in Medicine and Biology*, vol. 53, no. 13, p. 3501, 2008.

[8] M. Kemp, P. Taday, E. Cole, J. Cluff, A. Fitzgerald, and W. Tribe, “Security applications of terahertz technology,” in *Proc. of SPIE Vol*, vol. 5070, p. 45.

[9] J. Federici, B. Schulkin, F. Huang, D. Gary, R. Barat, F. Oliveira, and D. Zimdars, “THz imaging and sensing for security applicationsexplosives, weapons and drugs,” *Semiconductor Science and Technology*, vol. 20, p. S266, 2005.

[10] Y. Shen, T. Lo, P. Taday, B. Cole, W. Tribe, and M. Kemp, “Detection and identification of explosives using terahertz pulsed spectroscopic imaging,” *Applied Physics Letters*, vol. 86, p. 241116, 2005.

[11] M. McColl, M. F. Millea, and A. H. Silver, “The superconductor-semiconductor schottky barrier diode detector,” *Applied Physics Letters*, vol. 23, no. 5, pp. 263–264, 1973.

[12] D. E. Prober, “Superconducting terahertz mixer using a transition-edge microbolometer,” *Applied Physics Letters*, vol. 62, no. 17, pp. 2119–2121, 1993.

[13] K. Kawase, M. Sato, T. Taniuchi, and H. Ito, “Coherent tunable THz-wave generation from LiNbO[sub 3] with monolithic grating coupler,” *Applied Physics Letters*, vol. 68, pp. 2483–2485, Apr. 1996.

[14] F. Zernike and P. R. Berman, “Generation of far infrared as a difference frequency,” *Physical Review Letters*, vol. 15, no. 26, pp. 999–1001, 1965.

[15] E. R. Brown, F. W. Smith, and K. A. McIntosh, “Coherent millimeter-wave generation by heterodyne conversion in low-temperature-grown GaAs photoconductors,” *Journal of Applied Physics*, vol. 73, no. 3, p. 1480, 1993.

[16] N. S. Nishioka, P. L. Richards, and D. P. Woody, “Composite bolometers for submillimeter wavelengths,” *Applied Optics*, vol. 17, pp. 1562–1567, May 1978.

[17] N. R. Erickson, “A fast and sensitive submillimeter waveguide power meter,” in *10th Int. Space Terahertz Technol. Symp*, p. 501507, 1999.

[18] J. E. Walsh, J. H. Brownell, M. J. Goldstein, J. C. Swartz, J. Urata, and M. F. Kimmitt, "A new tunable coherent FIR-THz source," *Opt. Photon. News*, vol. 9, no. 12, p. 5152, 1998.

[19] E. R. Brown, K. A. McIntosh, K. B. Nichols, and C. L. Dennis, "Photomixing up to 3.8 THz in low-temperature-grown GaAs," *Applied Physics Letters*, vol. 66, p. 285, 1995.

[20] S. Matsuura, G. A. Blake, R. A. Wyss, J. C. Pearson, C. Kadow, A. W. Jackson, and A. C. Gossard, "A traveling-wave THz photomixer based on angle-tuned phase matching," *Applied Physics Letters*, vol. 74, p. 2872, 1999.

[21] T. Noguchi, A. Ueda, H. Iwashita, S. Takano, Y. Sekimoto, M. Ishiguro, T. Ishibashi, H. Ito, and T. Nagatsuma, "Millimeter wave generation using a uni-traveling-carrier photodiode," in *Proc. 12th Int. Symp. Space Terahertz Technology*, vol. 2001, pp. 73–80, 2001.

[22] C. Fattinger and D. Grischkowsky, "Point source terahertz optics," *Applied Physics Letters*, vol. 53, p. 1480, 1988.

[23] L. Xu, X. C. Zhang, and D. H. Auston, "Terahertz beam generation by femtosecond optical pulses in electro-optic materials," *Applied Physics Letters*, vol. 61, p. 1784, 1992.

[24] H. R. Fetterman, P. E. Tannenwald, B. J. Clifton, C. D. Parker, W. D. Fitzgerald, and N. R. Erickson, "Far-IR heterodyne radiometric measurements with quasioptical schottky diode mixers," *Applied Physics Letters*, vol. 33, p. 151, 1978.

[25] E. R. Mueller, J. L. Hesler, T. W. Crowe, D. S. Kurtz, and R. II, "Widely-Tunable laser-sideband THz source for spectroscopy & LO applications," in *Proc. 2001 Space THz Tech. Symp*, 2001.

[26] J. H. Smet, C. G. Fonstad, and Q. Hu, "Intrawell and interwell intersubband transi-

tions in multiple quantum wells for far-infrared sources," *Journal of Applied Physics*, vol. 79, p. 9305, 1996.

[27] B. Xu, Q. Hu, and M. R. Melloch, "Electrically pumped tunable terahertz emitter based on intersubband transition," *Applied Physics Letters*, vol. 71, p. 440, 1997.

[28] T. Sollner, W. D. Goodhue, P. E. Tannenwald, C. D. Parker, and D. D. Peck, "Resonant tunneling through quantum wells at frequencies up to 2.5 THz," *Applied Physics Letters*, vol. 43, p. 588, 1983.

[29] M. Reddy, S. Martin, A. Molnar, R. Muller, R. Smith, P. Siegel, M. Mondry, M. Rodwell, H. Kroemer, and S. Allen, "Monolithic schottky-collector resonant tunnel diode oscillator arrays to 650 GHz," *Electron Device Letters, IEEE*, vol. 18, no. 5, pp. 218–221, 1997.

[30] E. R. Brown, C. D. Parker, L. J. Mahoney, K. M. Molvar, and J. R. Soderstrom, "Oscillations up to 712 GHz in InAs/AlSb resonant-tunneling diodes," *Applied Physics Letters*, vol. 58, no. 20, p. 2291, 1991.

[31] C. C. Bradley, "Gain and frequency characteristics of a 20 mW c. w. water vapour laser oscillating at 118. 6 microns," *Infrared Physics*, vol. 12, pp. 287–299, 1972.

[32] I. Song and K. K. G. Park, "Frequency-Locked submillimeter wave generation from josephson junction arrays," *Japanese Journal of Applied Physics*, vol. 38, pp. 44–47, 1999.

[33] H. Wang, L. Samoska, T. Gaier, A. Peralta, H. Liao, Y. Leong, S. Weinreb, Y. Chen, M. Nishimoto, and R. Lai, "Power-amplifier modules covering 70-113 GHz using MMICs," *Microwave Theory and Techniques, IEEE Transactions on*, vol. 49, no. 1, pp. 9–16, 2001.

[34] J. Bruston, E. Schlecht, A. Maestrini, F. Maiwald, S. C. Martin, R. P. Smith, I. Mehdi, P. H. Siegel, J. C. Pearson, J. B. Breckinridge, and P. Jakobsen, "Development of 200-GHz to 2.7-THz multiplier chains for submillimeter-wave heterodyne receivers,"

in *UV, Optical, and IR Space Telescopes and Instruments*, vol. 4013, (Munich, Germany), pp. 285–295, SPIE, July 2000.

[35] S. Martin, B. Nakamura, A. Fung, P. Smith, J. Bruston, A. Maestrini, F. Maiwald, P. Siegel, E. Schlecht, and I. Mehdi, "Fabrication of 200 to 2700 GHz multiplier devices using GaAs and metal membranes," in *IEEE MTT S INT MICROWAVE SYMP DIG*, vol. 1, pp. 1641–1644, 2001.

[36] A. Staprans, E. McCune, and J. Ruetz, "High-power linear-beam tubes," *Proceedings of the IEEE*, vol. 61, no. 3, pp. 299–330, 1973.

[37] P. H. Siegel, A. Fung, H. Manohara, J. Xu, and B. Chang, "Nanoklystron: A monolithic tube approach to terahertz power generation," in *12th Int. Space Terahertz Technol. Symp*, (SanDiego, CA), p. 8190, 2001.

[38] G. Chin, "Optically pumped submillimeter laser heterodyne receivers: astrophysical observations and recent technical developments," *Proceedings of the IEEE*, vol. 80, no. 11, pp. 1788–1799, 1992.

[39] H. P. Rser, "Heterodyne spectroscopy for submillimeter and farinfrared wavelengths from 100 m to 500 m," *Infrared Phys*, vol. 32, pp. 385–407, 1991.

[40] J. Farhoomand, G. A. Blake, M. A. Frerking, and H. M. Pickett, "Generation of tunable laser sidebands in the far-infrared region," *Journal of Applied Physics*, vol. 57, pp. 1763–1766, Mar. 1985.

[41] J. Faist, F. Capasso, D. L. Sivco, C. Sirtori, A. L. Hutchinson, and A. Y. Cho, "Quantum cascade laser," *Science*, vol. 264, pp. 553–556, Apr. 1994.

[42] F. Capasso, R. Colombelli, R. Paiella, C. Gmachl, A. Tredicucci, D. L. Sivco, and A. Y. Cho, "Far-infrared and ultra-high-speed quantum-cascade lasers," *Opt. Photon. News*, vol. 12, no. 5, p. 4046, 2001.

[43] M. Rochat, J. Faist, M. Beck, U. Oesterle, and M. Ilegems, “Far-infrared (lambda = 88 mu m) electroluminescence in a quantum cascade structure,” *Applied Physics Letters*, vol. 73, pp. 3724–3726, Dec. 1998.

[44] B. Williams, S. Kumar, Q. Hu, and J. Reno, “Operation of terahertz quantum-cascade lasers at 164 k in pulsed mode and at 117 k in continuous-wave mode,” *Optics Express*, vol. 13, pp. 3331–3339, May 2005.

[45] B. S. Williams, “Terahertz quantum-cascade lasers,” *Nat Photon*, vol. 1, no. 9, pp. 517–525, 2007.

[46] S. Verghese, K. McIntosh, and E. Brown, “Highly tunable fiber-coupled photomixers with coherent terahertz output power,” *Microwave Theory and Techniques, IEEE Transactions on*, vol. 45, no. 8, pp. 1301–1309, 1997.

[47] D. Zimdars and J. V. Rudd, “Opening the THz window,” *Photon. Spectra*, p. 146148, 2000.

[48] D. Arnone, C. Ciesla, and M. Pepper, “Terahertz imaging comes into view,” *Physics World*, no. April, pp. 35–40, 2000.

[49] J. C. O’Gorman, P. McEvoy, D. McDonald, F. P. Logue, and P. M. Landais, “Optical waveguide and a method for providing an optical waveguide,” Patent W 6978057, 12 2005.

[50] S. Latkowski, P. Landais, F. Surre, and S. Lynch, “CW-THz wave generation using a multimode semiconductor laser at room temperature,” in *Lasers and Electro-Optics Society, 2007. LEOS 2007. The 20th Annual Meeting of the IEEE*, pp. 864–865, 2007.

[51] S. Latkowski, F. Surre, R. Maldonado-Basilio, and P. Landais, “Investigation on the origin of terahertz waves generated by dc-biased multimode semiconductor lasers at room temperature,” *Applied Physics Letters*, vol. 93, pp. 241110–3, Dec. 2008.

[52] A. Beck, G. Ducournau, M. Zaknoune, E. Peytavit, T. Akalin, J. Lampin, F. Mollot, F. Hindle, C. Yang, and G. Mouret, “High-efficiency uni-travelling-carrier photomixer at 1.55[emsp4 1/4-em space][micro sign]m and spectroscopy application up to 1.4[emsp4 1/4-em space]THz,” *Electronics Letters*, vol. 44, pp. 1320–1322, Oct. 2008.

[53] E. Peytavit, J. Lampin, T. Akalin, and L. Desplanque, “Integrated terahertz TEM horn antenna,” *Electronics Letters*, vol. 43, pp. 73–75, Jan. 2007.

[54] S. Latkowski, J. Parra-Cetina, R. Maldonado-Basilio, P. Landais, G. Ducournau, A. Beck, E. Peytavit, T. Akalin, and J. Lampin, “Analysis of a narrowband terahertz signal generated by a unitravelling carrier photodiode coupled with a dual-mode semiconductor Fabry-Pérot laser,” *Applied Physics Letters*, vol. 96, no. 24, p. 241106, 2010.

[55] L. A. Reichertz, W. Esch, H. P. Gemnd, J. Gromke, and E. Kreysa, “The MPIR 100 mK bolometer array for 2 mm continuum observations,” *Nuclear Instruments and Methods in Physics Research Section A: Accelerators, Spectrometers, Detectors and Associated Equipment*, vol. 444, pp. 423–426, Apr. 2000.

[56] J. C. Mather, “Bolometers: ultimate sensitivity, optimization, and amplifier coupling,” *Appl. Opt.*, vol. 23, pp. 584–588, Feb 1984.

[57] S. Latkowski, F. Surre, and P. Landais, “Terahertz wave generation from a dc-biased multimode laser,” *Applied Physics Letters*, vol. 92, pp. 081109–3, Feb. 2008.

Chapter 8

Conclusions and future

8.1 Conclusions

The study of multimode semiconductor lasers presented in this report demonstrated their feasibility as sources of the signals with the frequencies from microwaves to terahertz range.

In Chapter 3 passive mode-locking operation principle for single section laser diode was disclosed with an identification criterion of such a process. Demonstration of the RF signals and short pulse generation with use of various types of semiconductor laser structures operating in passive mode-locking regime was performed in Chapters 4 and 5, along with the PML process identification for each case. Behavior of PML semiconductor laser diode under an external signal injection was investigated in Chapter 6. Potential for all-optical clock extraction from data-streams at various bit-rates with use of DBR and QDash lasers was demonstrated.

In Chapter 7 direct and indirect generation of terahertz signals by a single section multimode laser diode, operating under DC-bias condition and in room temperature has been experimentally evidenced. The intra-cavity modulations at THz frequencies resulting from the longitudinal modes beating are responsible for mode-locking process and direct terahertz emission were demonstrated. Impact of these modulations on the optical signals emitted by such a laser was also analyzed. The THz signals produced were examined in the terms of spectral linewidth.

The above outcomes resulted in a number of publications in reviewed scientific journals and conferences which are listed in Appendix A of this report.

8.2 Future

The research work presented demonstrates clearly the potential of multimode semiconductor lasers for future applications, not only in telecommunications, but in all areas where a compact size, energy efficient, narrowband terahertz sources can be utilized. There are, however, a number of investigations which could be performed in future to complete those presented:

- Improved investigation of the linewidth of the THz signals generated in order to support the mode-locking identification criterion.
- Measurements of the amount of the produced terahertz radiation in both direct and indirect configurations.
- Optimization of the laser design in order to efficiently guide-out the terahertz signal.
- Polarization state characterization of generated terahertz signal.

According to the last point, polarization dependence of the emitted signal was preliminary investigated with use of the setup presented in Fig. 8.1. Output of the laser under test

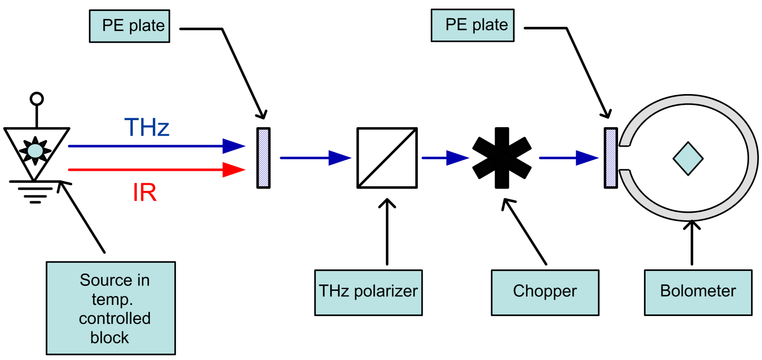

Figure 8.1: Experimental setup for THz signal polarization dependency. Wire-grid Thz polarizer is used at the IR filtered output of slotted FP LD under 88.7 mA of DC-bias.

operating at 88.8 mA is infrared filtered with two 5 mm thick polyethylene (PE) plates:

one at the window of the bolometer and the other at the front of the laser diode. Signal is passed through the wire-grid THz polarizer and chopper synchronized with lock-in amplifier for increased sensitivity of the detection setup. The recorded terhertz signal power (uncalibrated) as a function of angular position of the polarizer is depicted in Fig. 8.2.

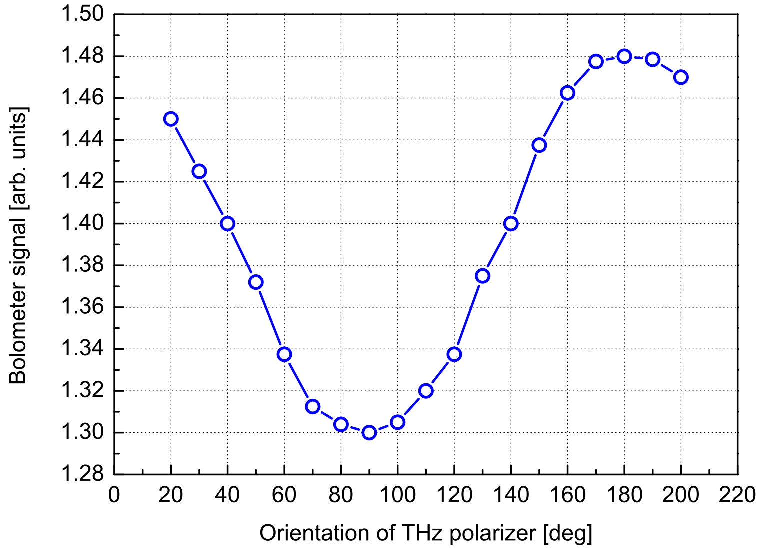

Figure 8.2: Terahertz signal polarization dependency. Terahertz signal power is uncalibrated.

The acquired data demonstrate that the terahertz signal emitted directly from the multimode slotted FP laser diode is polarized, however some more experimental work would be necessary in order to fully define the polarization condition of the THz wave generated in this way.

Appendix
List of Publications

Reviewed Journals:

1. S. Latkowski, F. Surre, and P. Landais, "Terahertz wave generation from a dc-biased multimode laser," *Applied Physics Letters*, vol. 92, pp. 081109-3, Feb. 2008.
   Selected for publication in Virtual Journal of Ultrafast Science.

2. S. Latkowski, F. Surre, R. Maldonado-Basilio, and P. Landais, "Investigation on the origin of terahertz waves generated by dc-biased multimode semiconductor lasers at room temperature," *Applied Physics Letters*, vol. 93, pp. 241110-3, Dec. 2008.

3. S. Latkowski, R. Maldonado-Basilio, and P. Landais, "Sub-picosecond pulse generation by 40-GHz passively mode-locked quantum-dash 1-mm-long Fabry-Pérot laser diode," *Optics Express*, vol. 17, pp. 19166-19172, Oct. 2009.
   Selected for publication in Virtual Journal of Ultrafast Science.

4. S. Latkowski, F. Surre, P. Landais, and G. Duan, "All-optical synchronization of a 40 GHz self-pulsating distributed bragg reflector laser to return-to-zero 10, 20 and 40 Gbit/s data streams," *Optics Communications*, vol. 282, pp. 2053-2058, May 2009.

5. S. Latkowski, R. Maldonado-Basilio, K. Carney, J. Parra-Cetina, S. Philippe, and P. Landais, "Semiconductor optical amplifier-based heterodyning detection for resolving optical terahertz beat-tone signals from passively mode-locked semiconductor lasers," *Applied Physics Letters*, vol. 97, no. 8, p. 081113, 2010.

6. S. Latkowski, J. Parra-Cetina, R. Maldonado-Basilio, P. Landais, G. Ducournau, A. Beck, E. Peytavit, T. Akalin, and J. Lampin, "Analysis of a narrowband terahertz signal generated by a unitravelling carrier photodiode coupled with a dual-mode semiconductor Fabry-Pérot laser," *Applied Physics Letters*, vol. 96, no. 24, p. 241106, 2010.

7. R. Maldonado-Basilio, S. Latkowski, F. Surre, and P. Landais, “Linewidth analysis of 40-GHz passively mode-locked multi-mode semiconductor lasers,” *Optics Communications*, vol. 283, pp. 299-303, Jan. 2010.

8. R. Maldonado-Basilio, J. Parra-Cetina, S. Latkowski, and P. Landais, “Timing-jitter, optical, and mode-beating linewidths analysis on subpicosecond optical pulses generated by a quantum-dash passively mode-locked semiconductor laser,” *Optics Letters*, vol. 35, pp. 1184-1186, Apr. 2010.
   Selected for publication in Virtual Journal of Ultrafast Science.

Conferences:

1. S. Latkowski, F. Surre, G. Pagny, and P. Landais, “Passive modelocking in bimodal laser,” *in Proceedings of the 2006 China-Ireland International Conference on Information and Communications Technologies (CIICT 2006)*, Hangzhou, China, p. 58, Sept. 2006.

2. S. Latkowski, P. Landais, F. Surre, and S. Lynch, “CW-THz wave generation using a multimode semiconductor laser at room temperature,” *in Lasers and Electro-Optics Society, 2007. LEOS 2007. The 20th Annual Meeting of the IEEE*, pp. 864-865, 2007.

3. S. Latkowski, F. Surre, and P. Landais, “RF or THz signals generated from DC biased multimode lasers,” *in Transparent Optical Networks, 2007. ICTON 07. 9th International Conference on*, vol. 3, pp. 257-260, 2007.
   Invited.

4. S. Latkowski, F. Surre, and P. Landais, “THz generation using multimode semiconductor laser,” *Photonics Ireland*, Galway, Ireland, p. 96, Sept. 2007.

5. S. Latkowski, F. Surre, P. Landais, B. Kelly, and S. Lynch, “Generation of THz signals with phase-locked longitudinal mode controlled laser diodes,” *Semiconductor and Integrated OptoElectronics conference*, Cardiff, Wales, Feb. 2007.

6. F. Surre, S. Latkowski, R. Maldonado-Basilio, P. Landais, and S. Lynch, "Generation of THz signal from Four-Wave-Mixing in multimode lasers due to material nonlinearities," *International Conference on Optical, Optoelectronic and Photonic Material and Applications*, London, UK, Aug. 2007.

7. K. Carney, S. Latkowski, R. Madonado-Basilio, F. Surre, and P. Landais, "Measurement of the linewidth enhancement factor using Cassidys method in a 370 GHz self-pulsating Fabry-Pérot laser," *IET Conference Publications: China-Ireland International Conference on Information and Communications Technologies (CIICT 2008)*, vol. 2008, pp. 668-671, Beijing, China, Sep. 2008.

8. S. Latkowski, F. Surre, E. Degirmenci, and P. Landais, "Mode-Locked multimode semiconductor laser: Novel narrowband terahertz signal source," *In: IOP ed.IOP Meeting THz sensing: Techniques and Applications*, London, UK, June, 2008.

9. S. Latkowski, F. Surre, E. Degirmenci, and P. Landais, "Passively phase-locked multimode semiconductor laser: From millimetre to terahertz wave generation," *in Lasers and Electro-Optics, 2008 and 2008 Conference on Quantum Electronics and Laser Science. CLEO/QELS 2008. Conference on*, pp. 1-2, 2008.

10. S. Latkowski, F. Surre, R. Maldonado-Basilio, and P. Landais, "Measurement of the THz signal generated by a multimode semiconductor laser," *European Semiconductor Laser Workshop 2008*, Eindhoven, Netherlands, Sept. 2008.

11. S. Latkowski, F. Surre, and P. Landais, "Passively phase-locked semiconductor lasers for clock recovery and terahertz generation," *IET Conference Publications: China-Ireland International Conference on Information and Communications Technologies (CIICT 2008)* , vol. 2008, pp. 661-664, Beijing, China, Sep. 2008.

12. S. Latkowski, F. Surre, and P. Landais, "Passively mode-locked semiconductor lasers and their applications," *in Transparent Optical Networks, 2008. ICTON 2008. 10th Anniversary International Conference on*, vol. 2, pp. 110-113, 2008.
Invited.

13. S. Latkowski, F. Surre, R. Maldonado-Basilio, and P. Landais. "THz generation using multimode semiconductor lasers," *Conference of the Science Fundation Ireland - Science Summit 2008, Convergence Worlds*, Kilkenny, Ireland, November 17-18, 2008.

14. S. Latkowski, R. Maldonado-Basilio, and P. Landais, "Short pulse generation with 40 GHz passively-mode locked q-dashed Fabry-Pérot laser," *in Transparent Optical Networks, 2009. ICTON 09. 11th International Conference on*, pp. 1-4, 2009. ***Invited***.

15. S. Latkowski, R. Maldonado-Basilio, and P. Landais, "Sub-picosecond pulse generation at 40GHz repetition rate by passively mode-locked quantum-dashed Fabry-Pérot laser," *Photonics Ireland*, Kinsale, Ireland, A62, Sept. 2009.

16. R. Maldonado-Basilio, S. Latkowski, and P. Landais, "All-optical tunable source at x40-GHz by passively mode-locked quantum-dash Fabry-Pérot semiconductor lasers," *Photonics Ireland*, Kinsale, Ireland, A68, Sept. 2009.

17. R. Maldonado-Basilio, S. Latkowski, and P. Landais, "720-fs pulse generation with 40 GHz passively-mode locked quantum-dash Fabry-Pérot laser," *in Optical Communication, 2009. ECOC 09. 35th European Conference on*, pp. 1-2, 2009.

18. R. Maldonado-Basilio, S. Latkowski, F. Surre, and P. Landais, "Linewidth study of 40-GHz passively mode-locked multimode semiconductor lasers," *in CLEO/Europe -EQEC 2009 - European Conference on Lasers and Electro-Optics and the European Quantum Electronics Conference*, Munich, Germany, pp. 1-1, 2009.

19. R. Maldonado-Basilio, S. Latkowski, and P. Landais, "Generation and compression of sub-picosecond pulses by a passively mode-locked QDash semiconductor laser," *Inspire Nanoweek Conference 2009*, County Cork, Ireland, 30 Nov to 1 Dec 2009.

20. K. Carney, S. Latkowski, R. Maldonado-Basilio, P. Landais, R. Lennox, and A. L. Bradley, "Characterization of a multi-electrode bulk-SOA for low NF in-line amplifi-

cation in passive optical networks," *in Transparent Optical Networks (ICTON), 2010 12th International Conference on*, pp. 1-4, 2010.

21. R. Maldonado-Basilio, S. Latkowski, F. Surre, and P. Landais, "Wave-mixing analysis for THz-signals generation in dc-biased semiconductor optical devices at room temperature, *in 2010 IEEE Photonics Society Winter Topicals Meeting Series (WTM)*, Majorca, Spain, pp. 9-10, 2010.

22. J. Parra-Cetina, S. Latkowski, R. Maldonado-Basilio, and P. Landais, "Timing jitter and linewidth analysis based on a Quantum-Dash Fabry-Pérot semiconductor laser with an All-Optical clock recovery application," *Semiconductor and Integrated OptoElectronics conference*, Cardiff, Wales, Mar. 2010.

23. J. Parra-Cetina, S. Latkowski, R. Maldonado-Basilio, and P. Landais, "Timing jitter and all-optical clock recovery based on a quantum-dash Fabry-Pérot semiconductor laser," *in Transparent Optical Networks (ICTON), 2010 12th International Conference on*, pp. 1-4, 2010.
    Invited.

24. J. Parra-Cetina, S. Latkowski, R. Maldonado-Basilio, and P. Landais, "Non-return-to-zero 40 Gb/s all-optical clock recovery and retiming, reshaping and re-amplification (3R) regenerator," *in International Conference on Coherent Non-linear Optics / Laser, Applications and Technology (ICONO/LAT)*, Kazan, Russia, 23-27 Aug, 2010.

25. G. Ducournau, A. Beck, E. Peytavit, T. Akalin, J-F. Lampin, S. Latkowski, J. Parra-Cetina, R. Maldonado-Basilio, and P. Landais, "Narrowband terahertz signal generation using a dual-mode semiconductor Fabry-Pérot laser and a uni-travelling carrier photodiode," *IRMMW-THz 2010, 35th International Conference on Infrared, Millimeter, and Terahertz Waves, IRMMW 2010*, Rome, Italy, September 5-10, 2010.

26. R. Maldonado-Basilio, S. Latkowski, and P. Landais, "Analysis of optical THz-signals from mode-locked semiconductor laser by using a semiconductor optical amplifier-

based detection scheme," *IRMMW-THz 2010, 35th International Conference on Infrared, Millimeter, and Terahertz Waves, IRMMW 2010*, Rome, Italy, September 5-10, 2010.

27. S. Latkowski, J. Parra-Cetina, R. Maldonado-Basilio, and P. Landais, "Short pulse generation at 320 GHz by dc-biased passively mode-locked QDash laser diode," *Scientific Meeting: The Laser at 50*, Belfast, Northern Ireland, September 13, 2010.

28. S. Latkowski, R. Maldonado-Basilio, and P. Landais, "320 GHz optical pulse-stream from quantum-dash mode-locked semiconductor laser diodes," *European Semiconductor Laser Workshop 2010*, Pavia, Italy, September 24 - 25, 2010.

29. R. Maldonado-Basilio, S. Latkowski, , and P. Landais, "All-optical 40 Gb/s 3R regeneration assisted by clock-extraction based on a passively mode-locked quantum-dash Fabry-Pérot laser," *Optical Communication, 2010. ECOC '10. 35th European Conference on*, 2010 , (accepted).

30. J. Parra-Cetina S. Latkowski, R. Maldonado-Basilio, and P. Landais, "All-optical clock recovery based on a quantum-dash Fabry-Prot semiconductor laser in a 3R regenerator with modulation format conversion at 40 Gb/s," *2010 China-Ireland International Conference on Information and Communications Technologies (CIICT 2010)* , Wuhan, China, Oct. 2010 (accepted).

31. S. Latkowski, J. Parra-Cetina, R. Maldonado-Basilio, P. Landais, G. Ducournau, A. Beck, E. Peytavit, T. Akalin, J-F. Lampin, "Narrowband terahertz signal generator based on dual-mode Fabry-Pérot semiconductor laser and unitravelling carrier photodiode." *TOM 2: Terahertz Science and Technology: EOS Annual Meeting 2010 (EOSAM 2010)*, Paris, France, October 26 - 29, 2010, (accepted).